The Porter Puddle Complex,

Petrology and Geochemistry of the Marmot Formation,

Northern Canadian Cordilleran Miogeocline

By

Benjamin P. Williams

A Thesis Submitted to
Saint Mary's University, Halifax, Nova Scotia
in Partial Fulfilment of the Requirements for
the Degree of Bachelor of Sciences, Honours.

May 2013, Halifax, Nova Scotia

Approved: Dr. Georgia Pe-Piper

Supervisor

Date: 29/04/2013

The Porter Puddle Complex, Petrology and Geochemistry of the Marmot Formation,

Northern Canadian Cordilleran Miogeocline

By Benjamin P. Williams

Abstract

The Porter Puddle Complex (PPC) of the Ordovician–Silurian Marmot Formation volcanics (MFV) is located in the northeastern Canadian Cordillera (NTS map sheet 106B/SE). The PPC has previously been interpreted as a rift-related submarine volcanic edifice within a carbonate platform and its seaward shale equivalent. It consists of potassic-ultrapotassic and alkalic volcanic rocks. Previous geochemical and mineralogical studies of these rocks are limited. New mapping by the Northwest Territory Geoscience Office in 2009-2012 applied newer stratigraphy and better delineated the PPC. Samples were collected from the PPC for mineralogical and geochemical study to better understand the petrogenesis of the volcanic rocks.

All samples have experienced considerable alteration under hydrothermal conditions at the seafloor and during burial diagenesis. Primary mineral assemblages include pseudomorphs after olivine, dominant clinopyroxene, phlogopite, K-feldspar, albite and Ba-feldspars of the celsian–hyalophane series. These minerals suggest a potassic-ultrapotassic, low-silica basaltic magma. Early crystal fractionation involved clinopyroxene, olivine, and spinel at pressures well above 30 kbar. REE patterns indicate a lack of plagioclase fractionation and presence of residual garnet in the source, also implying a predominant mantle origin for MFV magmas.

Ocelli textures suggest an immiscible phase in a silica-undersaturated, high-volatile basalt. Estimates for crystallization pressure for oxyhornblende in the ocelli suggest that later stage petrogenesis involved immiscible phases, K-feldspar fractionation, and crystallization of Ba-feldspar. Phlogopite associated with early clinopyroxene suggests magma evolved from a more hydrous system into a later stage of ocelli crystallization, further suggesting a hydrous-silica-undersaturated immiscibility. These multiple controls on petrogenesis may be responsible for the geochemical variability in the Marmot Formation volcanic rocks described in previous literature.

29/04/2013

Acknowledgements

I would like to express my very great appreciation to my supervisor, Dr. Georgia Pe-Piper, for her endless guidance, comments, and wealth of knowledge. I would also like to thank Dr. David Piper for his reviews and comments.

Financial support and logistics for this project was provided by the Northwest Territories Geoscience Office (NTGO) and Saint Mary's University Geology Department, in which I am very grateful. In particular, I would like to thank Beth Fischer, Valerie Jackson, and Luke Ootes for taking me into the field. They have taught me how to observe and learn in the field, as well as providing me with a fascinating project. Support and enthusiasm from David Knowlton and Kirsti Medig was greatly appreciated; both in the field, and in the months that followed.

I would like to thank the teaching, technical and support staff of the Geology Department at Saint Mary's University. You have taught me everything I know. In particular I would like to thank Dr. Jacob Hanley, Dr. Jarda Dostal, Dr. YuanYuan Zhang, Xing Yang, Randolph Corney, and Angeliki Papoutsa, for their assistance, discussions, insight, and guidance.

Finally, I wish to thank my family and friends for their continual support.

Table of Contents

Abstract ii
Acknowledgements iii
Table of Contents iv
List of Figures v
List of Tables vi
List of Abbreviations vii
Chapter 1: Introduction 1
Chapter 2: Geological Setting 2
Chapter 3: Methods 5
Chapter 4: Field Observations 7
4.1: Introduction 7
4.2: Marmot Formation Volcanic Rocks 7
Chapter 5: Analytical Results 11
5.1: Petrographic Observations 11
5.2: Mineral Chemistry 17
5.2.1: Clinopyroxene 17
5.2.2: Phlogopite 18
5.2.3: Amphiboles 19
5.2.4: Ba-Feldspars 22
5.3: Geochemistry 23
5.3.1: Whole Rock Geochemistry 23
5.3.2: Major Elements 29
5.3.3: Trace Elements 30
Chapter 6: Discussion 34
6.1: Interpretation of Mineral Data 34
6.1.1: Clinopyroxene 34
6.1.2: Phlogopite 37
6.1.3: Amphiboles 37
6.1.4: Ba-Feldspars 40
6.2: Effects of Alteration 40
6.3: Petrogenesis & Fractional Crystallization 43
6.4: Nature of Source 46
6.5: Comparison with Rift-related Volcanism 51
Chapter 7: Conclusions & Recommended Future Work 54
7.1: Conclusions 54
7.2: Recommended Future Work 55
Chapter 8: References 56
Appendices: 61
A: Mineral Chemistry by SEM/EDS 61
B: Backscatter Electron Images (BSE) 76

List of Figures:

Figure 2.1: Map of Lower Paleozoic paleogeoraphy 4
Figure 2.2: Cross-section through MCE 5
Figure 4.1: Simplified geology map 9
Figure 5.1.1: Petrographic images of clinopyroxene 13
Figure 5.1.2: Petrographic images of ocelli 14
Figure 5.1.3: Petrographic images of ocelli cores 15
Figure 5.1.4: Backscatter Electron images of Ba-feldspar 16
Figure 5.2.1: Ternary classification diagram of pyroxene 18
Figure 5.2.2: Ternary classification diagram of micas 19
Figure 5.2.3: Amphibole classification diagram 20
Figure 5.3.1A: Major elements vs. Zr plots 27
Figure 5.3.1B: Al_2O_3/Na_2O alteration index plots 28
Figure 5.3.2: Geochemistry discrimination diagrams 30
Figure 5.3.3: Chondrite & Primitive Mantle normalized spider diagrams for MFV 31
Figure 5.3.4: Trace elements vs. Cs plots 33
Figure 6.1: Plots of clinopyroxene chemistry 36
Figure 6.2: Spider diagrams showing effects of alteration for MFV 42
Figure 6.3: Incompatible trace and major elements vs. Zr plots 45
Figure 6.4.1: Trace element variation plots 47
Figure 6.4.2: Plots illustrating garnet lherzolite melting 48
Figure 6.5.1: Chondrite & Primitive Mantle normalized spider diagrams for EARS 53

List of Tables:

Table 4.2: Sample names, locations, and petrographic grouping 10
Table 5.2.3: Chemical analyses for amphiboles 21
Table 5.2.4: Chemical analyses for Ba-feldspars 23
Table 5.3.1: Major and Trace Element Geochemistry for MFV (this study) 25
Table 5.3.2: Major and Trace Element Geochemistry for MFV (from literature) 26
Table 6.1.3: Geobarometry results for amphiboles 38
Table 6.1.4: Calculated original bulk composition for ocelli 39
Table 6.4.1: Incompatible element ratios 50

List of Abbreviations:

Ba-fsp.....Ba-feldspar
cal.....Calcite
chl.....Chlorite
cpx.....Clinopyroxene
EARS .....East African Rift System
EDS.....Energy dispersive spectroscopy
fsp.....Feldspar
hbl .....Hornblende (Amphibole)
HFSE.....High field strength element
HREE.....Heavy rare earth elements
hya.....Hyalophane
ICP-MS .....Inductively-coupled plasma mass spectrometer
kfs.....K-feldspar
LILE.....Large ion lithophile element
LOI.....Loss on ignition
LREE.....Light rare earth elements
MCE.....Misty Creek Embayment
MFV.....Marmot Formation volcanic rocks
NT .....Northwest Territories
NTGO .....Northwest Territory Geoscience Office
NTS.....National topographic system
OIB.....Ocean island basalt
ol .....Olivine
phl .....Phlogopite
PPC .....Porter Puddle Complex
py.....Pyrite
qtz.....Quartz
REE.....Rare earth elements
SEM .....Scanning electron microscope
TAS.....Total alkalis vs. silica
xen.....Xenoliths
XRF.....X-ray fluorescence spectroscopy

1 INTRODUCTION

The Porter Puddle Complex (PPC) is located in the southeastern Bonnet Plume map sheet (NTS 106B/SE) in the northern Canadian Cordillera (Northwest Territories). The region, according to published reconnaissance-scale maps, is underlain by Lower Paleozoic Road River Group basinal strata, undivided Silurian-Devonian platformal carbonate rocks, and Middle Devonian Earn Group turbiditic siltstone and sandstone. The Lower Paleozoic strata were deposited in the Misty Creek paleo-embayment, an embayment of the Selwyn Basin thought to have formed by incipient rifting. Ordovician-Silurian volcanic rocks of the Marmot Formation have been identified and their extent is approximately mapped in several areas of southern NTS 106B.

The PPC has previously been interpreted as a submarine volcanic edifice that records shoaling, pertaining to the Marmot Formation. It consists of potassic-ultrapotassic and alkalic volcanic rocks. Previous studies of the geochemistry of these rocks are limited, and were summarized by grouping the rocks according to geographic and not stratigraphic location.

New mapping, carried out as part of the Northwest Territories Geoscience Office (NTGO) Selwyn-Mackenzie Shale Basins project during the 2009-2012 field seasons, has applied the newer stratigraphy to mapped areas, and better delineated the various horizons of the PPC. The purpose of this study is to expand the understanding of the Porter Puddle Complex, through detailed petrological, mineralogical, and geochemical analyses. We will further address the issue of multiple geochemical classifications

(potassic - alkaline) (Goodfellow et al. 1995) for the same geographical localities. Based on petrography, mineral chemistry, and trace element controls of petrogenesis, we will examine the control on the source region, as well as compare our samples with those from a similar tectonic history.

Eleven samples of mafic flows from various parts of the complex were collected for polished-thin section, and whole rock major and trace element geochemical analysis. Initial examinations of these mafic rocks reveal euhedral-subhedral seriate-textured to subophitic textured phenocrysts of olivine, zoned pyroxenes, and biotite or phlogopite set in a pilotaxitic fine-grained altered chloritic matrix. Local carbonate alteration of the groundmass is present, originating from late-stage quartz and calcite veining associated with tectonism, and/or from seawater-sourced fluids close to the time of deposition. Further petrogaphic and geochemical analysis are in addressed in later sections of this thesis.

2 GEOLOGICAL SETTING

The Early Paleozoic evolution of the western Canadian Cordillera was marked by the development of a passive margin built on the western edge of ancestral North America as a result of supercontinent Rodinia breakup in Neoproterozoic time (Devlin and Bond 1988; Fritz et al. 1991; Gordey and Anderson 1993; Cecile et al. 1997). Variations in stratigraphic thicknesses and anomalous sedimentary facies, combined with the presence of local accumulations of mainly alkaline mafic volcanic rocks, suggest

renewed extension of the passive margin occurred episodically throughout much of the Paleozoic (Fritz et al. 1991; Goodfellow et al. 1995). During this time the northern passive continental margin shoaled eastward, which accompanied the development of expansive carbonate platforms (e.g., Mackenzie, Redstone and Ogilvie platforms). These platform areas pass to the west to embayments, basins and troughs (Fig. 2.1; Fritz et al. 1991).

To the south and west of the Mackenzie Platform, the strata grade into basinal facies siliciclastic rocks deposited in what is termed the Selwyn Basin (Fig. 2.1; Gordey and Anderson 1993). An irregular rifted basin termed the Misty Creek Embayment (MCE) (Fig 2.1; Cecile 1978; 1982) occurs along the margin between the Mackenzie Platform and the Selwyn Basin. The approximately 100 x 150 km MCE represents a lower Paleozoic basin developed as a result of three superimposed stages of rifting. The first rifting event coincides with the initial breakup of the supercontinent Rodinia in the latest Neoproterozoic. This rifting event was marked with the emplacement of voluminous mafic igneous rocks (e.g., the Tsezotene Sills; Ootes et al. 2008) into the Neoproterozoic Mackenzie Mountains Supergroup. The second rifting event coincides with the development of the lower Paleozoic passive margin and marks a time of substantial subsidence and infill of basinal facies strata (Cambrian rifting of Figure 2.2). This rifting event formed the initial geometry of the MCE in Early to Middle Cambrian time. The third rifting event was superimposed on the second event and culminated in Late Cambrian to Early Ordovician time (Cecile 1978, 1982; Cecile et al. 1997). As with the second rifting event, considerable subsidence is recorded in the strata; however, this rifting event is also characterized by voluminous submarine (predominantly) alkaline

mafic magmatism (Ordovician rifting of Figure 2.2). These volcanic deposits, which comprise the Marmot Formation, are interstratified with upper Lower and Middle Ordovician basinal shale facies in the center of the MCE.

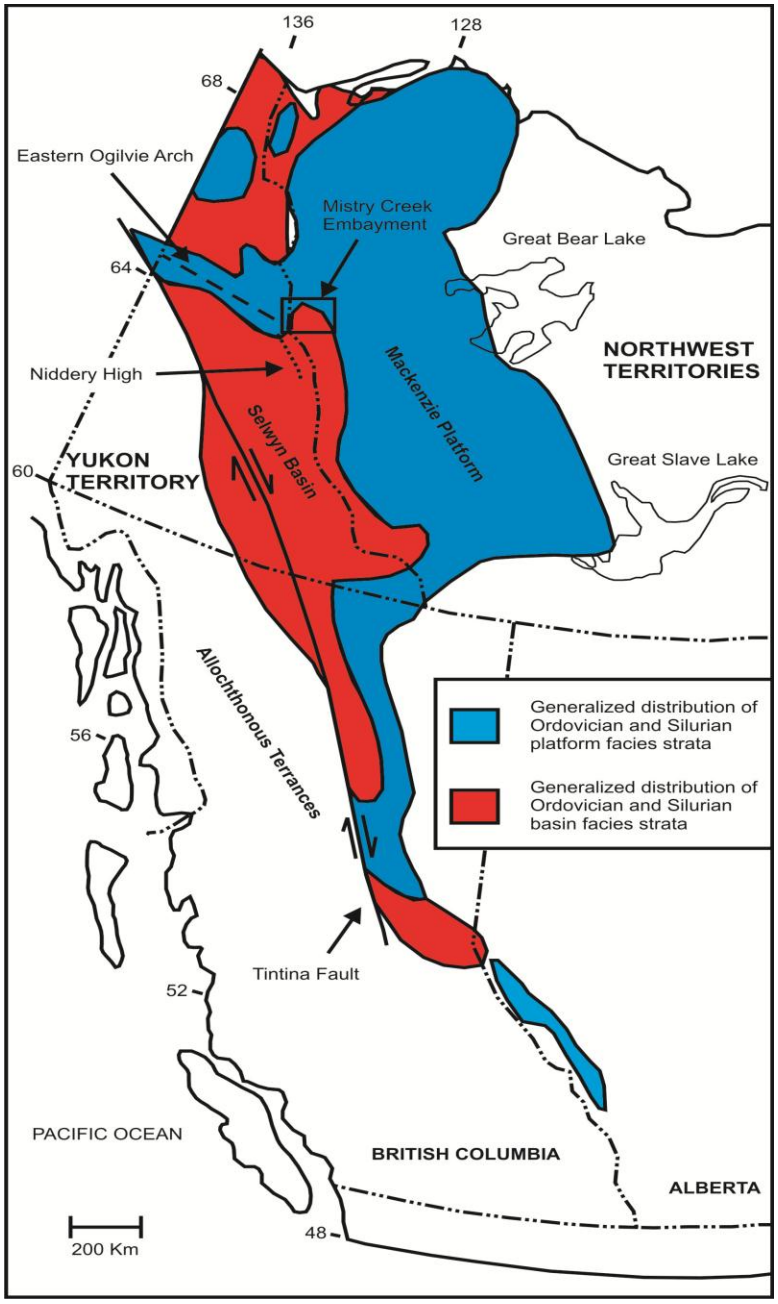

Figure 2.1 Map of Lower Paleozoic paleogeography with location of the Misty Creek Embayment (modified from Cecile et al. 1997). Box represents location of Figure 4.1

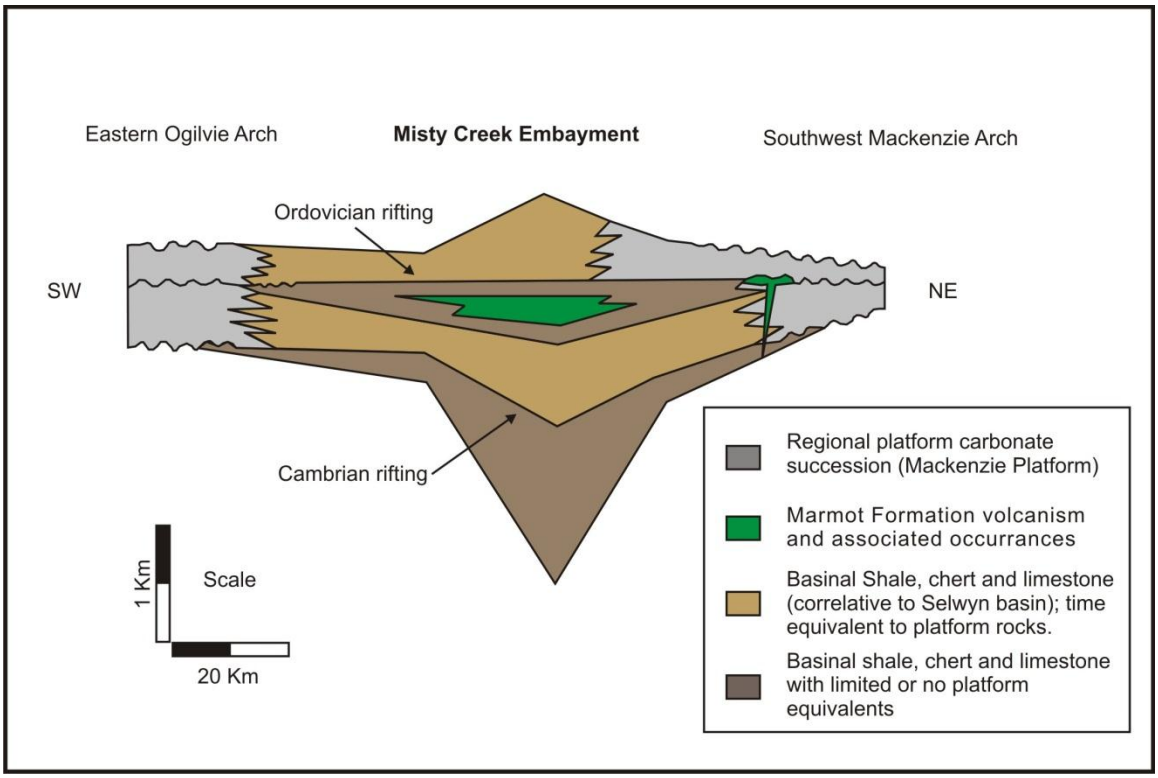

Figure 2.2 Southwest to northeast schematic cross-section through the Misty Creek Embayment showing two classic rift 'steers-head' profiles (modified from Cecile et al. 1997).

3 METHODS

Samples of the Marmot Formation volcanic rocks (hereafter abbreviated MFV) were collected from seventeen different localities throughout the MCE, during the 2012 summer field season. This sampling was carried out in part with a regional 1:60,000 scale bedrock mapping project in collaboration with the Northwest Territories Geoscience Office.

The petrography is based on examination of polished thin sections from representative samples using a polarizing and reflected light microscope, in conjunction with scanning electron microscope (SEM) analyses of selected samples. Major and trace elements of whole rocks were determined for eleven samples, and have been compared with pre-existing geochemical data from Goodfellow et al. (1995).

Rock powders for whole-rock geochemistry were prepared by removing all altered surfaces and obvious xenoliths from the samples, chipping and then washing the chips in de-ionized water to remove any loose contaminants. Samples were crushed using a shatter box with an iron bowl at the Minerals Engineering Centre of Dalhousie University. Major and trace elements were determined by Acme Analytical Laboratories according to their Code 4X and Code 4B packages, which combine XRF whole rock and ICP-MS trace element packages. Whole rock geochemical data are given in Table 5.3.1.

The Scanning Electron Microscope (SEM) at the Regional Analytical Centre at Saint Mary's University was used to determine chemical mineralogy of selected samples. It is a LEO 1450 VP SEM with a maximum resolution of 3.5nm at 25kV, with a detection limit of 0.1%. The SEM uses a tungsten filament to supply electrons to produces a back-scatted electron image (BEI) of the grains on the polished thin section and return an atomic number. The SEM was also used to confirm the identification of minerals that were not easily identified by petrographic microscope through the use of energy dispersive spectroscopy (EDS) (Appendices A, B).

4 FIELD OBSERVATIONS

4.1 INTRODUCTION

The predominantly alkaline magmatism of Ordovician age within the MCE has been divided into multiple distinct suites that were grouped based upon whole rock geochemical signatures (Goodfellow et al. 1995). The Marmot Formation comprise many lithofacies defined by Cecile (1982), consisting of lapilli tuff, fine grained breccia, sandstone, siltstone, argillite, massive amygdaloidal flows, conglomerate, sills, and pillow breccia. Herein the term 'Marmot Formation' (MFV), will be used to describe group (II) of Goodfellow et al. (1995), consisting of the volcanic components described later. Previous speculations on the correlation of the Marmot Formation with other volcanic suites in the region have been made by Cecile (1982) and Goodfellow et al. (1995) on the basis of limited geochemical data.

4.2 MARMOT FORMATION VOLCANIC ROCKS

The Marmot Formation, as described by Cecile (1982), is mainly exposed in the center of the MCE (Fig. 4.1). The greater part of the Formation comprises volcanic, volcaniclastic and epiclastic material that is interstratified with Ordovician siliclastic and carbonate rocks (Cecile 1982). At the top of the Marmot Formation type section, however, Cecile (1982) identified a two-hole crinoid fossil in a limestone bed that is

interstratified with volcanic rocks and tuffs. The presence of a two-holed crinoid suggests a late Early to early middle Devonian age for the cessation of volcanism. It is possible that the volcanism in the MCE persisted to this time; however, the bulk of MCE volcanism is Ordovician in age (Cecile 1982; Goodfellow et al. 1995) and is the focus of this study.

The dominant MFV occurrences comprise texturally coherent thick accumulations of mafic volcanic rocks that overlie basinal facies carbonates of the Middle Ordovician Duo Lakes Formation. This suite also contains brecciated coherent material such as those deposits interpreted to reflect volcanic vents. Additionally, the MFV suite also includes hyaloclastites, brecciated pillowed basalts, amygdaloidal basalts, and strata bound lapilli tuffs. A list of sample locations, field names, and short form name can be found in Table 4.2, as well as their field locations plotted on Figure 4.1. Sample numbering was based on field notes/ locations, outcrop, lithology, and number of samples. For example, 456B1 and 456B2 represent two slightly different lithologies from the same outcrop.

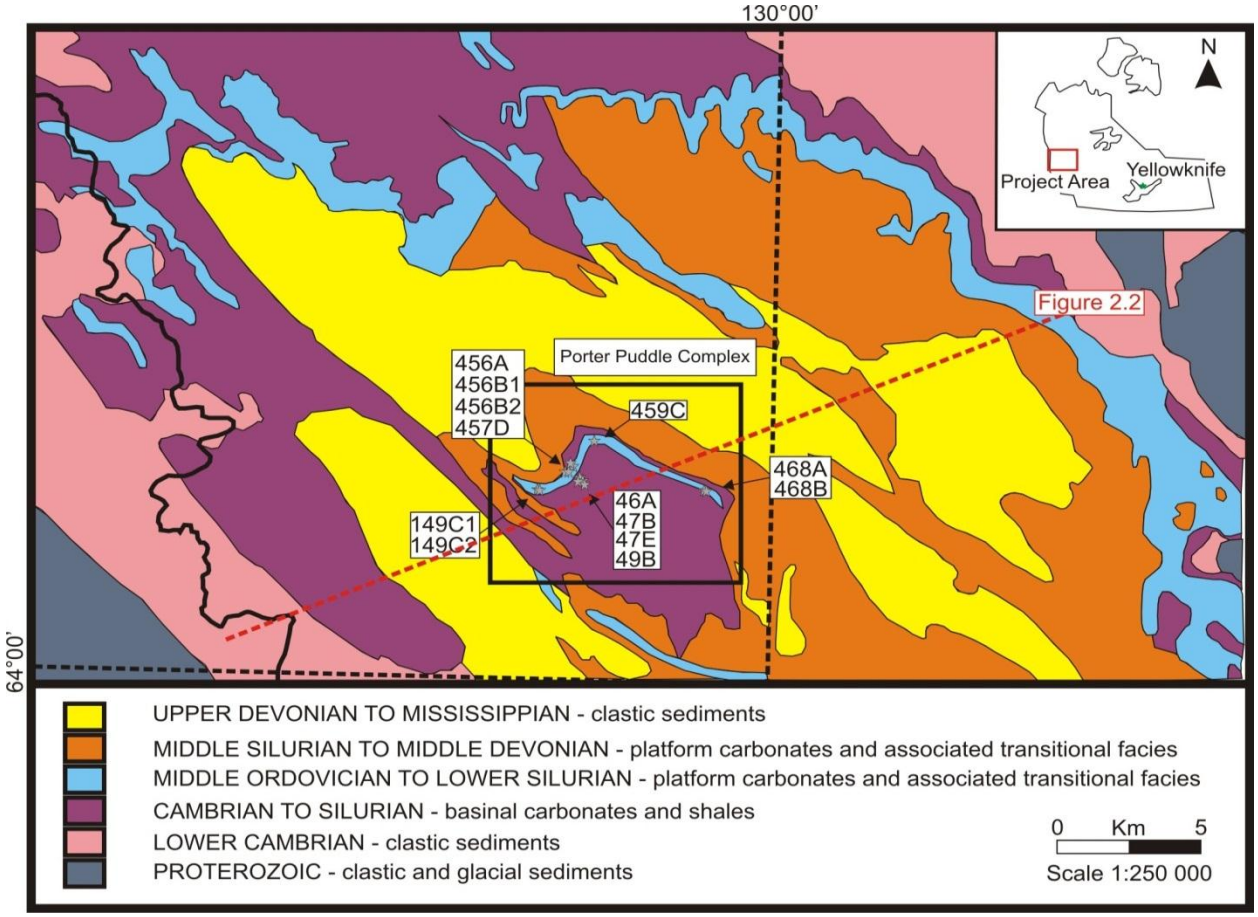

Figure 4.1 Simplified geology map of the study area showing locations of samples of the Marmot Formation and related intrusive and volcaniclastic rocks. Geology from Blusson (1974). Red dashed line denotes the location for the cross section presented in Figure 2.

			UTM - Zone 9		Decimal Degrees			Phenocrysts and Major
Sample Shorthand	Sample ID	Field Name	Easting (m)	Northing (m)	Latitude	Longitude	Petrographic group	Alteration Minerals Present
46A	12BF46A	mafic volcanic flow	436977.764	7115050.303	64.15609739	-130.2957794	1	phl, fsp, cpx, ol, xen, chl
47B	12BF47B	amygdaloidal pillow basalt	436793.532	7115064.184	64.1561882	-130.2995719	1	phl, fsp, cpx, ol, cal, qtz, py
47E	12BF47E	microcrystic basalt	436838.817	7115065.247	64.15620604	-130.2986416	3	phl, fsp, cpx, cal, chl, qtz, py
49B	12BF49B	pyritic volcanic tuff	436113.935	7115430.764	64.15935174	-130.3136961	4	cal, cpx, xen, chl, qtz, py
149C1	12BF149C1	mafic volcanic flow	435140.299	7114237.095	64.1484611	-130.3331966	1	phl, fsp, cpx, ol, cal, qtz, py
149C2	12BF149C2	mafic volcanic flow	435140.486	7114237.095	64.14846113	-130.3331928	1	phl, fsp, cpx, ol, cal, qtz, py
456A	12KM456A	microcrystic basalt	435793.539	7115173.779	64.1569867	-130.3201727	3	phl, fsp, cpx, cal
456B1	12KM456B1	microcrystic basalt	435633.850	7115257.907	64.15771168	-130.3234911	3	phl, fsp, cpx, chl
456B2	12KM456B2	massive flow basalt	435633.850	7115257.907	64.15771168	-130.3234911	2	phl, fsp, cpx, chl
457D	12KM457D	phenocrystic basalt	435579.219	7115381.945	64.15881428	-130.3246671	2	phl, fsp, cpx, cal
459C	12KM459C	massive amygdaloidal basalt	436180.846	7116803.556	64.17168008	-130.3129027	1	phl, fsp, cpx, cal, chl
468A	12KM468A	massive amygdaloidal basalt	440963.451	7115891.829	64.1643527	-130.2141839	1	phl, fsp, cpx, ol, chl, cal
468B	12KM468B	flow top breccia	440960.028	7115885.590	64.16429614	-130.2142518	4	cal, cpx, xen, chl
G-R4	CJA-83-26-R4	basalt flow						
G-137	BP0137	tuff						
G-19	CJA79-08-19	basalt flow						
G-51	CJA79-48-51	basalt flow						

Table 4.2 Sample identification, field names, locations, petrographic group, and phenocrysts and major alteration minerals present. Symbols: phl = phlogopite, fsp = feldspars, cpx = clinopyroxene, ol = olivine, cal = calcite, chl = chlorite, qtz = quartz, py = pyrite, xen = xenoliths (of wollastonite and alstonite).

5 ANALYTICAL RESULTS

5.1 PETROGRAPHIC OBSERVATIONS

All Marmot Formation Volcanic (MFV) rocks are variably altered, primarily by carbonate, ± quartz, chlorite, sericite, and serpentine, and in some cases all primary volcanic textures and mineralogy are overprinted (Appendix B). In most cases this alteration is too strong to petrographically classify these rocks on the basis of mineralogy; therefore, the following petrographic observations are primarily focused on samples with an identifiable primary mineralogy.

1) Coarse-grained mafic volcanic rocks typically contain euhedral clinopyroxene macrocrysts as well as clinopyroxene and minor olivine microphenocrysts set in a plagioclase, clinopyroxene, and glass bearing groundmass (Appendix B).

2) Other coarse grained samples contain glomeroporphyritic textures that comprise clinopyroxene phenocrysts set in a feldspar, clinopyroxene, and glass bearing groundmass.

3) Fine grained intergranular mafic volcanic rocks that make up a large portion of the MFV suite.

4) Volcaniclastic rocks which consist of lapilli sized juvenile clasts displaying the typical MFV mineral assemblage, with a carbonate and lithic clast dominated interclast matrix. Spinel, clinopyroxene and locally phlogopite comprise identifiable fresh mineral phases in these deposits.

It seems that these samples are directly crystalized from a liquid, and do not show cumulate textures. Clinopyroxene macrocrysts in the coarse-grained rocks of these samples, show concentric zoning, classic hour-glass zoning and simple core and rim zoning. Individual macrocrysts show subhedral cores with euhedral rims, that are variably resorbed and with sieve texture (Fig. 5.1.1). The question of whether these macrocrysts are phenocrysts or xenocrysts will be addressed in a later section.

Oxyhornblende occurs in a few samples, concentrated in ellipsoidal bodies, 0.5 - 2 mm in diameter, interpreted as ocelli. They contain varying amounts of dendritic and plumose texture hornblendes, with some psudomorphed by chlorite, and minor calcite (Fig. 5.1.2). The darker rims of the plumose structure are common among oxyhornblendes (Deer et al. 1997), identified as very fine grained crystals of ilmenite (Fig. 5.1.2 and Fig. 5.1.3). Small 0.25 - 0.5 mm pockets of Ba-rich feldspars are present within the ocelli cores (Fig. 5.1.3 and Fig. 5.1.4). Further discussion on the occurrence of hornblende and ocelli will be presented in a later section.

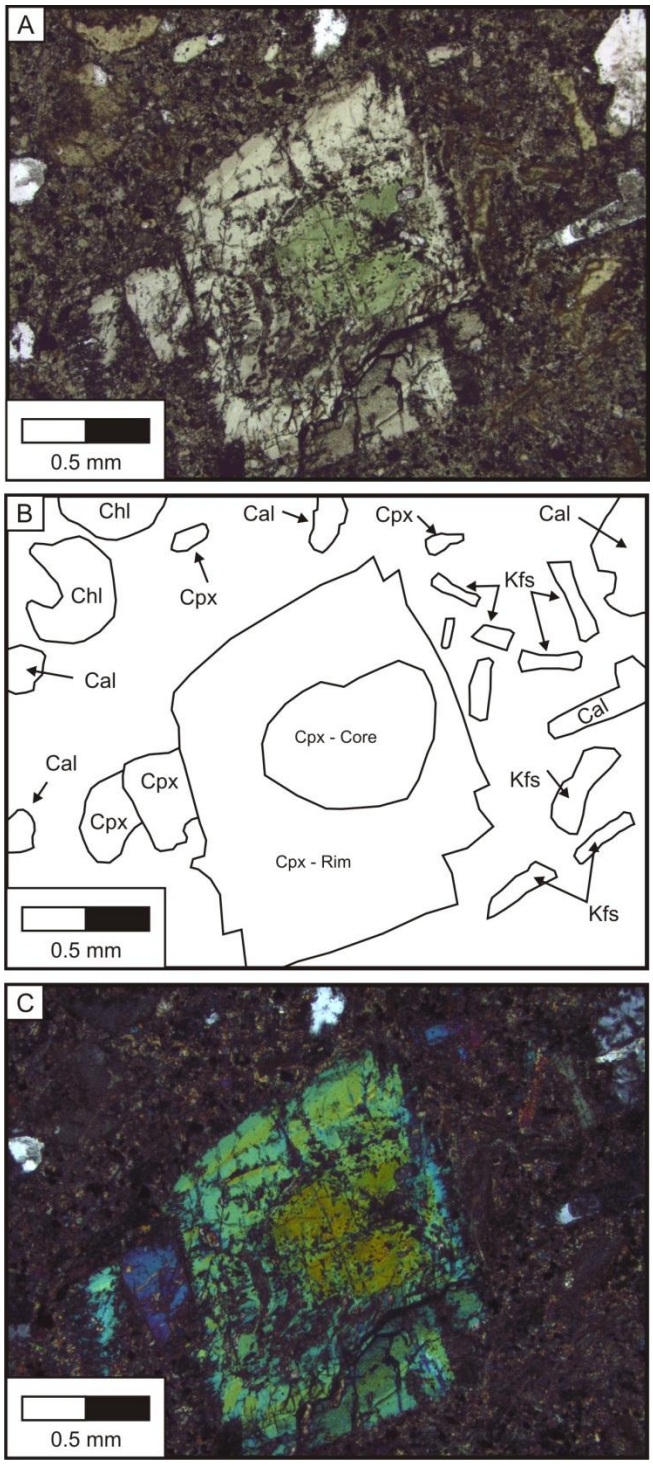

Figure 5.1.1 (A) Plain polarized light, (B) sketch with labeled minerals, (C) Crossed polarized light, of zoned clinopyroxene grains.

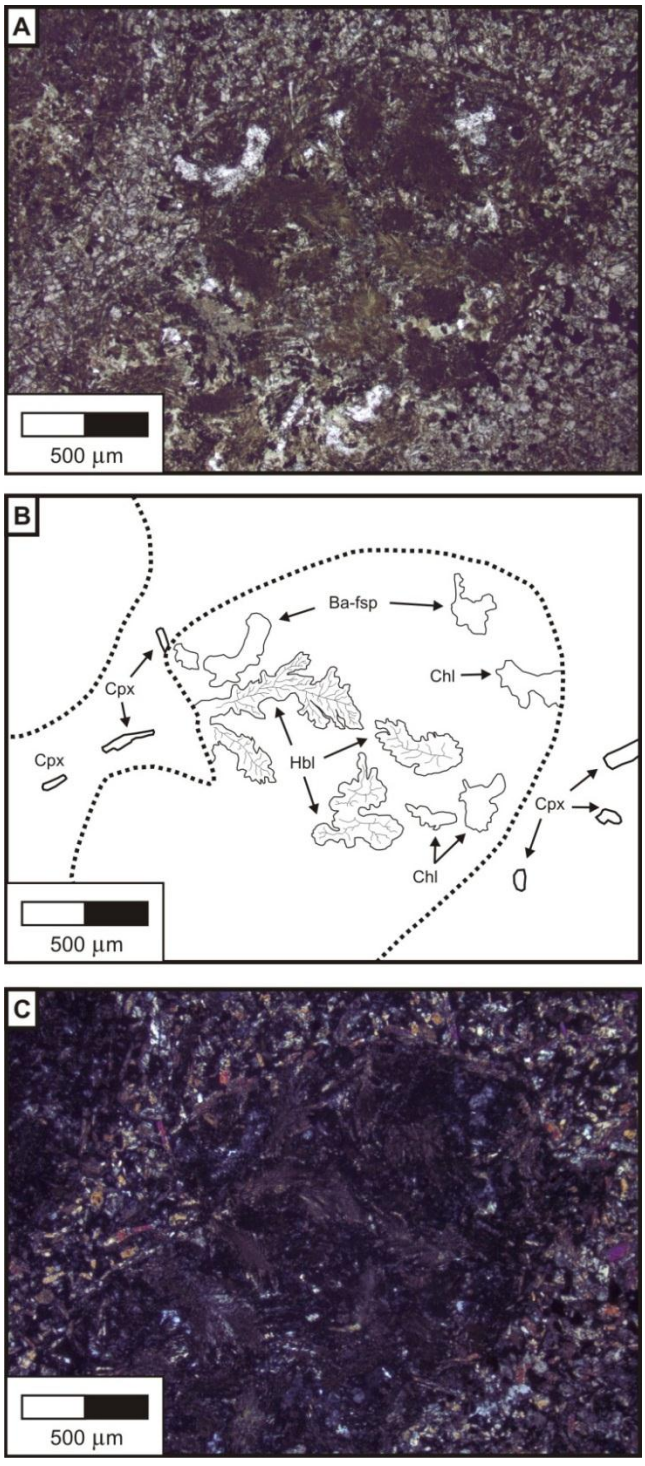

Figure 5.1.2 (A) Plain polarized Light, (B) sketch with labeled minerals, (C) crossed polarized light, showing ellipsoidal/spherical ocelli body (outline as dotted line in sketch), with dendritic and plumose hornblende. Ocelli occur in fine grained matrix of clinopyroxene, plagioclase, and assorted alteration minerals.

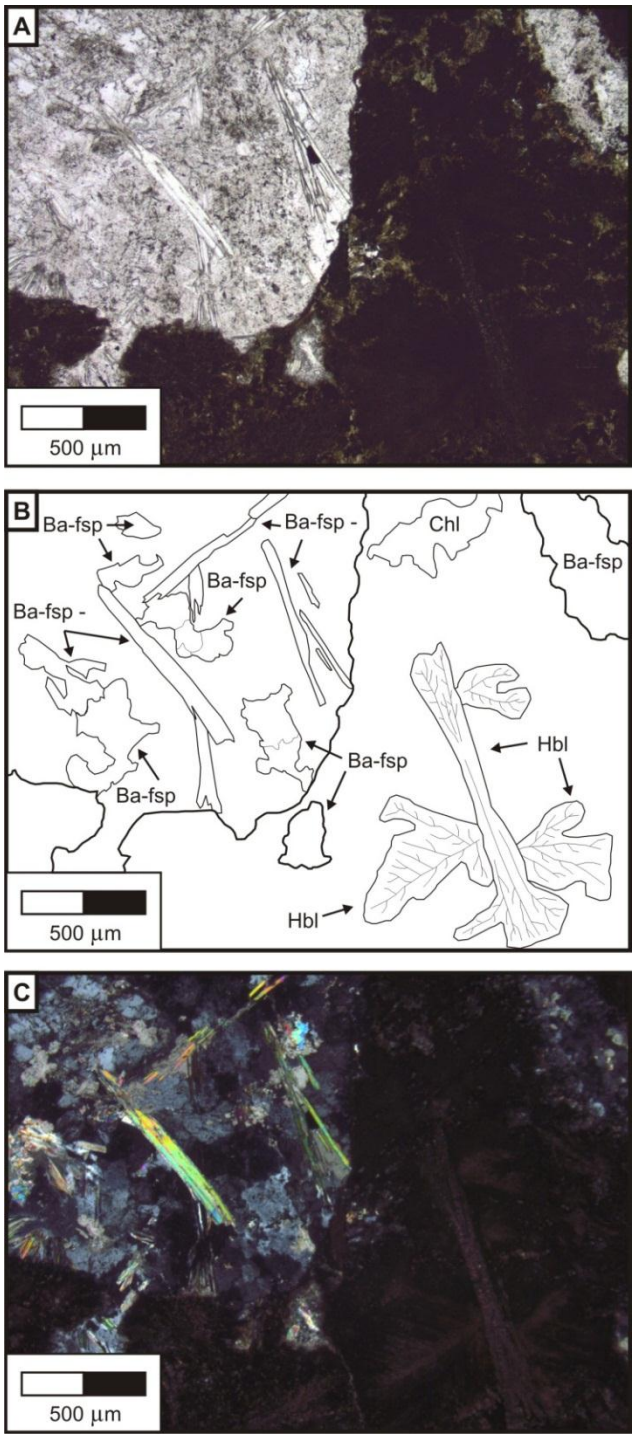

Figure 5.1.3 (A) Plain polarized light, (B) sketch with labeled minerals, (C) crossed polarized light. Showing ellipsoidal/spherical ocelli cores (top left of images) with two phase Ba-rich feldspars, and ocelli body (bottom right of images) with dendritic and plumose hornblende, and minor alteration minerals.

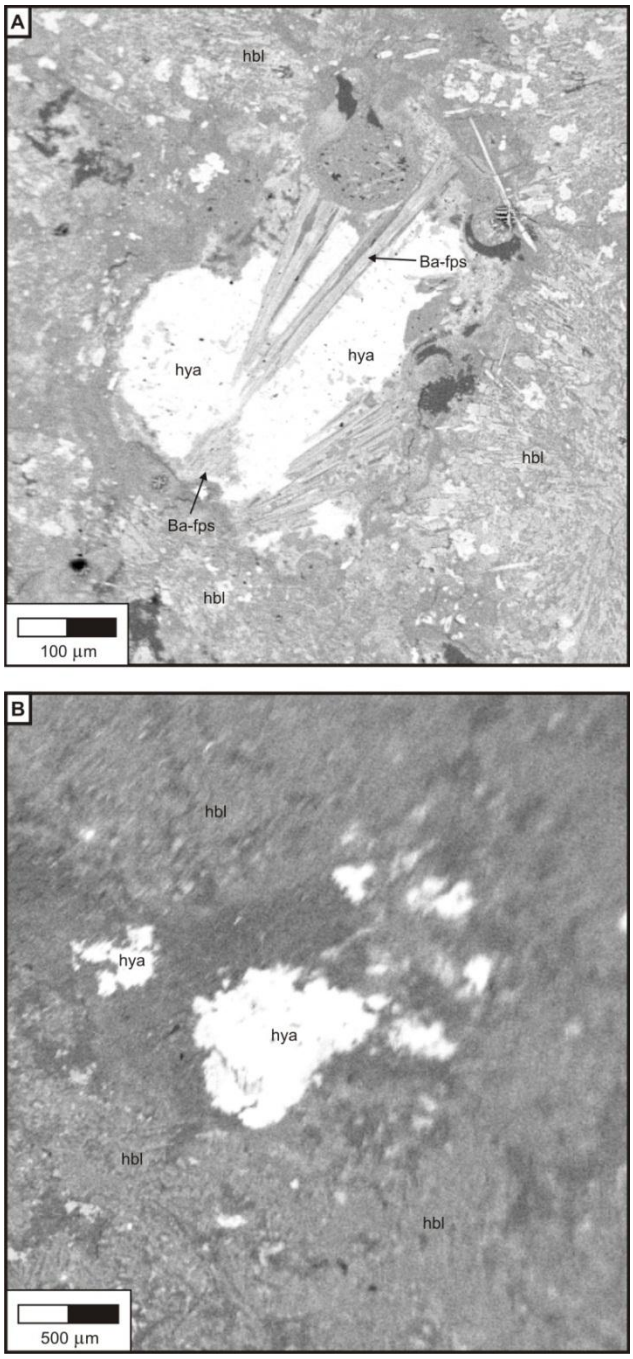

Figure 5.1.4 BSE images (A) from sample 456B2 site 1, and (B) from sample 456B1 site 4, showing re-absorbed textures. Symbols: hya: hayolphane, Ba-fsp = Ba-rich feldspars, hbl = hornblende (Oxyhornblende).

5.2 MINERAL CHEMISTRY

5.2.1 Clinopyroxene

Fresh, unaltered clinopyroxene is the typical mineral for MFV samples, especially for those comprising the massive clinopyroxene phyric mafic volcanic flows exposed near the center of the MCE (i.e. sample 456A). Mineral chemistry studies were conducted on clinopyroxene crystals from samples 46A, 456A, 456B1, and 456B2, as they offer distinct insight into two stages of clinopyroxene growth (cores and rims). In most MFV occurrences, clinopyroxene grains are typically the most abundant and freshest primary mineral preserved; therefore SEM/EDS analysis on these grains was used to offer constraints on magmatic evolution.

All clinopyroxene cores and rims analyzed from the massive mafic volcanic rocks (i.e. sample 456A) are classified as diopsides and augites (Fig. 5.2.1). Cores contain variable TiO_2 (0.83 – 1.1 wt. %) and Cr_2O_3 (0 – 0.58 wt. %), whereas the rims with TiO_2 (1.85 – 2.85 wt. %) and Cr_2O_3 (0-26 wt. %) are generally augite. Al_2O_3 contents in the cores are low (3.31 – 6.2 wt. %), whereas the rims yield contents higher Al_2O_3 (5.91 – 8.35 wt. %). Mg numbers (100 *Mg/ (Fe^{2+} + Mg)) for cores (79.9 – 86.8) are higher than Mg numbers for the rims (72.4 – 78.9).

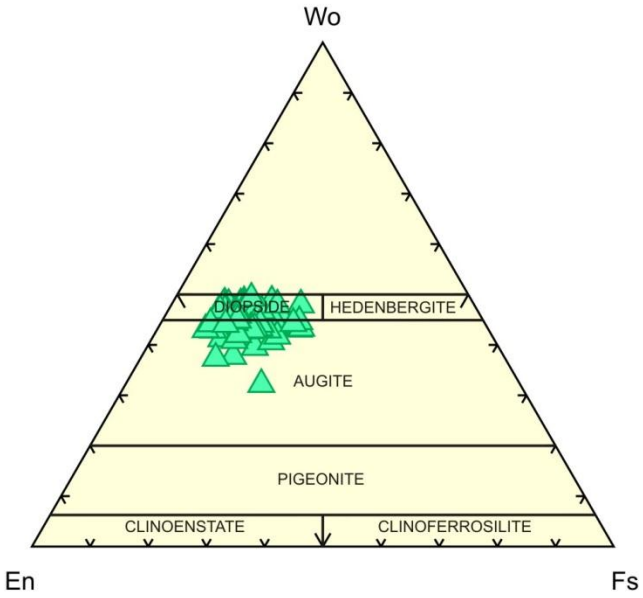

Figure 5.2.1 Ternary classification diagram of pyroxene from all samples

5.2.2 Phlogopite

Mica grains were analyzed in sample 46A, from large phlogopite macrocrysts (up to 0.5cm in width) and smaller grains also present in the groundmass assemblage. All larger macrocrysts are remarkably fresh, with no integral alteration or zoning; however, all grains are typically subhedral and show resorbed grain boundaries (Fig Appendix B, Sample 46A, Sites 3 and 4).

In conventional mica Mg-Al-Fe plot (Fig. 5.2.2), all macrocrysts grains are classified as phlogopites, and four analyses are classified as biotite, related to the finer grained groundmass grains. Macrocrysts are aluminous (7.12 – 8.04 wt. %) with high TiO_2 (16.61 – 17.46 wt. %), variable FeO_t (8.83 – 10.05 wt. %), with Mg numbers

ranging from 82.7 to 84.6 (refer to Appendix B for data). Most groundmass grains are geochemically similar to their macrocrystic counterparts.

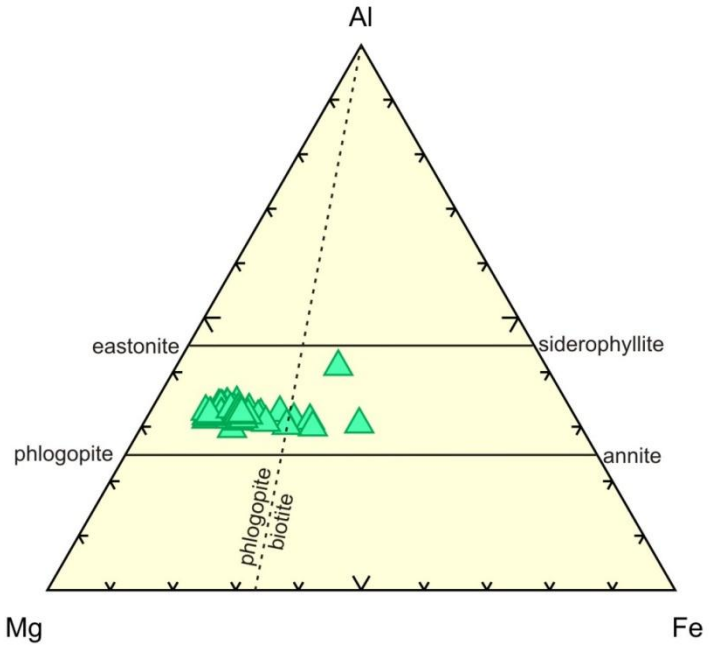

Figure 5.2.2 Ternary classification diagram of micas from all samples

5.2.3 Amphiboles

Analyses of amphiboles in MFV are hornblende, occurring in many samples (i.e. 46A, 456A, 456B1, and 456B2) concentrated in globular bodies interpreted as ocelli. Comparing their chemical composition with Deer et al. (1997), they appear to be oxyhornblende. These oxyhornblendes are aluminum rich (10.01 – 16.53 wt. % Al_2O_3), with MgO values from 10 to 15 wt. %, and FeO_t values ranging from 12.9 to 16.53 wt.

%. Likewise they have relatively high TiO_2 (1.75 – 3.52 wt. %) and moderate CaO values (10.12 - 16.59 wt. %) (Table 5.2.3).

Classification of these amphiboles (Table 5.2.3) was conducted using structural formula calculations and based on the classification scheme of Leake et al. (1997). We used 23 oxygens, with the Fe^{2+} / Fe^{3+} ratio estimated by assuming 13 cations. Further classification can be made on the following calcic amphibole (Ca_B >= 1.50) discrimination diagram (Figure 5.2.3). Two types for these amphiboles occur, based on whether $(Na+K)_A$ is less (Fig. 5.2.3A) or greater (Fig. 5.2.3B) than 0.5, classifying the amphiboles as (ferro-) tschermakite hornblende, and (ferro-) edenite.

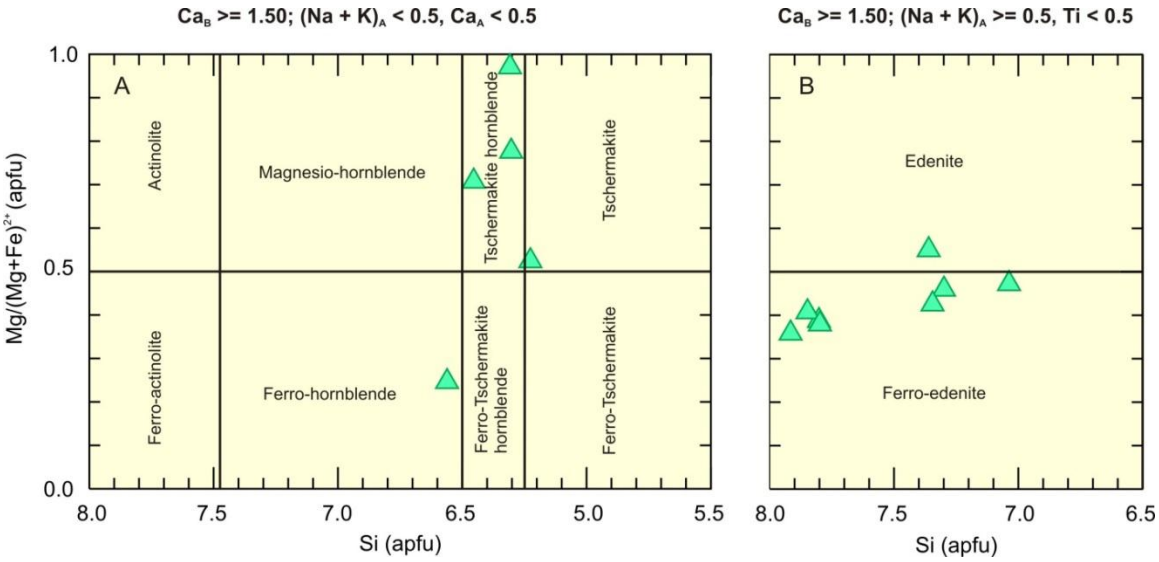

Figure 5.2.3 Amphibole classification diagram for selected oxyhornblende samples, based on 13 cations and on structural formulae criteria (modified from Leake et al. 1997).

Sample	46A	456A	456B1	456B1	456B1	456B1	456B1	456B1	456B1	456B1	456B1	456B1	456B1
SiO_2	42.96	37.61	46.33	45.12	45.59	45.93	45.42	48.24	46.01	41.97	45.91	45.46	44.99
TiO_2	3.52	2.32	2.14	2.29	2.44	1.75	3.40	2.75	2.75	2.69	2.30	2.35	3.65
Al_2O_3	13.23	15.32	13.40	11.00	13.00	14.06	11.47	13.49	12.26	12.17	13.72	12.70	10.56
FeO	14.95	16.53	9.83	10.45	11.12	10.27	8.86	8.67	10.65	12.59	10.46	10.77	12.49
MnO											0.40	0.30	
MgO	10.81	16.86	10.93	13.99	11.26	11.66	11.54	8.39	10.83	12.35	10.02	10.60	11.71
CaO	11.10	10.12	11.54	12.96	11.42	11.29	14.13	12.16	13.24	14.20	12.28	12.65	16.59
Na_2O	0.66			0.00	0.98	1.78							
K_2O	2.12	1.24	3.44	1.66	2.87	3.28	2.83	4.34	2.65	1.41	3.59	2.98	
Total	99.35	100.00	97.61	97.47	98.68	100.02	97.65	98.04	98.39	97.38	98.68	97.81	99.99
Structural formulae (on the basis of 13 cations)													
T-site													
Si	6.218	6.308	6.717	6.561	6.597	6.552	6.621	6.934	6.484	6.303	7.025	7.299	7.36
Al^{iv}	1.782	1.262	1.283	1.439	1.403	1.448	1.379	1.066	1.516	1.697	0.975	0.701	0.64
C-site													
Al^{vi}	0.475	0	1.007	0.446	0.815	0.916	0.591	1.219	0.52	0.457	1.499	1.703	1.396
Ti	0.383	0.044	0.233	0.25	0.266	0.188	0.373	0.297	0.292	0.304	0.265	0.284	0.449
Fe^{3+}	0.522	2.02	0	0.146	0	0	0	0	1.255	1.581	1.339	1.446	1.709
Fe^{2+}	1.288	0	1.192	1.125	1.346	1.225	1.08	1.042	0	0	0	0	0
Mn	0	0	0	0	0	0	0	0	0	0	0.052	0.041	0
Mg	2.332	3.673	2.362	3.033	2.429	2.48	2.508	1.798	2.275	2.765	2.286	2.537	2.856
B-site													
Ca + Na	1.721	1.584	1.793	2.019	1.771	1.726	2.207	1.873	1.999	2.285	2.013	2.176	2.908
A-Site													
Na	0.185	0	0	0	0.275	0.492	0	0	0	0	0	0	0
K	0.391	0.231	0.636	0.308	0.53	0.597	0.526	0.796	0.476	0.27	0.701	0.61	0
Total	17.3	17.12	17.22	17.33	17.43	17.62	17.29	17.02	16.82	17.66	18.15	18.8	19.32
Amphibole classification (Leake et al., 1997)													
	Ca	Ca	Ca	Ca	Ca	Ca	Ca	Ca	Ca	Ca	Ca	Ca	Ca
(Ca+Na) (B-site)	1.907	1.584	1.793	2.019	2.000	2.000	2.207	1.873	1.999	2.285	2.013	2.176	2.908
Na (B-site)	0.185	0.000	0.000	0.000	0.229	0.274	0.000	0.000	0.000	0.000	0.000	0.000	0.000
(Na+K) (A-site)	0.391	0.231	0.636	0.308	0.575	0.815	0.526	0.796	0.476	0.270	0.701	0.610	0.000
$Mg/(Mg+Fe^{2+})$	0.644	1.000	0.665	0.729	0.643	0.669	0.699	0.633	1.000	1.000	1.000	1.000	1.000
$Fe^{3+}/(Fe^{3+}+Al^{vi})$	0.524	1.000	0.000	0.246	0.000	0.000	0.000	0.000	0.707	0.776	0.472	0.459	0.550

Table 5.2.3 Sample amphibole compositions (wt. %), and structural formulae (after Leake et al., 1997)

5.2.4 Ba-Feldspars

Pockets of Ba-rich feldspars are found within the cores of ocelli (Fig. 5.1.2 and 5.1.3). SiO_2 values range 45.09 - 54.34 wt. %, Al_2O_3 range 20.05 – 38.17 wt. %, and K_2O ranges from 4.36 – 9.9 wt. %. Two types of Ba-feldspar are present. Lath-like radial Ba-feldspars (Fig. 5.1.4A) have lower BaO values (2.24 - 7.77 wt. %), and are interpreted as Ba-feldspar. The more massive, intergrown Ba-feldspars (Fig. 5.1.4A, B) have higher BaO values (13.46 – 28.37 wt. %), appear to be re-absorbed, are interpreted as hyalophane (13.46-24.60 wt. % BaO) and celsian (25.40-28.37 wt. %. BaO) (Melluso et al. 2011). See Table 5.2.4 for sample analysis (derived from Appendix B) of Ba-feldspars. Further discussion on the occurrence of Ba-feldspars will be addressed in a later section.

Sample (*)	Site	Pos.	Mineral (**)	SiO_2	Al_2O_3	FeO	MgO	CaO	Na_2O	K_2O	ZnO	BaO	Total
46A (1)	2	11	hya (oo)	50.57	20.09	1.48	1.23	2.17		6.42	1.15	16.87	99.98
46A (1)	4	37	hya (oo)	49.48	23.11	5.11	3.35			5.50		13.44	99.99
46A (1)	7	3	cln (oo)	42.31	23.05	1.03	0.86			4.36		28.37	99.98
46A (1)	7	9	hya (oo)	51.21	20.43	0.75	0.65	0.62	1.11	7.24		18.00	100.01
46A (1)	7	11	hya (oo)	46.74	20.44	2.01	2.22		0.49	6.53		21.57	100.00
456B1 (3)	3	5	hya (io)	47.49	23.37				0.85	5.97		22.32	100.00
456B1 (3)	4	1	hya (io)	47.06	24.17					6.40	0.46	21.92	100.01
456B2 (2)	1	1	hya (io)	53.05	22.16					8.44		16.36	100.01
456B2 (2)	1	3	Ba-fsp (io)	45.48	38.89					8.17		7.48	100.02
456B2 (2)	1	4	Ba-fsp (io)	51.73	31.78					9.90		6.58	99.99
456B2 (2)	1	2	Ba-fsp (io)	45.54	38.17					8.52		7.77	100.00
456B2 (2)	1	5	hya (io)	53.09	22.92					8.59		15.41	100.01
456B2 (2)	1	9	hya (io)	45.61	24.81					4.99		24.60	100.01
456B2 (2)	2	5	Ba-fsp (io)	51.92	21.26	7.17	6.53	3.65		7.22		2.24	99.99
456B2 (2)	2	6	hya (io)	53.82	22.18					8.72		15.26	99.98
456B2 (2)	2	7	hya (io)	54.34	21.33					9.48		14.86	100.01
456B2 (2)	4	4	cln (oo)	45.42	24.38					4.71		25.50	100.01
456B2 (2)	4	5	hya (oo)	51.79	22.84					7.08		18.28	99.99
456B2 (2)	4	9	cln (oo)	45.37	24.81					4.42		25.40	100.00

Table 5.2.4 Chemical analyses of representative Ba-feldspars. (*) represents lithology, see Table 4.2 and section 5.1. (**) represents occurrence: io = occurring in ocelli, oo = outside of ocelli. Mineral symbols: hya: hayolphane, cln: celsian, Ba-fsp: Ba-feldspars.

5.3 GEOCHEMISTRY

5.3.1 Whole Rock Geochemistry

Whole rock geochemical analyses were determined for a representative suite of samples of the Marmot Formation. Lithogeochemical data are presented in Table 5.3.1 (this study) and Table 5.3.2 (from Goodfellow et al. 1995).

An attempt was made to select the least altered samples for analyses based on field and petrographic observations; however, it is inferred that low-grade seawater and carbonate alteration has affected the majority of these samples to some extent. Petrographic studies indicate that typical alteration minerals apparent in most MFV samples are clay minerals, carbonate, chlorite, serpentine, and minor quartz. Also, due to

the fact that volcanic occurrences are hosted within regional carbonate strata, carbonate derived fluids are secondary volatiles that were fundamental in these alteration processes. Therefore, major elements (i.e. SiO_2, Na_2O, K_2O, and CaO) and LILE (i.e. Cs, Rb, Ba, Sr, etc.) concentrations in these samples are suspect, owing to the mobility of these elements during low grade alteration (Piercey et al. 2002). In addition, the high LOI (loss on ignition) values from these rocks, ranging up to 19 wt. %, support the likelihood of elemental mobility.

However, major elements such as Al_2O_3, TiO_2, and P_2O_5 and HFSE and REE were likely relatively immobile during low grade alteration process (Piercey et al. 2002). To test that these elements remained immobile, we plotted key compatible elements and incompatible element ratios in this chapter against the Al_2O_3/Na_2O alteration index (Fig. 5.3.1B) of Spitz and Darling (1987). It is clear that for the most part there is little to no correlation between Ti, other HFSE and REE and the alteration index, indicating that these elements were likely immobile during the aforementioned conditions. The lack of correlation within the MFV suite permits us to use only these elements for discussion. We base our interpretations of primary igneous geochemistry of the sample suite primarily on immobile elements to avoid element mobility and erroneous interpretations.

We use Zr as our fractionation monitor for volcanic evolution, because Zr is usually relatively immobile during alteration and its concentration will likely reflect primary volcanic fractionation trends (Piercey et al. 2002) (Figure 5.3.1A). Elements that do not define a linear trend with Zr are interpreted to have been mobile and to reflect non-volcanic processes. Further discussion on the effects of alteration will be addressed in a later section.

Sample	46A	47B	49B	149C1	149C2	456A	456B1	456B2	457D	468A	468B
SiO2	35.20	35.70	30.80	30.50	29.40	42.50	39.50	40.00	40.40	26.50	45.60
Al_2O_3	11.14	11.62	9.72	13.89	13.25	11.32	11.34	11.49	10.19	10.27	16.15
Fe_2O_{3t}	14.65	10.40	9.04	20.66	20.00	10.19	12.25	12.23	9.30	11.15	11.29
CaO	11.36	13.04	20.05	6.72	8.49	11.09	14.18	14.04	14.98	18.62	2.71
MgO	10.15	7.76	1.18	10.71	10.20	13.46	12.02	11.75	11.00	11.13	9.68
Na_2O	0.13	1.44	4.34	0.39	0.38	1.71	0.76	0.76	2.29	0.18	1.68
K_2O	1.47	2.45	0.86	1.47	1.34	1.09	1.50	1.73	0.44	0.34	4.75
MnO	0.19	0.13	0.09	0.06	0.06	0.17	0.24	0.25	0.19	0.14	0.10
TiO_2	4.82	4.00	2.99	2.87	2.69	2.36	2.52	2.50	1.96	2.01	2.15
P_2O_5	0.56	0.42	0.55	0.57	0.53	1.01	1.09	1.10	0.71	0.73	0.59
LOI	9.08	9.86	10.14	10.22	9.83	4.40	3.96	4.30	8.03	19.03	5.55
SUM	99.26	97.81	89.81	98.13	96.23	99.60	99.78	100.60	99.60	100.10	100.60
TOT/C	1.36	2.21	4.49	1.33	1.79		0.15	0.15	1.05	4.07	0.03
TOT/S	0.19	0.25	4.68			0.05			0.34	0.14	
Ba	4169.00	8319.00	342.00	455.00	362.00	2448.00	3400.00	3564.00	1312.00	224.00	2909.00
Be			2.00		1.00	2.00		3.00	3.00	7.00	
Co	40.10	42.80	32.00	87.00	81.30	53.60	46.00	45.80	42.40	74.50	39.50
Cs	5.80	1.20		2.80	2.60	3.50	1.40	1.50	0.80	1.40	1.00
Ga	19.60	15.90	13.50	15.70	15.20	11.30	12.40	11.40	11.40	12.90	16.70
Hf	7.40	5.80	6.10	4.30	4.80	4.30	3.60	3.50	4.40	4.00	3.30
Nb	86.70	56.30	78.70	67.70	37.80	160.80	148.10	141.90	97.40	80.30	75.60
Rb	43.90	41.70	9.90	36.60	34.80	64.00	37.10	43.30	15.90	9.60	68.60
Sn	2.00	1.00	1.00	1.00			1.00	1.00	2.00	1.00	
Sr	659.60	170.70	269.80	217.30	233.10	540.60	726.30	750.10	532.40	508.00	326.30
Ta	5.00	3.60	4.20	3.90	4.00	8.20	6.90	7.50	4.40	5.00	3.70
Th	7.30	4.70	6.70	5.70	5.30	17.30	15.50	16.00	9.90	5.90	5.20
U	1.60	1.10	1.40	1.40	1.40	3.80	3.50	3.30	2.40	1.50	1.20
V	439.00	381.00	311.00	302.00	289.00	224.00	248.00	256.00	216.00	218.00	118.00
W	0.50	0.90	1.20			0.60		1.20	3.70	4.00	1.60
Zr	269.20	200.60	253.60	188.80	178.80	196.10	190.40	184.50	179.70	159.50	144.50
Y	23.10	18.30	21.30	12.80	11.70	27.10	27.90	28.20	20.60	17.50	18.10
La	59.10	38.90	48.20	41.70	43.30	127.00	126.00	127.60	73.80	40.20	56.90
Ce	113.70	77.70	95.70	76.60	79.10	229.20	227.70	225.20	138.80	72.10	104.80
Pr	12.81	9.20	10.89	8.05	8.23	23.04	23.18	22.70	15.60	8.46	11.32
Nd	50.30	39.10	43.20	32.40	30.70	82.90	81.30	76.10	56.20	33.60	43.00
Sm	9.32	7.28	7.71	5.24	5.18	12.34	12.01	12.13	8.58	6.45	7.06
Eu	2.42	1.89	2.29	4.11	1.69	3.51	3.65	3.52	2.25	1.81	1.95
Gd	8.15	6.19	6.82	4.31	4.16	9.55	9.41	9.34	7.06	5.49	5.58
Tb	1.04	0.80	0.92	0.60	0.58	1.14	1.22	1.15	0.89	0.78	0.74
Dy	5.03	4.11	4.79	2.96	3.11	5.79	6.26	5.59	4.47	3.89	3.49
Ho	0.89	0.68	0.82	0.49	0.50	0.98	0.97	0.97	0.80	0.71	0.71
Er	2.27	1.76	2.05	1.25	1.30	2.41	2.61	2.67	2.05	1.71	1.69
Tm	0.28	0.22	0.30	0.18	0.17	0.32	0.33	0.33	0.27	0.22	0.21
Yb	1.68	1.27	1.81	1.14	1.08	2.18	2.09	1.93	1.96	1.36	1.39
Lu	0.20	0.16	0.24	0.13	0.11	0.27	0.26	0.27	0.25	0.19	0.22
Mo	1.10	1.10	0.60	0.60	0.60	0.40	0.30	0.20	1.30	0.30	
Cu	88.00	98.10	34.80	1.20	2.10	194.50	74.00	80.80	61.10	55.40	2.00
Pb	3.40	0.80	9.30	0.60	1.00	4.50	9.10	7.30	4.55	4.90	1.90
Zn	86.00	63.00	23.00	77.00	78.00	75.00	72.00	70.00	60.00	54.00	70.00
Ag			0.10			0.10					
Ni	107.50	169.90	94.70	373.90	349.80	229.00	179.40	180.90	200.80	275.50	118.30
Cr	177.89	437.89	608.94	622.62	567.89	526.83	431.05	396.84	465.26	540.52	355.78
As			3.80					0.60	1.10	1.90	
Au	3.20	1.40	3.50	1.00		1.90	2.00	2.50			
Cd									0.10		
Sb			0.50								
Hg			0.04							0.01	
Tl						0.20					

Table 5.3.1 Major (in wt. %) and Trace Elements (in ppm) of Rocks Analyzed in this study.

Sample	G-R4	G-137	G-19	G-51
LOI	10.09	6.21	9.43	16.05
SiO_2	37.80	51.37	39.00	37.60
Al_2O_3	14.00	16.99	11.40	12.70
Fe_2O_{3t}	13.81	9.33	9.45	10.67
CaO	9.40	3.06	11.80	6.35
MgO	5.10	7.24	13.70	8.60
Na_2O	1.10	4.64	1.00	0.25
K2O	3.29	1.92	0.95	3.03
MnO	0.18	0.06	0.20	0.10
TiO_2	4.90	2.86	2.31	4.15
P_2O_5	1.45	0.57	0.98	0.44
SUM	101.12	104.25	100.22	99.94
Ba	3770.00	1000.00	2608.00	4478.00
Co	16.00	14.00	56.00	48.00
Nb	130.00	151.00	78.00	86.00
Rb	40.00	21.00	26.00	63.00
Sr	1900.00	186.00	274.00	551.00
U	4.10	3.20	0.40	0.60
V	300.00	246.00	400.00	336.00
Zr	580.00	455.00	241.00	234.00
Y	45.00	23.00	27.00	21.00
La		116.00		
Ce		236.00	214.00	131.00
Yb			0.90	
Mo	8.00	4.00	5.00	5.00
Cu	12.00	18.00	123.00	87.00
Pb	12.00	5.00	5.00	5.00
Zn	151.00	62.00	107.00	107.00
Ag	0.10	0.10	0.50	0.50
Ni	7.00	8.00	122.00	72.00
As	0.80	2.00	0.20	0.50
Cd	0.20	0.20	1.00	1.00
Sb	0.20	17.00	0.20	0.20
Hg	37.00	35.00	25.00	25.00
Se	0.20	1.00	0.20	0.20

Table 5.3.2 Major (in wt. %) and Trace Elements (in ppm) of selected samples from Goodfellow et al. (1995).

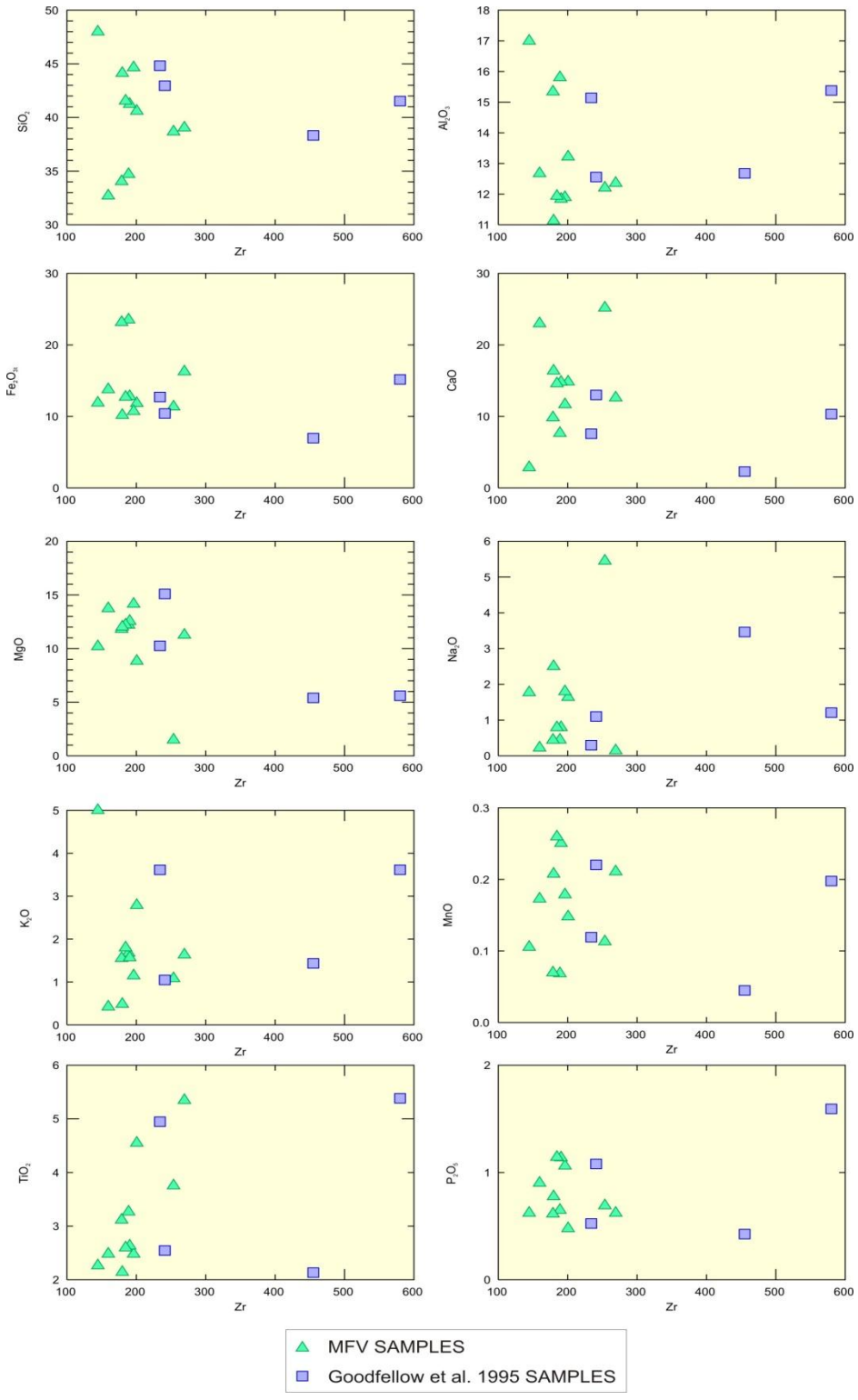

Figure 5.3.1A Plots of major elements vs. Zr, illustrating mobility/immobility. Major elements are recalculated on a volatile free basis.

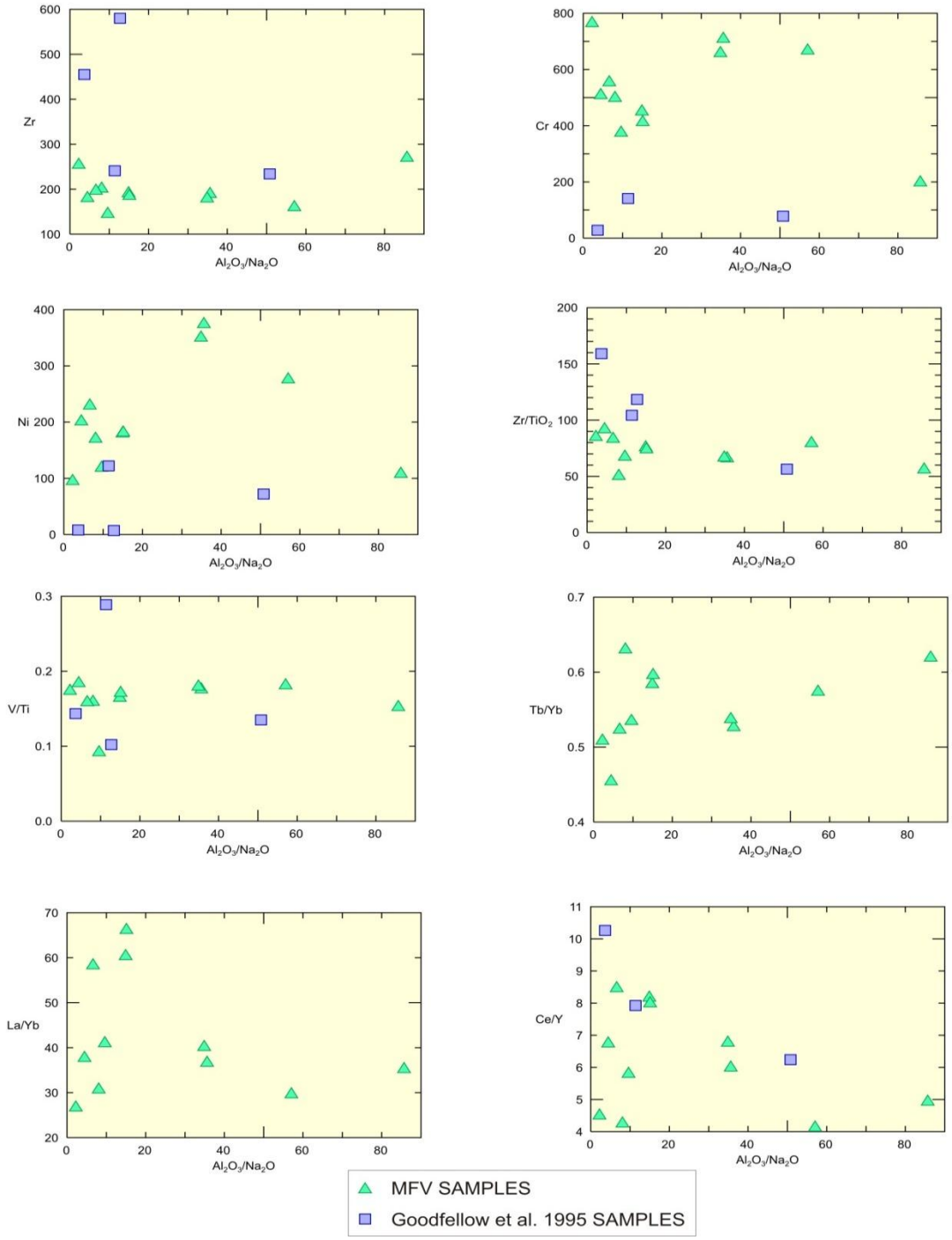

Figure 5.3.1B Plots of key compatible elements, compatible element ratios, and incompatible element ratios versus Al_2O_3/Na_2O alteration index of Spitz and Darling (1978).

5.3.2 Major Elements

Confirming field observations, LOI values are high for the MFV samples (ranging from 3.96 - 19.03 wt. %) (Table 5.3.1). There is a limited range in some major elements contents within the MFV suite (Al_2O_3 9.72 – 16.15 wt. %; TiO_2 1.96 – 4.82 wt. %), suggesting less mobility of these elements. Some major elements on the other hand show substantial compositional ranges (MgO 1.71 – 12.01 wt. %; CaO 2.71 – 20.05 wt. %), which likely reflects element mobility and alteration processes. In addition, some carbonate may derive from the underlying carbonate platform, as evidenced by the presence of wollastonite and alstonite xenoliths (Table 1, appendices A, B). Owing to the high LOI values, and Al_2O_3/Na_2O ratios > 25 (see Piercey et al. 2004) we do not utilize major elements (Figure 5.3.1A) for characterizing the MFV petrogenesis, with further discussion on the effects of alteration will be addressed in a later section.

Furthermore, there is a wide range in compositions in total alkalis vs. silica (TAS) diagram (Fig. 5.3.2A). On the basis of petrography we can preclude using this diagram and use the major elements, in favor of immobile element diagrams (Fig. 5.3.2B) for lithological classification of the MFV suite. Normative mineralogy is not reported here, due to the nature of major elements during alteration. However, we suggest that the Zr/TiO_2 remains relatively immobile during alteration, as evidence by its consistent grouping (Fig. 5.3.1B).

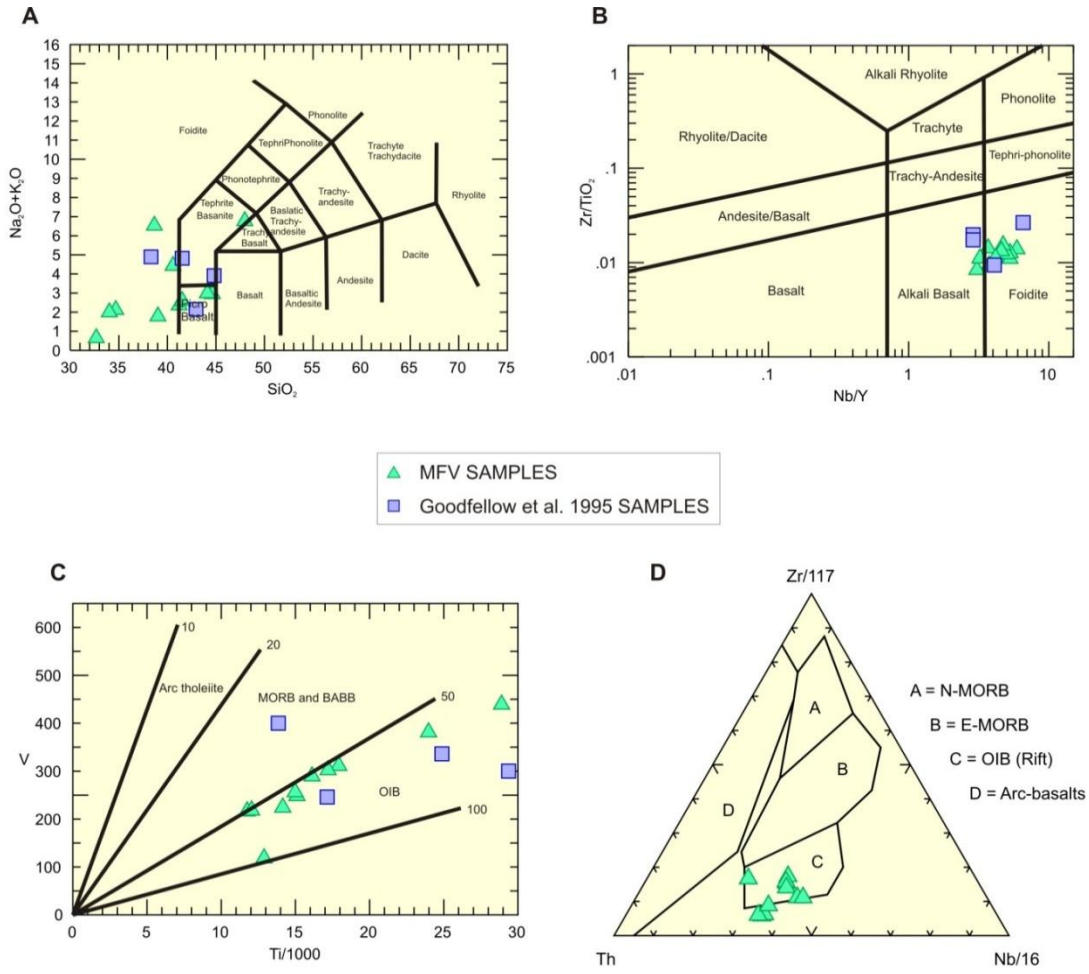

Figure 5.3.2 (A) Total alkalis vs. silica (TAS) diagram for volcanic rocks, after Le Bas et al. (1986), Elements are recalculated on a volatile free basis. (B) Zr/TiO2 vs. Nb/Y diagram (Pearce 1996). (C) V vs. Ti discrimination diagram of Shervais (1982). (D) Th-Zr-Nb tectonic discrimination diagram of Wood (1980)

5.3.3 Trace Elements

Trace element composition is important in the MFV because of the apparent mobility of many major elements (Fig. 5.3.1A). In the Zr/TiO_2 vs. Nb/Y classification of Pearce (1996) (Fig. 5.3.2B), MFV rocks are characterized by basaltic affinity (Zr/TiO_2 =

50-208) and are moderate to extremely alkalic (Nb/Y = 2.5 – 7.4). They can therefore be geochemically classified as alkali basalts to foidites (Fig 5.3.2B). This generally confirms the interpretation from the TAS diagram where most of the samples plotted as basalt or foidite.

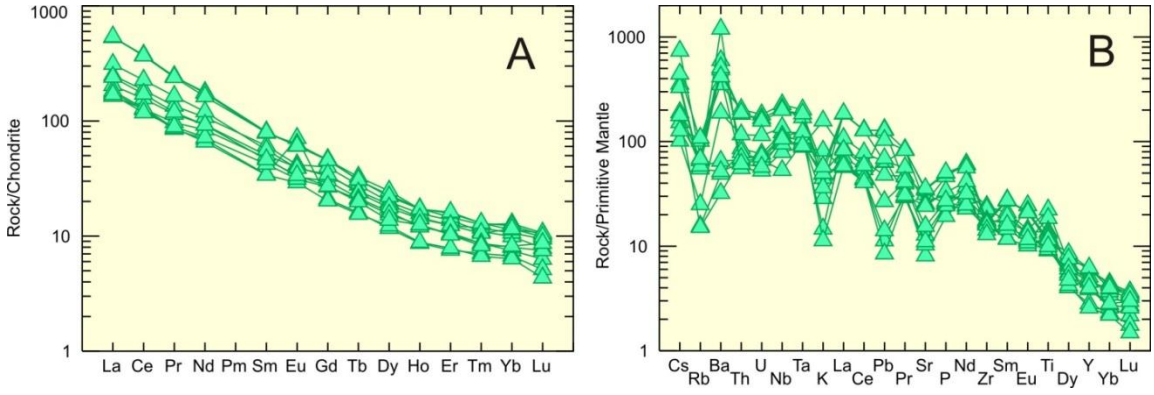

Figure 5.3.3 (A) Chondrite normalized rare earth element plot. (B) Primitive mantle normalized incompatible element plot. Chondrite and primitive mantle values from Sun and McDonough (1989).

Chondrite normalized rare earth elements (REE) patterns (Fig. 5.3.3A) for all MFV samples are quite similar, with moderate enrichment in light REE (LREE), and less enrichment in the heavy REE (HREE). Primitive mantle normalized patterns (Fig. 5.3.3B) again are quite similar, with the exception of some LILE (e.g. Rb, Ba, K, Pb) showing negative anomalies. Plots of Cs vs. select LILE elements (Fig. 5.3.4), showing that the mobility/immobility of these elements (e.g. Rb, Ba, K, etc.), which has been suggested to be controlled by K-feldspar fractional crystallization (Gast, 1968; Icenhower and London, 1996). Possible mobility of these elements may also be partly derived from volatile-influence in a wide range of geological environments (Greenough and Fryer

2008). However, due to the mobility in LILE implied by Fig. 5.3.3B, we can negate the use of LILE to infer primary geochemistry.

The Th-Zr-Nb plot (Fig 5.3.2D) of Wood (1980) indicates that all samples are characteristic of an OIB source. All samples fall within or near the OIB array on a V-Ti plot (Fig 5.3.2C) of Shervais (1982) with the exception of one sample, owing to the low TiO_2 content.

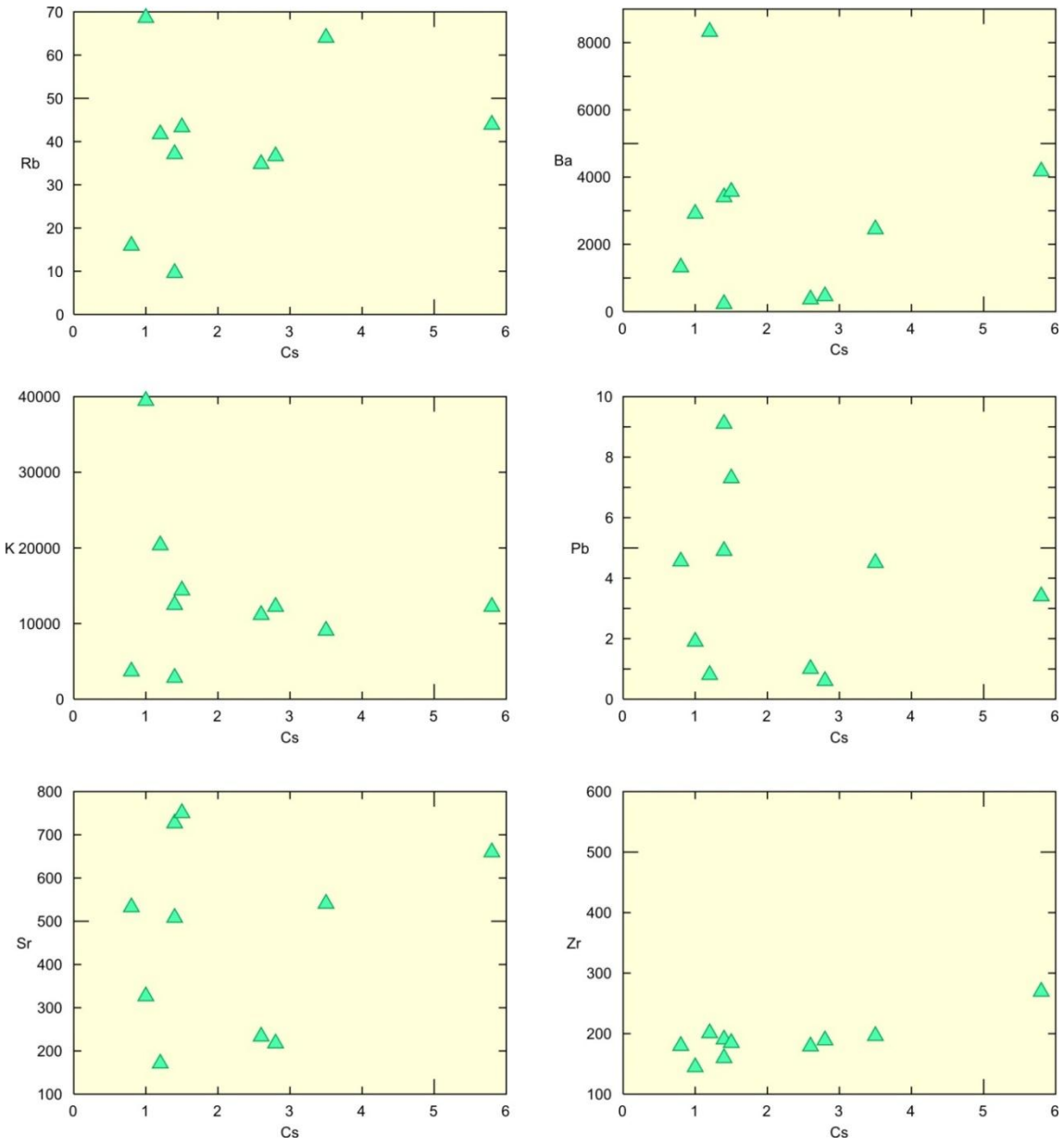

Figure 5.3.4 Plots of select trace elements vs. Cs, showing possible mobility or influence of partitioning coefficients. Ba, K, and Zr show slight linear trends (with the exception of one sample).

6 DISCUSSION

6.1 INTERPRETATION OF MINERAL DATA

6.1.1 Clinopyroxene

Clinopyroxene in mafic igneous rocks has been shown by previous authors to provide geochemical clues into the mantle source and magmatic evolution of basalts (Nisbet and Pearce 1977; Bindi et al. 1999, Dobosi et al. 1991). This is in part due to wide range of chemical substitutions into the crystal structure of clinopyroxene and its overall resilience to late stage alteration. The observation of zoning in clinopyroxene grains (Fig. 5.1.1) from massive mafic volcanic rocks of MFV represents typical clinopyroxene fractionation, with higher contents of Mg, Si, and Cr in the core, but lesser contents of Fe, Ti, and Al than in the rims.

Petrographic observations show that this transition from core to rim is sharp (Fig. 5.1.1), possibly suggesting there was a rapid change in pressure and temperature conditions during magmatic evolution. Furthermore, Cr has a higher clinopyroxene/melt distribution coefficient (Dobosi et al. 1991) and will therefore be enriched in clinopyroxene during early stages of crystallization (i.e. cores) at higher pressures. Additionally, Ti accommodation in clinopyroxene is favored at lower pressure and temperature conditions; thus Ti contents should be higher in the rims of crystals (Dobosi et al. 1991). Many grains display slightly resorbed cores surrounded by euhedral rims (Fig. 5.1.1).

The resorbed nature of these cores may be a result of unstable conditions related to changing pressure and temperature. This scenario was also suggested for clinopyroxene grains with similar textures from alkali basalts in work by Dobosi et al. (1991). A simple clinopyroxene crystallization evolution is inferred for the massive mafic volcanic rocks based on the linearity and continuity in the data on variation diagrams (Fig. 6.1 A, B). Any deviation from this trend would record different crystallizing magma conditions, with clustering of data suggesting two stages of crystallization at unique pressure and temperature conditions from the same evolving alkaline to peralkaline magma (Fig 6.1A).

In a plot of Al_2O_3 vs. SiO_2 (Fig. 6.1A) used to constrain crystallizing magma alkalinity, cores are characterized by chemical compositions reflecting alkaline crystallization conditions (high SiO_2, low Al_2O_3), whereas rims reflect peralkaline crystallization conditions (Nisbet and Pearce, 1977), with low SiO_2 and high Al_2O_3 (Fig. 6.1A).

Based on consistency of mineral chemistry from sample 456A, as well as euhedral habits of rims and significant lack of other phenocrystic phases within these samples, we interpret that the host basalt to reflect magma from which clinopyroxene crystallized, and that none of the clinopyroxene grains are xenocrystic in origin.

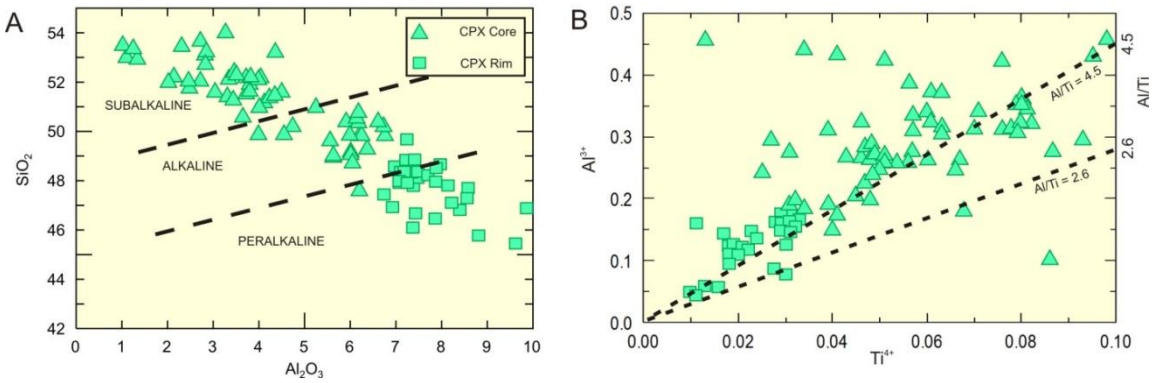

Figure 6.1 Plots of clinopyroxene chemistry from sample 456A. (A) SiO_2 vs. Al_2O_3 with alkalinity fields from Nisbet and Pearce (1977). (B) Al^{3+} vs. Ti^{4+} showing Al/Ti ratios, the 2.6 line denotes a pressure of crystallization corresponding to ~30 kbars (Lloyd 1981).

A plot of Al^{3+} vs. Ti^{4+} (Fig 6.1B) has been used to constrain depths of clinopyroxene crystallization (Lloyd 1981 and Lloyd et al. 1985). This is based on experimental work (Edgar et al. 1976) in which these authors grew synthetic clinopyroxene crystals (+/- olivine, phlogopite, and minor illite) at different temperatures and pressures from an ultra-potassic starting material. The synthetic clinopyroxene that crystallized during experiments by Edgar et al. (1976) are similar to clinopyroxene grains from the MFV (i.e. Ca/(Ca+Mg) > 0.5, and low TiO_2 contents ranging from 0.75 – 3.07 wt. %), similar to our cores. These authors suggested that Al/Ti ratio from clinopyroxene of 2.6 marks a pressure of crystallization at around 30 kbars and temperatures around 1250 °C, and that there is a positive correlation between Al/Ti ratio and the pressure and temperature conditions during crystallization (Edgar et al. 1976). Our results from MFV (sample 456A) yield higher average Al/Ti ratios of approximately 4.5. The higher Al/Ti ratios reflect a higher pressure than 30 kbar during crystallization of the cores then that of the rims, and thus suggest a deep source of crystallization.

6.1.2 Phlogopite

As noted by Arai (1984), aluminum contents of phlogopite from ultrapotassic rocks are controlled fundamentally by the equilibrium pressure and as such might be used as a geobarometer. The average Al_2O_3 contents of groundmass phlogopites from sample 46A is 16.87 wt. %, which is similar to the Al_2O_3 contents from the macrocrystic phlogopite samples (17.23 wt. %), suggesting that groundmass phlogopite was in pressure equilibrium with these macrocrysts. The rounding of grain boundaries in the ground mass phlogopites may represent a late stage chemical phenomenon in the highly volatile melt in which they were transported to the surface. Closer inspection of these grain boundaries in BSE images (APPENDIX B, Sample 46A, Site 3and 4), shows that for the most part, rounding appears to be chemically destructive (i.e. erosion of grain edges giving the grain margins a jagged and irregular appearance). There may also be an earlier phase of mechanical rounding as evidenced by some grains.

6.1.3 Amphibole

Samples examined in this study contain ocelli, which are interpreted as potassium-rich, and of oxyhornblende composition (Table 6.1.3). Examining the modal mineralogy observed in ocelli throughout samples 46A, 456A, 456B1, and 456B2, an approximate (average) composition for ocelli was determined to be: 80% oxyhornblende, 5% Ba-feldspar, 5% titanite, 3% chlorite, and 2% calcite by volume. Two amphibole

types, (ferro-) tschermakite hornblende and (ferro-) edenite, are present based on mineral analysis. They account for the backscatter contrast visible in the dendritic/plumose textures observed (Fig. 5.1.2) in the ocelli. These textures suggest crystallization of two suites of hornblende, with ilmenite rims, brought on by a moderate - high degree of undercooling with low nucleation rates (Deer et al. 1997).

An attempt was made to determine the depth at which the ocelli were quenched (crystallization of oxyhornblende). Using two geobarometers (Hammarstrom and Zen, 1986 and Schmidt, 1992 for Ca-amphiboles), for selected analyses, pressure of crystallization was determined (Table 6.1.3) to range from 5.6 – 8.8 kbars.

	Sample	46A	456B1	456B1	456B1	456B1	456B1	456B1	456B1	456B1	456B1	456B1
Geobarometer	Hammarstrom & Zen 86	7.4	7.6	5.6	7.2	8.0	6.0	7.6	6.3	6.9	8.5	8.5
P (kbar)	Schmidt 92	7.7	7.9	6.0	7.5	8.2	6.4	7.9	6.7	7.2	8.8	8.8

Table 6.1.3 Geobarometry results for select amphiboles, using Ca-amphiboloe geobarometry from Hammarstrom & Zen (1986) and Schmidt (1992).

Using mineral analysis and the PELE program (Boudreau 1999) an attempt was made to calculate the bulk original composition of the ocelli. Utilizing a range of confining pressures (Table 6.1.3), an acceptable temperature range for mafic magmas, and allowing for a range of volatiles (H_2O) outlined by Barclay and Carmichael (2004) and Moore et al. (1998), a normalized composition was determined for ocelli from different samples (Fig 6.1.4) . Our data suggests that the ocelli were derived from a silica-poor (39.19 - 46.38 wt. %), volatile-rich (3.27 – 3.77 wt. % H_2O) liquid.

Sample	46A	456A	456B1	456B2
SiO_2	42.3	39.2	46.4	45.2
TiO_2	3.5	1.0	2.1	2.3
Al_2O_3	13.0	16.0	13.4	11.0
FeO_t	13.2	11.7	8.9	9.4
MnO	0.0	0.0	0.0	0.0
MgO	10.6	16.3	10.9	14.0
CaO	10.9	9.7	11.6	13.0
Na_2O	0.7	0.0	0.0	0.0
K_2O	2.1	2.7	3.4	1.7
H_2O	3.8	3.6	3.3	3.3
Total	100.0	100.0	100.0	100.0

Table 6.1.4 Calculated original bulk compositions for ocelli, from normalized modal mineralogy (discussed above), and average composition of mineral phases (Table 5.2.3, Table 5.2.4, and Appendices A,B, sample 456B2, sites 1,2).

Ocelli may result from immiscibility of two magmatic phases. The concept of immiscibility in silicate liquids, preserved as glasses or patches/zones of mineralization relating enrichment/depletion of elements, has been widely accepted by igneous petrologists (Roeder et al., 1979 and Philpotts, 1982). Textural evidence of ocelli found by Bogoch and Magaritz (1983) further supports the presence of an immiscible phase in silicate systems. Work by Conticelli et al. (1992), Greenough and Fryer (2008), and Vegas et al. (2011) suggest immiscibility in silicate systems for alkaline rocks is partially controlled by lower viscosity due to enrichment in volatiles. Our interpretation of modal mineralogy for ocelli supports the idea of an immiscible phase caused by a low-silica – high-volatile system in the MFV alkali rocks.

6.1.4 Ba-feldspar

Crystals of hyalophane (Ba-feldspar) occurring in the observed ocelli (Fig. 5.1.2, and Fig. 5.1.3), show patchy, re-absorbed grain boundaries, and are therefore interpreted as being a primary mineral. The Ba-rich K-feldspar minerals, having a radiating and lathlike structure, occurring both inside the ocelli and within the matrix material are interpreted to be secondary. Work by Melluso et al. (2011) suggests that the association of Ba-feldspars and an immiscible phase related to volatile content in alkaline magmas is possible for systems in which K-feldspar is sufficiently alkali-rich and silica-undersaturated, in the presence of feldspathoids. However, this study was unable to identify any feldspathoids through petrographic or mineral geochemistry, perhaps due to overprinting by diagenetic or hydrothermal processes. Therefore, we are unable petrographically address any possible relationship that would be expected to occur between Ba-feldspar and oxyhornblende (ocelli), and between Ba-feldspar and phlogopite. Trace element geochemistry for this relationship is discussed in a later section.

6.2 EFFECTS OF ALTERATION

Inspection of Table 5.3.1 suggests that there are five groups of samples, each with differing geochemical signature of alteration (Fig. 6.2). One group (samples 456A, 456B1 and 456B2) has relatively low LOI (~4 %). Another group (samples 46A, 47B and

457D) is geochemically similar, but has LOI of 8–10%. Two samples (149C1 and 149C2) have exceptionally high Fe_2O_{3T} (~20%). Two other samples (49B and 468A) have exceptionally high CaO (~20%) and one (468B) has very low CaO (<3%).

Trace elements and REE (Fig. 6.2B) show some systematic variation with these five geochemical types of alteration. The samples with 8–10% LOI have a very slight negative Eu anomaly. The samples with high Fe_2O_{3t} have a positive Eu anomaly. Positive Eu anomalies have been described from modern sea-floor hydrothermal alteration involving the precipitation of ochre (Goulding et al., 1998), which would increase the Fe_2O_{3t} content of any host rock.

Plots of incompatible elements normalised to primitive mantle abundances (Fig. 6.2A) can be used to interpret relative enrichment or depletion in trace elements during hydrothermal alteration and diagenesis. Sample G-R4 of Goodfellow et al. (1995), although it has LOI of 10%, shows a very smooth spidergram pattern except for Ba and Rb and on the basis of lack of apparent enrichment or depletion of K and Sr relative to adjacent elements in the plot might be considered the sample least affected by seafloor hydrothermal metasomatism. All other samples show relative depletion in Sr and most show relative depletion in K, elements that are typically mobile in seafloor hydrothermal systems (Staudigel et al. 1981).

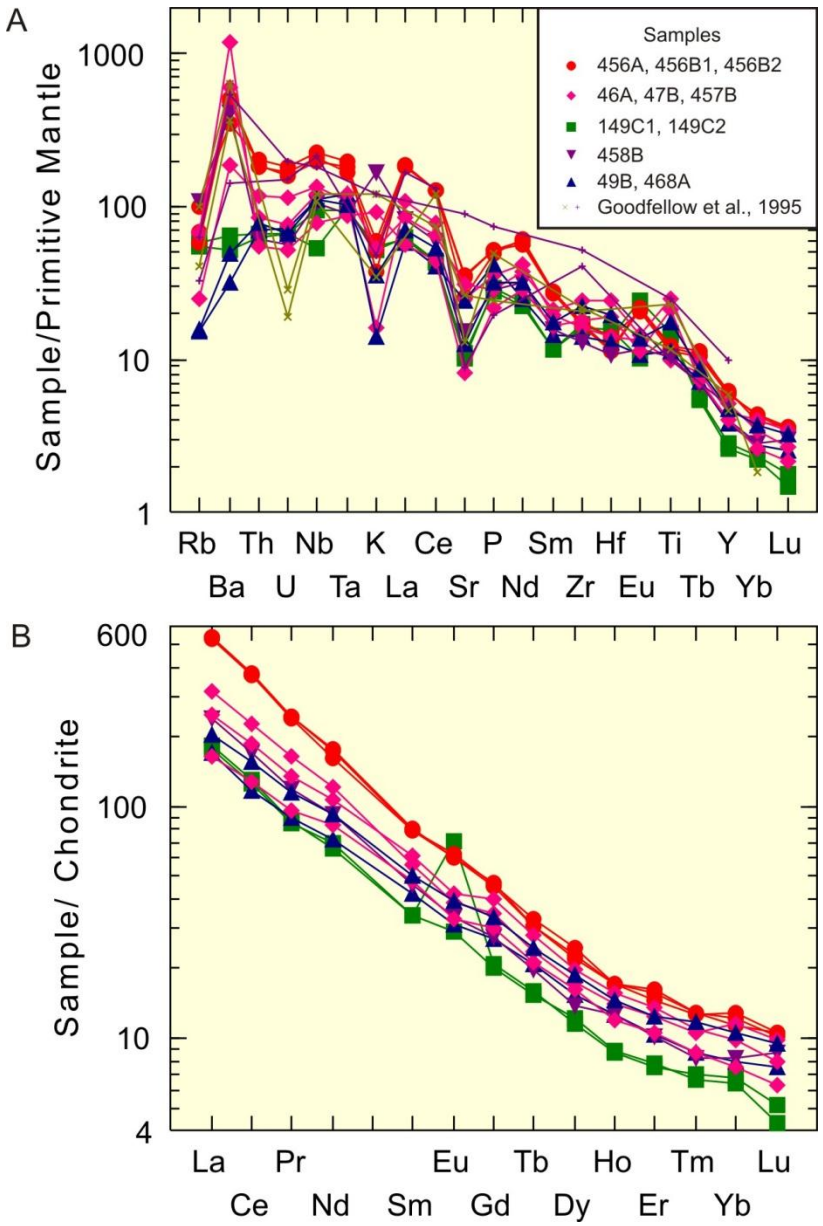

Figure 6.2. (A) Primitive mantle normalized incompatible element plot, (B) Chondrite normalized rare earth element plot. Chondrite and primitive mantle values from Sun and McDonough (1989).

The high Fe_2O_{3T} samples are relatively depleted in heavy and middle REE, Sr, and the LILE U, Th and Ba, but have Rb and K similar to less altered samples. Samples with high CaO are similarly depleted in Sr, U and Th, but show much stronger relative depletion in K, Ba and particularly Rb. Similar addition of CaO and loss of LILE with increasing K/Rb ratio is known from hydrothermal alteration of modern ocean crust (Staudigel et al. 1981). The sample with very low CaO shows K enrichment relative to other LILE and less Sr depletion than most other samples.

6.3 PETROGENESIS & FRACTIONAL CRYSTALLIZATION

Trends in both major and trace elements were examined, to identify potential petrogenesis and fractional crystallization patterns for MFV. There are minor geochemical variations found in the MFV samples examined in this study. For example, Al_2O_3/TiO_2 values range from 2.9 – 8.4. These values are significantly lower than the typical primitive mantle ratios (~22) or the normal mid-ocean-ridge basalts (~9.4), but are more similar to typical ocean island basalts (~5) (values from Sun and McDonough 1989). Lack of variation implies that geochemical composition of all samples is largely controlled by mantle processes or mantle compositions (Jung and Masberg 1998), and that fractional crystallization in high-level magma chambers was not important.

Clinopyroxene was observed as the most dominant phenocryst in most samples; where preserved, suggesting that it had an important constituent in the evolution of the melt. Petrographic evidence, resorbed margins of cores and sharp optical contrast with

rims (Fig. 5.1.1) of clinopyroxene macrocrysts indicate at least two stages of crystal growth. However, the observed continuity in clinopyroxene chemical compositions (Fig. 6.1), suggests normal (or simple) clinopyroxene fractionation. Additional evidence of clinopyroxene fractionation is indicated by a negative slope in a plot of Cr vs. Zr (Fig. 6.3A). This plot suggests that spinel was also a fractionating phase. The negative correlation depicted in a plot of Ni vs. Zr (Fig. 6.3B) is consistent with olivine fractionation. Plots of Nb vs. Zr and V vs. Zr (Fig. 6.3C, D) and plots Y vs. Zr and La vs. Zr (Fig. 6.3D, E) show that REE and HFSE fractionation is not straightforward, and that some other processes, perhaps source area variation, has occurred (van Westrenen et a. 2001).

The absence of a prominent negative Eu anomalies in REE plots (Fig. 5.3.3A, B) suggest that a low-pressure plagioclase fractionation has not occurred. These features together show that an early crystal fractionation process involving clinopyroxene, olivine, and spinel largely controlled the petrogenesis and evolution of the Marmot Formation, with later petrogenetic controls derived in part by an immiscible phase represented by ocelli (oxyhornblende and volatiles).

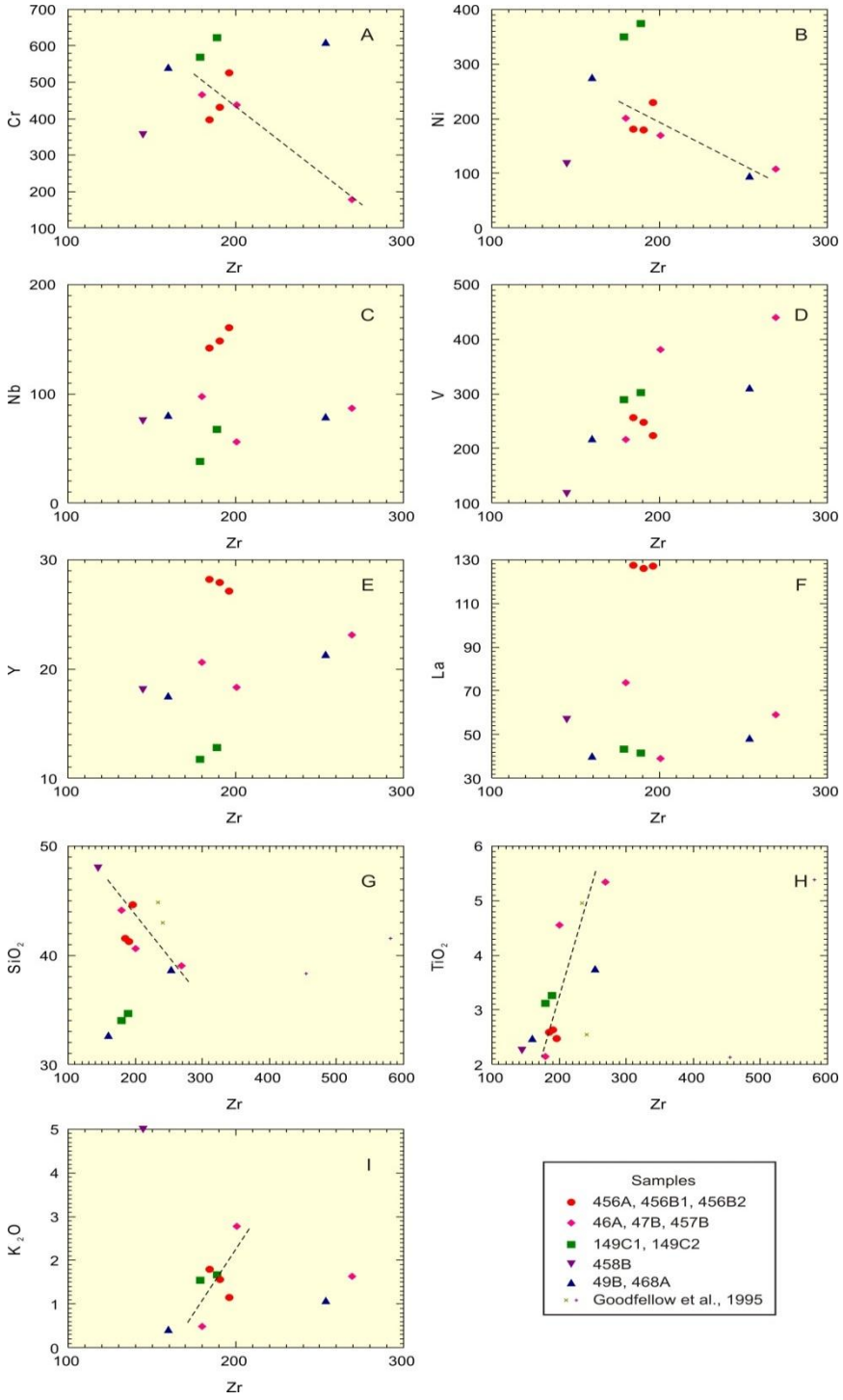

Figure 6.3 Incompatible nature of selected major and trace elements: (A) Cr vs. Zr, (B) Ni vs. Zr, (C) Nb vs. Zr, (D) V vs. Zr, (E) Y vs. Zr, (F) La vs. Zr, (G) SiO2 vs. Zr, (H) TiO2 vs. Zr, and (I) K2O vs. Zr plots. Symbols depict alteration groups (see section 6.2)

6.4 NATURE OF SOURCE

The absence of lower crustal or mantle derived xenoliths in MFV, inferences concerning the mineralogical and geochemical composition of the source are speculative. Therefore the following discussion is primarily based on trace element geochemistry. Low silica basalts are sourced from the mantle, due to the crust being too silicic to produce silica-poor basalt by partial melting (Sun and McDonough 1989). Geobarometric estimates for clinopyroxene and lack of Eu anomaly (plagioclase fractionation) also suggests mantle conditions for source of the magma. Potassic-ultrapotassic rocks require small degrees of partial melting of enriched or metasomatised mantle (Conticelli and Peccerillo, 1992), loosely termed OIB, common in rift settings.

MFV samples are petrographically similar, therefore utilizing incompatible elements with similar bulk partition coefficients in a binary plot, we can assess the potential of different sources for genesis for MFV. For example, plots of incompatible element ratios all show a positive correlation (Fig 6.4.1) away from primitive mantle suggesting that the derivation of the parental Marmot Formation was from a primitive mantle source. An OIB-like source for MFV is confirmed by the Th-Zr-Nb plot (Fig 5.3.2D) in which all samples fall in the OIB field.

The source composition was garnetiferous as evidenced by the substantial enrichment of LREE over HREE (average $La_N/Y_N = 23$). Yttrium is preferentially incorporated into garnet and left in the residuum, and thus melts derived from a garnet bearing source should be depleted in Y with respect to LREE (e.g. high La_N/Y_N). The

plot of Ce/Y vs. Zr/Nb (Fig 6.4.2A) also indicates that the source was predominantly garnet bearing.

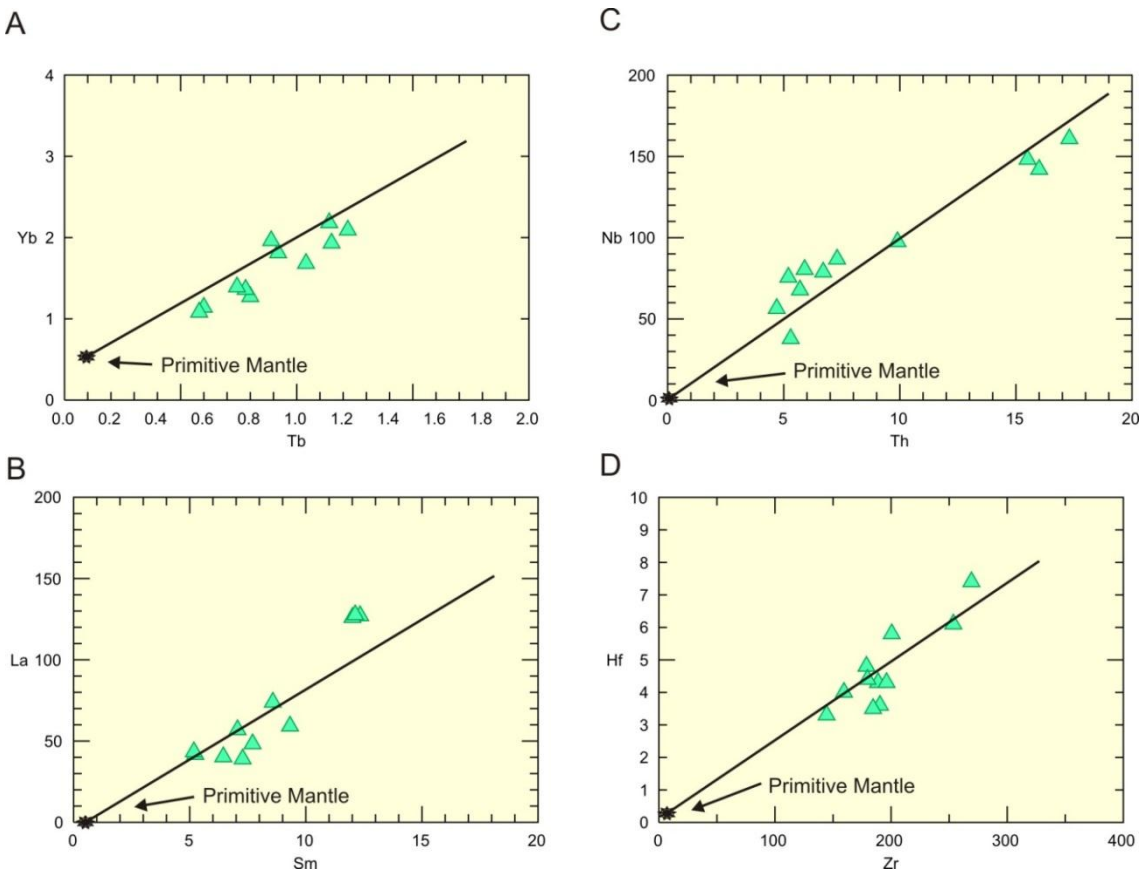

Figure 6.4.1 (A) Yb vs. Tb, (B) Nb vs. Th, (C) La vs. Sm, and (D) Hf vs. Zr variation plots. Primitive mantle values from Sun and McDonough 1989).

In a Tb/Yb vs. La/Yb plot (Fig 6.4.2.B), our least fractionated samples plotted between 2-4 % modal amounts of garnet on this diagram based on the value of the Tb/Yb ratio (Fig. 6.4.2.B). These curves were derived from geochemical modeling of fertile lherzolite mantle (Macdonald et al. 2001). On the basis of these constraints, the source that was melted to generate the primary magma for the MFV was likely a garnet bearing-

lherzolite, corresponding to a few percent garnets in source, again confirming mantle conditions, likely greater then 60 km depth or 20 kbar pressures.

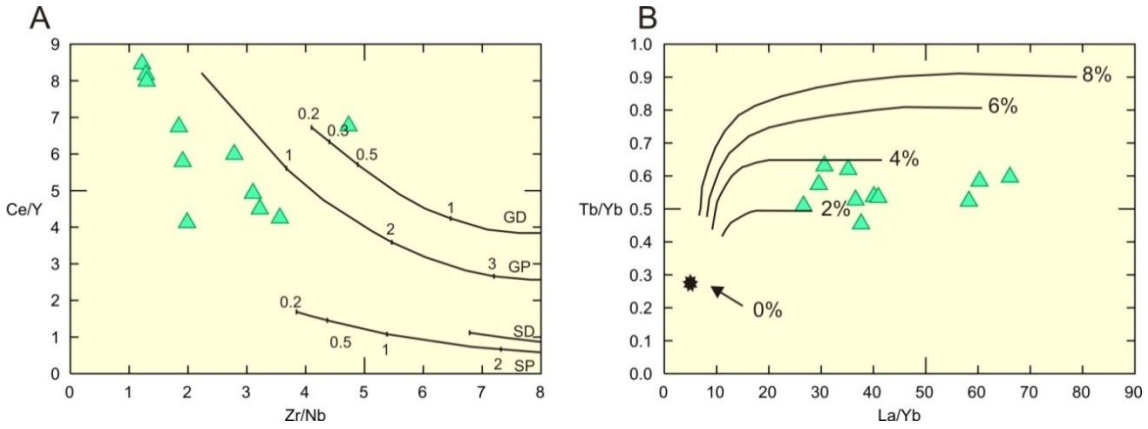

Figure 6.4.2 (A) Ce/Y vs. Zr/Nb plot. The continuous lines are melting curves calculated by Hardarson and Fitton (1992) for mantle compositions (GD = depleted lherzolite; GP = primitive garnet lherzolite; SD = depleted spinel lherzolite; SP = primitive spinel lherzolite), numbers on curves refer to percentage of melts. (B) Tb/Yb vs. La/Yb plot, continuous lines are for melting of fertile lherzolite mantle calculated by Macdonald et al (2001). Numbers on curves represent modal amounts of garnet.

The presence of phlogopite as a macrocryst, and probably a phenocrystic phase in some of MFV samples, suggests that there was a hydrous phase present in the source, further supported by the presences of amphiboles in the form of ocelli (discussed earlier). Identifying which of these phases was predominant in controlling petrogenesis and evolution of MFV, can be done by utilizing element data, especially those elements indicative of phlogopite and amphibole with characteristic partition coefficients such as K, Rb, Ba, and Sr (Fig 5.3.3B and work by Furnam 2007, and Icenhower and London

1996). However, these incompatible elements were probably mobile during low-grade alteration that our rocks have experienced (discussed earlier).

Mantle metasomatism typically leads to the modification of mantle peridotite and crystallization of incompatible element enriched minerals (e.g. phlogopite and amphibole) (Halliday et al. 1995, and Spath et. al 2001). Metasomatic processes are generally interpreted to enrich peridotitic mantle in incompatible elements. High La/Yb, Na/La and Na/Tb ratios with very high Zr/Hf and very low Ti/Eu ratios with respect to primitive mantle values are characteristic of cabonatitc metasomatism (Karmalkar et al. 2005). Our samples show average values for Nb/La, Nb/Ta, Zr/Hf and Ti/Eu ratios, and high values for La/Yb ratio (Table 6.4.1), which indicate enrichment with respect to typical primitive mantle values from Sun and McDonough (1989). Therefore variations in incompatible element ratios are probably in response to some varying effects of metasomatic processes within the source (Piercey et al. 2006).

Sample	La/Yb	Nb/La	Nb/Ta	Zr/Hf	Ti/Eu
46A	35.2	1.5	17.3	36.4	13241
47B	30.6	1.4	15.6	34.6	14426
49B	26.6	1.6	18.7	41.6	9825
149C1	36.6	1.6	17.4	43.9	4762
149C2	40.1	0.9	9.5	37.3	11045
456A	58.3	1.3	19.6	45.6	4234
456B1	60.3	1.2	21.5	52.9	4320
456B2	66.1	1.1	18.9	52.7	4421
457D	37.7	1.3	22.1	40.8	5703
468A	29.6	2.0	16.1	39.9	8212
468B	40.9	1.3	20.4	43.8	6954
Average	42.0	1.4	17.9	42.7	7922
Primitive Mantle *	1.5	1.0	17.4	36.2	7619

Table 6.4.1 Incompatible element ratios, * Primitive mantle values from Sun and McDonough (1989).

Similarly, highly incompatible element ratios such as Zr/Hf and Nb/Ta (Table 6.4.1) indicate derivation from a metasomatically altered source when compared to primitive mantle, as evidence in calcification of amphiboles (see above, and work by Green 1995). The partition coefficients of these incompatible elements (e.g. Nb and Ta) in amphibole and phlogopite are similar in alkaline melts (Green et al. 1993; Adam and Green 2006) and such these elements should behave in a similar manner. Therefore distinguishing between amphibole and phlogopite on the basis of incompatible elements is also unreliable. However with the presence of both amphibole and phlogopite in our samples, we can infer a residual metasomatic enrichment of our source.

6.5 COMPARISON WITH RIFT-RELATED VOLCANISM

Possibly comparable OIB-like volcanism is geochemically variable, but typically displays alkaline signatures, an enrichment in LILE (Cs, Rb, K, Ba, etc.) and HFSE (Th, U, Ce, Zr, Hf, etc.). MFV geochemistry is consistent with an OIB source. However this does not require that MFV erupted into an ocean island setting derived from a mantle source. Continental rift settings, such as East African Rift System (EARS) contain large quantities of alkaline rocks of OIB type geochemistry (Furman 1995, Rogers et al 2000, Spath et al 2001, Macdonald et al. 2001, and Chakrabarti et al. 2009). The geneses of such volcanoes are related to substantial mantle upwelling below a divergent margin with the magmas derived from partial melting of metasomatized lithospheric mantle. We will thus examine the tectonic setting and geochemistry from East African Rift (Chakrabarti et al. 2009) and our MFV.

The tectonic model for the EARS involves continental extension concentrating along weakened zones within Proterozoic basement (Macdonald et al. 2001). This extension is believed to begin with lithospheric thinning (pre-rift) and was followed by development of graben structures accompanied with coeval mafic volcanism (rifting). The lithospheric thickness below these active rifts is significantly thinner than that of distal cratonic basement (~20-35 km thick crust, Macdonald et al. 2001). The tectonic nature of the MCE is believed to have involved a simple graben structure as a result of crustal extension, and is associated with mafic volcanism (MFV) (Cecile 1978; 1982; Cecile et al. 1997). Difference between MFV and EARS is dramatically different scale of

crustal extension and the nature of the pre-rift thickness of the underlying crust. Thinning of lithospheric crust below MCE occurred approximately 300 Ma before the formation of the MCE, during the break up of supercontinent Rodinia (Colpron et al. 2002). Reactivation of these older crustal structures led to the formation of MCE. Lithospheric thickness in the Ordovician in western North America is unknown, but a modern analog for a passive margin (e.g., the Norwegian passive margin), comprises approximately 26-35 km crust, and approximately 125 km thick lithosphere (Sheck-Wenderoth and Maystenko 2008). Therefore it is reasonable to expect a similar crust and lithosphere thicknesses beneath MCE. Following rifting, the depth to the asthenosphere-lithosphere transition would likely decrease due to upwelling of the asthenosphere (i.e. thinner lithosphere). Geochemistry of the MFV (discussed above) indicates that magmas represent melts of enriched mantle, similar to EARS, although significantly overprinted by diagenetic and hydrothermal alteration.

Geochemical evidence for this relationship between EARS and MFV is evident in the chondrite normalized REE and primitive mantle normalized plots (Fig. 6.5.1A, B). There are marked similarities between these localities. Similarities include enrichment of LILE relative to HFSE, positive Nb and Ta anomalies, negative Zr anomalies, and a negative Pb anomaly (relating to post entrapment leaching, Chakrabarti et al. 2008). On the basis of trace element modeling, Chakrabarti et al. (2008) suggested the Virunga volcanism of the EARS were derived from comparatively greater depths by very low degrees of partial melting of a phlogopite-bearing, volatile rich (carbonated) mantle source assemblage. These constraints are similar to melting and source constraints that we have inferred for MFV; however we cannot constrain the role of phlogopite (or

amphibole) in MFV petrogenesis due to the mobility of Rb, Ba, and K (see above). Based on the similarities discussed above, we can interpret MFV to represent rift related magmatism derived from small degrees of partial melting of variably enriched metasomatized OIB-like source.

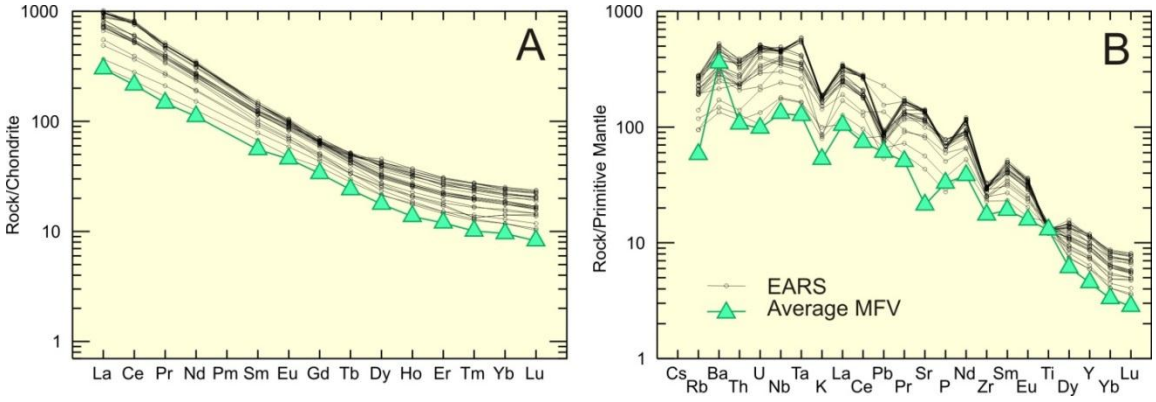

Figure 6.5.1 (A) Chondrite normalized rare earth element plot. (B) Primitive mantle normalized incompatible element plot. Chondrite and primitive mantle values from Sun and McDonough (1989), East African Rift System (EARS) values from Chakrabarti et al. (2009).

7 CONCLUSIONS & RECOMMENDED FUTURE WORK

7.1 CONCLUSIONS

Mineral assemblages suggest potassic-ultrapotassic low-silica basaltic source magma for the Marmot Formation volcanics in the Porter Puddle Complex. Similarly, REE and stable HFSE are similar to those of ultrapotassic magmas in the East African Rift System. Controls on an early crystal fractionation process were determined to involve clinopyroxene, olivine, and spinel at pressures well above 30 kbar. With the lack of plagioclase fractionation (no negative Eu anomaly) and HREE indicating presence of residual garnet in the source, a predominant mantle origin for MFV magmas is inferred.

Evidence of ocelli textures suggests an immiscible phase in a silica-undersaturated – high-volatile basalt system. Estimations for crystallization pressure for oxyhornblende (5.6-8.8 kbar), suggests a later stage petrogenetic controls derived in part by an immiscible phases, K-feldspar fractionation, and change in phlogopite-amphibole crystallization.

The presence of phlogopite associated with early clinopyroxene suggest that magma evolved from a more hydrous system into a later stage of ocelli crystallization, further suggesting a hydrous-silica-undersaturated immiscibility. These multiple controls on petrogenesis may be responsible for geographical and geochemical variation in the Marmot Formation volcanic rocks in previous literature.

7.2 RECOMMENDED FUTURE WORK

We recommend additional mapping of the MFV occurrences at all geographical locations, especially the Porter Puddle Complex, with the intent to identify separate flows, or volcanic events to better constrain the role of phlogopite-amphibole controls on petrogenesis. However, due to isolation, poor exposure, and the high degree of alteration of MFV, such a mapping project would be costly and time consuming.

Mapping of individual flows with a tighter sample collection (intended for petrology and geochemistry) would give more insight into the silicate immiscible phase. In addition isotopic geochemistry could provide further information on the nature of the source, and provide a stronger model for the evolution of the Marmot Formation.

8 REFFERENCES

Adam, J., and Green, T. 2006. Trace element partitioning between mica- and amphibole-bearing garnet lherzolite and hydrous basanitic melt: 1. Experimental results and the investigation of controls on partitioning behavior. Contribtuiions to Mineralogy and Petrology, v. 152, p. 1-17.

Arai, S. 1984. Pressure-temperature dependent compositional variation of phlogopitic micas in upper mantle peridotites. Contributions to Mineralogy and Petrology, v. 87, p. 206-264.

Barclay, J., and Carmichael, I.S.E. 2004. A hornblende-bearing basalt from Western Mexico: water-saturated phase relations constrain a pressure-temperature window of eruptability. Journal of Petrology, v. 45, p. 485-506.

Bindi, L., Cellai, D., Melluso, L., Conticelli, S., Morra, V., and Menchetti, S. 1999. Crystal chemistry of clinopyroxene from alkaline undersaturated rocks of the Monte Vulture Volcano, Italy. Lithos, v. 46, p. 259-274.

Blusson, S.L. 1974. Operation Stewart (northern Selwyn basin): Mount Eduni (106A), Bonnet Plume Lake (106B), Nadaleen River (106C), Lansing (105N) and Niddery Lake (105O). Geological Survey of Canada, Open File 205.

Bogoch, R., and Magaritz, M. 1983. Immiscible silicate-carbonate liquids as evidence from ocellar diabase dykes, southeast Sinai. Contributions to Mineralogy and Petrology, v. 82, p. 227-230.

Boudreau, A.E. 1999. PELE = a version of the MELTS software program for the PC platform. Computers & Geosciences, v. 25, p. 201-203.

Cecile, M.P. 1978. Report on Road River stratigraphy and Misty Creek Embayment, Bonnet Plume (106B) and surrounding map areas, Northwest Territories. In: Current Research, Part A; Geological Survey of Canada, paper 78-1A, p. 371-377.

Cecile, M.P. 1982. The lower Paleozoic Misty Creek Embayment, Selwyn Basin, Yukon and Northwest Territories. Geological Survey of Canada, Bulletin 335, 78p.

Cecile, M.P., Morrow, D.W., and Williams, G.K. 1997. Early Paleozoic (Cambrian to Early Devonian) tectonic framework, Canadian Cordillera. Bulletin of Canadian Petroleum Geology, v. 45, p. 54-74.

Chakrabarti, R., Basu, A.R., Santo, A.P., Tedesco, D., and Vaselli, O. 2009. Isotopic and geochemical evidence for a heterogeneous mantle plume origin of the Virunga volcanics, Western rift, East African Rift system. Chemical Geology, v. 259, p. 273-289.

Colpron, M., Logan, J.M., and Mortensen, J.K. 2002. U-Pb zircon age constraint for late Neoproterozoic rifting and initiation of the lower Paleozoic passive margin of western Laurentia. Canadian Journal of Earth Science, v. 39, p. 133-143.

Conticelli, S., Manetti, P., Menichetti, S. 1992. Mineralogy, geochemistry and Sr-isotopes in orendites from south Tuscany, Italy: constraints on their genesis and evolution. European Journal of Mineralogy, v. 4, p. 1359-1375.

Conticelli, S. and Peccerillo, A. 1992. Petrology and geochemistry of potassic and ultrapotassic volcanism in Central Italy: petrogenesis and inferences on the evolution of the mantle sources. Lithos, v. 28, p. 221-240.

Deer, W.A., Howie, R.A., and Zussman, J. 1997. Rock-forming Minerals, 2B, Double-Chain Silicates, (2nd ed.). Geological Society of London, 764p.

Devlin, W.J., and Bond, G.C. 1988. The initiation of the early Paleozoic Cordilleran miogeocline: evidence from the uppermost Proterozoic –Lower Cambrian Hamill Group of southeastern British Columbia. Canadian Journal of Earth Sciences, v. 25, p.1-19.

Dobosi. G., Schultz-Güttler, R., Kurat, G., and Kracher, A. 1991. Pyroxene chemistry and evolution of alkali basaltic rocks from Burgenland and Styria, Austria. Mineralogy and Petrology, v. 43, p. 275-292.

Edgar, A.D., Green, D.H., and Hibberson, W.O. 1976. Experimental Petrology of a highly potassic magma. Journal of Petrology, v. 17, p. 339-356.

Fritz, W.H., Cecile, M.P., Norfor, B.S., Morrow, D., and Geldsetzer, H.H.J. 1991. Cambrian to Middle Devonian assemblages. In: Gabrielse, H. and Yorath, C.J. (eds). Geology of the Cordilleran orogeny in Canada. Geological Survey of Canada, Geology of Canada 4, p. 153-218.

Furman, T. 1995. Melting of metasomatized subcontinental lithosphere: undersaturated mafic lavas from Rungwe, Tanzania. Contributions to Mineralogy and Petrology, v. 122, p. 97-115.

Furnam, T. 2007. Geochemsitry of East African Rift basalts: An overview. Journal of African Earth Sciences, v. 48, p. 147-160.

Gast, P.W. 1968. Trace element fractionation and the origin of tholeiitic and alkaline magma types. Geochimica et Cosmochimica Acta, v. 32, p. 1057-1086.

Goodfellow, W.D., Cecile, M.P., and Leybourne, M.I. 1995. Geochemistry, petrogenesis, and tectonic setting of lower Paleozoic alkalic and potassic volcanic rocks, Northern Canadian Cordilleran Miogeocline. Canadian Journal of Earth Sciences, v. 32, p. 1236-1254.

Goulding, H.C., Mills, R.A., Nesbit, R.A. 1998. Precipitation of hydrothermal sediments on the active TAG mound: implications for ochre formation. In: Mills, R.A., & Harrison, K. (eds).

Modern Ocean Floor Processes and the Geological Record. Geological Society, London, Special Publications, v. 148, p. 201-216.

Gordey, S.P. and Anderson, R.G. 1993. Evolution of the Northern Cordilleran Miogeocline, Nahanni map area (105I), Yukon and Northwest Territories. Geological Survey of Canada, Memoir 428, 214 p.

Green, T.H. 1995. Significance of Nb/Ta as an indicator of geochemical processes in the crust-mantle system. Chemical Geology, v. 120, p.347-359.

Green, T.H., Adam, J., and Site, S.H. 1993. Proton microprobe determined trace element partition coefficients between parasite, augite and silicate or carbonatitc melts. EOS, Transactions of the American Geophysical Union, v. 74, 340p.

Greenough, J.D, and Fryer B.J. 2008. Trace-element evidence for volatile-influenced differentiation in a flow of alkali basalt, Peng Hu island, Taiwan. Canadian Mineralogist, v. 46, p. 305-315.

Halliday, A., Lee, D., Tommasini, S., Davies, G., Paslick, C., Godfrey Fitton, J., and James, D. 1995. Incompatible trace elements in OIB and MORB and source enrichment in the sub-oceanic mantle. Earth and Planetary Science Letters, v. 133, p. 379-395.

Hammarstrom, J.M., and Zen, E. 1986. Aluminum in hornblende: An emerical igneous geobarometer. American Mineralogist, v. 71, p. 1297-1313.

Icenhower, J., and London, D. 1996. Experimental partitioning of Rb, Cs, Sr, and Ba between alkali feldspar and peraluminous melt. American Mineralogist, v. 81, p. 719-734.

Jung, S., and Masberg, P. 1998. Major- and trace-elementsystematics and isotope geochemistry of Cenozoic mafic volcanic rocks from the Vogelsberg (central Germany) Constraint on the origin of continental alkaline and tholeiitic basalts and their mantle sources. Journal of Volcanology and Geothermal Research, v. 86, p. 151-177.

Karmalkar, N., Rege, S., Griffin, W., and Oreilly, S. 2005. Alkaline magmatism from Kutch, NW India: implications for plume-lithosphere interaction. Lithos, v. 81, p. 101-119.

Leake, B.E., Woolley, A.R., Arps, C.E.S., Birch, W.D., Gilbert, M.C., Grice, J.D.,Hawthorne, F.C., Kato, A., Kisch, H.J., Krivovichev, V.G., Linthout, K., Laird,J., Mandarino, J.A., Maresch, W.V., Nickel, E.H., Rock, N.M.S., Schumacher, J.C., Smith, D.C., Stephenson, N.C.N., Ungaretti, L., Whittaker, E.J.W., and Youzhi, G. 1997. Nomenclature of amphiboles: Report of the Subcommittee on Amphiboles of the International Mineralogical Association, Commission on New Minerals and Mineral Names. American Mineralogist, v. 82, p. 1019–1037.

Lloyd, F.E. 1981. Upper-mantle metasomatism beneath a continental rift: Clinopyroxenes in alkali mafic lavas and nodules from South West Uganda. Mineralogical Magazine, v. 44, p. 315-323.

Lloyd, F.E., Arima, M., and Edgar, A.D. 1985. Partial melting of a phlogopite-clinopyroxenite nodule from south-west Uganda: an experimental study bearing on the origin of highly potassic continental rift volcanics. Contributions to Mineralogy and Petrology, v. 91, p. 321-329.

Macdonald, R., Rogers, N., Fitton, J.G., and Black, S. 2001. Plume-lithosphere interations in the generation of the basalts of the Kenya Rift, East Africa. Journal of Petrology, v. 42, p. 877-900.

Melluso, L., Morra, V., De Dennaro, R. 2011. Coexisting Ba-feldspar and melilite in a melafoidite lava at Mt. Vulture, Italy: Role of volatiles and alkaline earths in bringing a petrological incompatibility. Canadian Mineralogist, v. 49, p. 983-1000.

Moore, G., Vennemann, T., Carmichael, I.S.E. 1998. An empirical model for the solubility of H2O in magmas to 3 kilobar. American Mineralogist, v. 83, p. 36-42.

Nisbet, E., and Pearce, J. 1977. Clinopyroxene composition in mafic lavas from different tectonic settings. Contributions to Mineralogy and Petrology, v. 63, p. 149-160.

Ootes, L., Sandeman, H., Lemieuq, Y., and Leslie, C. 2008. The 780 Ma Tsezontene Sills, Mackenzie Mountains: a field, petrographical, and geochemical study. Northwest Territories Geoscience Office, NWT Open Report 2008-011, 21p.

Pearce, J.A. 1996. A user's guide to basalt discrimination diagrams. In: Wyman, D.A. eds., Trace element geochemistry of volcanic rocks: applications for massive sulphide exploration. Geological Association of Canada, Short Course Notes, v. 12, p. 79-113.

Philpotts, A.R. 1982. Composition of immiscible liquids in volcanic rocks. Contributions to Mineralogy and Petrology, v. 80, p. 201-218.

Piercey, S., Mortensen, J., Murphy D., Paradis, S., and Creaser, R. 2002. Geochemistry and tectonic significance of alkalic mafic magmatism in the Yukon-Tanana terrane, Finlayson Lake region, Yukon. Canadian Journal of Earth Sciences, v. 39, p. 1729-1744.

Piercey, S.J., Murphy, D.C., Mortensen, J.K., and Creaser, R.A. 2004. Mid-Paleozoic initiation of the northern Cordilleran marginal backarc basin: Geologic, geochemical, and neodymium isotope evidence from the oldest magmatic rocks in the Yukon-Tanana terrane, Finlayson Lake district, southwest Yukon, Canada. Geological Society of America Bulletin, v. 116, p. 1087-1106.

Roeder, P.L., Campbell, I.H., and Jamieson, H.E. 1979. A re-evaluation of the olivine-spinel geothermometer. Contributions to Mineralogy and Petrology, v. 68, p. 325-334.

Rogers, N., Macdonald, R., Fitton, J.G., and George, R. 2000. Two mantle plumes beneath the East African rift system: Sr, Nd and Pb isotope evidence from Kenya Rift basalts: Earth and Planetary Science Letters, v. 176, p. 387-400.

Schmidt, M.W. 1992. Amphibole composition as a function of pressure: an experimental calibration of the Al-in-hornblende barometer. Contributions to Mineralogy and Petrology, v. 110, p. 304-310.

Sheck-Wenderoth, M., and Maystenko, Y. 2008. How warm are passive continental margins? A 3-D lithosphere-scale study from the Norwegian margin. Geology, v. 36, p. 419-422.

Shervais, J.W. 1982. Ti-V plots and the petrogenesis of modern and ophiolitic lavas. Earth and Planetary Science Letters, v. 59, p. 101-118.

Spath, A., Le Roex, A., and Opiyo-Akech, N. 2001. Plume-lithosphere Interaction and the Origin of Continental Rift-related Alkaline Volcanism-the Chyulu Hills Volcanic Province, Southern Kenya. Journal of Petrology, v. 42. P. 768-787.

Spitz, G., and Darling, R. 1978. Major and minor element lithogeochemcial anomalies surrounding the Louvem copper deposit Val d'Or, Quebec. Canadian Journal of Earth Sciences, v. 15, p. 1161-1169.

Staudigel, H., Hart, S.R., and Richardson S.H. 1981. Alteration of the oceanic crust: processes and timing. Earth and Planetary Science Letters, v. 52, p. 311-327.

Sun, S.-s., and McDonough, W.F. 1989. Chemical and isotopic systematics of oceanic basalts: Implications for mantle compositions and processes. In: Saunders, A.D., and Norry, M.J. (eds). Magmatism in the ocean basin. London, UK, Geological Society Special Publications, v. 42, p. 313-345.

van Westrenen, W., Blundy, J.D., and Wood B.J. 2001. High field strength element/rare earth element fractionation during partial melting in the presence of garnet: Implications for identification of mantle heterogeneities, Geochemistry. Geophysics. Geosystems, v. 2.

Vegas, N., Rodriguez, J., Cuevas, J., Siebel, W., Esteban, J.J., Tubia, J.M., Basei, M. 2011. The sphene-centered ocellar texture: An effect of grain-supported flow and melt migration in a hyperdense magma mush. Journal of Geology, v. 119, p. 143-157.

Wood, D.A. 1980. The application of the Th-Hf-Ta diagram to problems of tectonomagmatic classification and to establishing the nature of crustal contamination of basaltic lavas of the British Tertiary volcanic province: Earth and Planetary Science Letters, v. 50, p. 11-30.

APPENDIX A

Mineral Chemistry by SEM/EDS

(in wt.% oxide)

Sample	Site	Pos.	Mineral	SiO_2	TiO_2	Al_2O_3	FeO_t	MnO	MgO	CaO	Na_2O	K_2O	P_2O_5	SO_3	F	Cl	V_2O_5	Cr_2O_3	CoO	NiO	ZnO	SrO	ZrO_2	MoO_3	BaO	La_2O_3	Ce_2O_3	Yb_2O_3	WO_3	PbO	Total
46A	1	1	Pyrite				27.81							72.19																	100
46A	1	2	Wollastonite	52.22			1.21	0.74		45.84																					100.01
46A	1	3	Fluoroapatite							48.23			43.54		8.23														0		100
46A	1	4	Calcite						3.18	96.81																					99.99
46A	1	5	Pyrite				27.44							72.56																	100
46A	1	6	Pyrite				27.96							72.07																	100.03
46A	1	7	Pyrite	0.66			26.89							72.44																	99.99
46A	1	8	Quartz	86.72		2.46	4.03		3.6	2.45		0.72																			99.98
46A	1	9	Calcite	3.79			2.43			93.77																					99.99
46A	1	10	Calcite	15.27		8.31	9.67		8.8	57.93																					99.98
46A	1	11	Fluoroapatite							52.85			47.16																		100.01
46A	1	12	Pyrite	2.8		0.81	26.39		2.19					67.2						0.62											100.01
46A	1	13	Wollastonite	66.4		3.04	4.64		3.17	22.75																					100
46A	1	14	Wollastonite	68.99		2.8	4.03		3.8	20.39																					100.01
46A	1	15	Oxyhornblende (Alt)	42.96	3.52	13.23	14.95		10.81	11.1	0.66	2.12	0.66																		100.01
46A	2	1	Phlogopite	39.85	5.49	16.5	15.27		15.44			7.44																			99.99
46A	2	2	Fluoroapatite	8.34		5.59	5		6.04	39.61			34.88								0.55										100.01
46A	2	3	Fluoroapatite	1.39			0.72			47.45			43.72		6.73																100.01
46A	2	4	Chlorite	34.21		21.69	22.96		20.36	0.78																					100
46A	2	5	Phlogopite	39.47	5.25	16.46	16.61		14.63			7.58																			100
46A	2	6	Calcite				1.79			98.21																					100
46A	2	7	Calcite				5.47			94.54																					100.01
46A	2	8	Calcite				1.75			98.25																					100
46A	2	9	Alstonite				3.46			43.99											1.42				51.13						100
46A	2	10	Calcite	17.43		4.97	6.3		3.81	67.5																					100.01
46A	2	11	Ba-feldspar	50.57		20.09	1.48		1.23	2.17		6.42									1.15				16.87						99.98
46A	2	12	Quartz	94.87			1.65		1.36	2.11																					99.99
46A	2	13	Phlogopite	41.39	6.42	14.59	10.54		18.32			8.74																			100
46A	2	14	Chlorite + K2O	39	2.82	16.48	21.29		16.53			3.89									0										100.01
46A	2	15	Titanite	24.64	52.41	2.15	1.39			19.39											0										99.98
46A	2	16	Chlorite + K2O	38.7		19.75	20.2		19.8	0.52		1.04																			100.01
46A	2	17	Calcite	12.9			1.87			85.24																					100.01
46A	2	18	Quartz	86.72		1.21	2.42		2.4	7.23																					99.98
46A	2	19	Chlorite + K2O	39.96		20.29	13.33		9.78	12.58		4.05																			99.99
46A	2	20	Chlorite + K2O	44.02		24.64	15.81		11.29			4.22																			99.98
46A	2	21	Titanite	34.21	29.31	6.65	6.07		3.83	17.53		1.4									0.98										99.98
46A	3	1	Phlogopite	38.83	5.54	17.54	14.09		16.17			7.84																			100.01
46A	3	2	Phlogopite	38.74	5.42	16.99	13.59		18.12			7.15																			100.01
46A	3	3	Phlogopite	39.6	7.26	16.99	9.7		18.16			8.3																			100.01
46A	3	4	Chlorite + K2O	41.31		22.79	17.88		14.66			3.35																			99.99
46A	3	5	Calcite	13.65		9.47	9.85		8.14	58.88																					99.99
46A	3	6	Titanite	34.03	30.91	4.69	3.01		2.44	24.92																					100
46A	3	7	Titanite	32.99	33.43	4.97	4.14		2.35	20.83		0.93				0.35															99.99
46A	3	8	Quartz	96.14		1.25	1.25		1.36																						100
46A	3	9	Titanite	34.91	28.74	6.2	5.36		3.6	20.53		0.65																			99.99
46A	3	10	Fluoroapatite							46.83			44.64		8.52																99.99
46A	3	11	Phlogopite	39.9	6.41	16.61	9.6		18.8			8.71																			100.03
46A	3	12	Titanite	28.47	44.67	3.21	1.22			22.42																					99.99
46A	3	13	Titanite	32.9	33.46	4.57	3.62		2.77	22.68																					100

Sample	Site	Pos.	Mineral	SiO_2	TiO_2	Al_2O_3	FeO_t	MnO	MgO	CaO	Na_2O	K_2O	P_2O_5	SO_3	F	Cl	V_2O_5	Cr_2O_3	CoO	NiO	ZnO	SrO	ZrO_2	MoO_3	BaO	La_2O_3	Ce_2O_3	Yb_2O_3	WO_3	PbO	Total
46A	4	1	Phlogopite	40.24	6.61	16.08	8.63		18.79			8.48															1.18				100.01
46A	4	2	Phlogopite	40.77	6.66	15.74	8.39		19.45			9																				100.01
46A	4	3	Fluoroapatite							47.67			43.22		9.12																100.01
46A	4	4	Fluoroapatite	6.93		3.16	2.19		2.14	45.67		1	38.91																		100
46A	4	5	Calcite	20.62		4.25	5.96		3.81	65.36																					100
46A	4	6	Phlogopite	40.47	6.91	16.08	8.56		19.3			8.67																			99.99
46A	4	7	Titanite	21.93	57.36	2.7	1.12			16.9																					100.01
46A	4	8	Clinopyroxene	48.56	3.92	7.97	5.43		12.8	21.3																					99.98
46A	4	9	Titanite	34.83	28.66	5.14	2.11		1.87	24.21													3.17								99.99
46A	4	10	Titanite	24.43	53.36	2.82	1.16			18.23																					100
46A	4	11	Titanite	27.19	47.79	3.34	0.93			20.76																					100.01
46A	4	12	Phlogopite	39.83	6.52	16.06	10.24		18.55			8.79																			99.99
46A	4	13	Phlogopite	39.94	6.96	16.99	11.09		16.98			8.06																			100.02
46A	4	14	Clinopyroxene	47.92	2.85	7.05	6.41		14.79	20.97																					99.99
46A	4	15	Phlogopite	40.07	7.26	16.02	10.77		17.48			8.41																			100.01
46A	4	16	Titanite	35.21	31.83	4.42	1.79		1.04	25.7																					99.99
46A	4	17	Calcite	4.28		2.19	2.55			90.99																					100.01
46A	4	18	Phlogopite	39.1	7.34	17.46	10.05		17.48			8.58																			100.01
46A	4	19	Phlogopite	39.17	8.04	17.36	9.16		17.78			8.48																			99.99
46A	4	20	Phlogopite	39.17	7.91	17.52	8.8		18.55			8.06																			100.01
46A	4	21	Phlogopite	39.23	7.82	16.84	9.65		18.59			7.88																			100.01
46A	4	22	Phlogopite	40.28	7.26	16.31	8.41		18.95			8.79																			100
46A	4	23	Phlogopite	39.64	7.59	16.25	8.32		19.47			8.72																			99.99
46A	4	24	Phlogopite	39.94	6.64	17.4	8.94		18.89			8.19																			100
46A	4	25	Phlogopite	39.45	7.66	16.91	8.13		19.52			8.32																			99.99
46A	4	26	Phlogopite	39.17	8.82	17.14	9.08		17.48			8.31																			100
46A	4	27	Phlogopite	40.92	7.12	15.72	9.37		18.01			8.87																			100.01
46A	4	28	Phlogopite	39.51	4.85	15.89	20.25		11.81			7.67																			99.98
46A	4	29	Phlogopite	38.12	8.41	16.87	8.83		17.83	2.38		7.58																			100.02
46A	4	30	Phlogopite	40.41	7.22	16.61	9.01		18.31			8.47																			100.03
46A	4	31	Quartz	85.87		3.02	4.14		3	3.95																					99.98
46A	4	32	Titanite	35.7	30.43	4.95	1.88		1.71	25.34																					100.01
46A	4	33	Titanite	34.72	30.99	4.29	2.92		2.49	24.6																					100.01
46A	4	34	Clinopyroxene	51.15	2.4	4.12	8.31		13.27	20.75																					100
46A	4	35	Clinopyroxene	51.36	1.22	4.23	8.76		14.86	19.57																					100
46A	4	36	Chlorite	37.24		17.61	21.41		20.78	2.97																					100.01
46A	4	37	Ba-feldspar	49.48		23.11	5.11		3.35			5.5													13.44						99.99
46A	4	38	Titanite	32.67	32.19	4.72	5.06		4.86	20.5																					100
46A	4	39	Quartz	94.23		1.72	2.44		1.61																						100
46A	4	40	Quartz	94.19		1.1	1.36			3.34																					99.99
46A	4	41	K-feldspar	49.99	0.75	23.05	11.69		7.88			6.61																			99.97
46A	4	42	Quartz	93.87			1.21		1.24	3.69																					100.01
46A	4	43	Chlorite +K2O	35.62		20.94	24.58		18.47			0.4																			100.01
46A	5	1	Phlogopite	39.79	6.47	16.61	12.32		16.75			8.05																			99.99
46A	5	2	Phlogopite	39.64	7.71	17.02	8.71		17.96		0.9	8.06																			100
46A	5	3	Phlogopite	39.79	7.17	17.16	9.55		16.76	1.12		8.46																			100.01
46A	5	4	Phlogopite	38.72	7.24	16.67	9.57		18.94			8.87																			100.01
46A	5	5	Phlogopite	39.06	3.29	16.87	18.44		15.84	1.02		5.49																			100.01
46A	5	6	Phlogopite	40.17	6.39	16.27	11.24		18.64			7.29																			100

Sample	Site	Pos.	Mineral	SiO_2	TiO_2	Al_2O_3	FeO_t	MnO	MgO	CaO	Na_2O	K_2O	P_2O_5	SO_3	F	Cl	V_2O_5	Cr_2O_3	CoO	NiO	ZnO	SrO	ZrO_2	MoO_3	BaO	La_2O_3	Ce_2O_3	Yb_2O_3	WO_3	PbO	Total
46A	5	7	Phlogopite	39.83	5.92	17.04	9.6		19.3			8.3																			99.99
46A	5	8	Chlorite	36.37		20.31	22.71		19.07	1.55																					100.01
46A	5	9	Clinopyroxene	50.96	1.7	5.25	7.02		15.82	19.24																					99.99
46A	5	10	Calcite				4.63		3.66	91.69																					99.98
46A	5	11	Calcite				12.63		5.32	82.05																					100
46A	5	12	Quartz	94.98		0.93	2.01		1.54	0.53																					99.99
46A	5	13	Titanite	25.95	50.46	2.61				20.99																					100.01
46A	5	14	Titanite	33.2	37.16	3.25	1.25			25.14																					100
46A	5	15	Titanite	33.16	35.93	4.52	1.05			25.34																					100
46A	5	16	Chlorite + SiO2	59.11		10.52	14.56		15.8																						99.99
46A	5	17	Calcite				15.01		6.4	78.58																					99.99
46A	5	18	Phlogopite	39.87	6.69	16.14	11.98		16.65			8.67																			100
46A	5	19	Titanite	27.81	41.5	3.59	1.84		1.67	23.58																					99.99
46A	5	20	Mix	52.88		19.75	7.73		6.25			7.96													5.43						100
46A	5	21	Phlogopite	39.32	6.62	17.48	10.2		18.19			8.19																			100
46A	5	22	Phlogopite	39.38	6.79	16.93	10.66		17.53			8.71																			100
46A	5	23	Phlogopite	36.84	6.37	16.14	9.93		16.86	5.86		8.01																			100.01
46A	5	24	Alstonite							36.51												4.32			59.18						100.01
46A	5	25	Mix	36.39	10.39	13.02	14.4		17.44	8.34																					99.98
46A	5	26	Phlogopite	41.37	6.72	16.14	8.28		18.84			8.65																			100
46A	5	27	Phlogopite	39.34	7.21	17.31	9.89		18.19			8.08																			100.02
46A	5	28	Chlorite	37.84		18.65	22.82		20.26			0.42																			99.99
46A	5	29	Phlogopite	43.9		23.52	16.58		11.33			4.67																			100
46A	5	30	Mix	19.77		13.45	16.16		11.59	39.02																					99.99
46A	5	31	Chlorite	37.65		19.35	23.08		19.91																						99.99
46A	6	1	Calcite				1.97			98.04																					100.01
46A	6	2	Calcite				15.35		5.69	78.96																					100
46A	6	3	Titanite	33.44	35.7	3.31	1.22		1.24	25.09																					100
46A	6	4	Titanite	20.81	59.73	2.85	1.09			15.52																					100
46A	6	5	Titanite	31.32	40.38	4.02	1.79		1.56	20.95																					100.02
46A	6	6	Quartz	94.45		1.38	2.12		2.04																						99.99
46A	6	7	Titanite	30.36	39.47	4.1	2.24		1.04	22.79																					100
46A	7	1	Phlogopite	38.68	6.61	15.4	14.67		15.69		0.55	8.4																			100
46A	7	2	Phlogopite	36.92	8.76	16.55	10.03		17.1		0.57	8.91															1.16				100
46A	7	3	Celsian	42.31		23.05	1.03		0.86			4.36													28.37						99.98
46A	7	4	Calcite	10.14		4.95	4.84	0.85	2.64	75.71		0.87																			100
46A	7	5	Phlogopite	37.54	8.04	15.46	10.68		17.53		0.47	9.35															0.94				100.01
46A	7	6	Phlogopite	37.2	9.21	15.85	10.14		17.11			9.18															1.29				99.98
46A	7	7	Phlogopite	37.16	7.09	16.5	13.62		17.51			8.11																			99.99
46A	7	8	Phlogopite	35.13	8.29	15	10.42		16.57	4.55	0.57	8.48															1.01				100.02
46A	7	9	Ba-feldspar	51.21		20.43	0.75		0.65	0.62	1.11	7.24													18						100.01
46A	7	10	Calcite	1.6		0.76	2.6	1.55	1.58	91.93																		0			100.02
46A	7	11	Ba-feldspar	46.74		20.44	2.01		2.22		0.49	6.53													21.57						100
46A	7	12	Phlogopite	34.27	8.89	15.08	10.34		15.85	5.85	0.51	8.09															1.1				99.98
46A	7	13	Phlogopite	36.88	9.36	16.06	10.38		16.96		0.51	8.65															1.21				100.01
46A	7	14	Calcite	1.9		1.04	3.96		3.1	90																					100
47E	1	1	Chlorite	36.34		20.31	21.99		20.33												1.03										100
47E	1	2	Quartz	99.41																	0.59										100
47E	1	3	Pyrite				27.29							72.27							0.46										100.02

Sample	Site	Pos.	Mineral	SiO_2	TiO_2	Al_2O_3	FeO_t	MnO	MgO	CaO	Na_2O	K_2O	P_2O_5	SO_3	F	Cl	V_2O_5	Cr_2O_3	CoO	NiO	ZnO	SrO	ZrO_2	MoO_3	BaO	La_2O_3	Ce_2O_3	Yb_2O_3	WO_3	PbO	Total
47E	1	4	Pyrite				27.23							72.07							0.72										100.02
47E	1	5	Pyrite				27.36							71.97							0.67										100
47E	1	6	Pyrite				27.18							72.17							0.65										100
47E	1	7	Pyrite				27.45							72.04							0.52										100.01
47E	1	8	Mix	49.69		19.61	11.27		12.88		3.9	1.84									0.81										100
47E	2	1	Pyrite				28.01							71.99																	100
47E	2	2	Pyrite				26.69							73.31																	100
47E	2	3	Pyrite				27.87							72.14																	100.01
47E	2	4	Pyrite				27.47							72.54																	100.01
47E	2	5	Barite											38.83											61.19						100.02
47E	2	6	Quartz	99.99																											99.99
47E	2	7	Quartz	99.99																											99.99
47E	2	8	Quartz	99.99																											99.99
47E	2	9	Olivine	37.01		19.5	18.9		24.59																						100
47E	2	10	Titanite	34.16	37.21	2.78				25.84																					99.99
47E	2	11	Quartz	96.11						1.93			1.95																		99.99
47E	2	12	Barite											39.08											60.92						100
47E	2	13	Barite											38.6											61.4						100
47E	2	14	Barite											38.33											61.68						100.01
47E	2	15	Barite											40.2											59.8						100
47E	2	16	Barite											39.4											60.6						100
47E	2	17	Barite											38.23											61.78						100.01
47E	3	1	Pyrite				27.53							72.46																	99.99
47E	3	2	Pyrite				27.32							72.69																	100.01
47E	3	3	Pyrite				27.74							72.27																	100.01
47E	3	4	Pyrite				27.54							72.46																	100
47E	3	5	Alstonite + Qartz	53.74		18.4				10.02		8.46													9.39						100.01
47E	3	6	Calcite							100																					100
47E	3	7	Pyrite				27.54							72.46																	100
47E	3	8	Chlorite	36.71		20.07	20.71		22.5																						99.99
49B	1	1	Pyrite				28.03							71.97																	100
49B	1	2	Calcite				1.09			98.91																					100
49B	1	3	K-feldspar	65.67		18.14						15.37													0.8						99.98
49B	1	4	Albite	69.42		18.44					12.13																				99.99
49B	1	5	Calcite				1.3			98.7																					100
49B	1	6	Calcite							100																					100
49B	1	7	Pyrite				27.85							72.14																	99.99
49B	1	8	Calcite					0.8		99.19																					99.99
49B	1	9	Albite	69.14		18.69					12.19																				100.02
49B	1	10	Mix	67.88		18.9	0.75				9.3	3.17																			100
49B	1	11	Calcite	2.18						97.16		0.66																			100
49B	1	12	Albite	69.03		18.61					12.36																				100
49B	1	13	Calcite				1.22			98.78																					100
49B	1	14	K-feldspar	66.42		17.8						15.78																			100
49B	1	15	K-feldspar	66.42		17.74						15.82																			99.98
49B	1	16	Pyrite				27.96							72.04																	100
49B	2	1	Pyrite				27.81							71.84							0.35										100
49B	2	2	Pyrite				27.45							72.04							0.52										100.01
49B	2	3	K-feldspar	65.93		17.84						15.74									0.49										100

Sample	Site	Pos.	Mineral	SiO_2	TiO_2	Al_2O_3	FeO_t	MnO	MgO	CaO	Na_2O	K_2O	P_2O_5	SO_3	F	Cl	V_2O_5	Cr_2O_3	CoO	NiO	ZnO	SrO	ZrO_2	MoO_3	BaO	La_2O_3	Ce_2O_3	Yb_2O_3	WO_3	PbO	Total
49B	2	4	Albite	69.07		18.25					12.21										0.46										99.99
49B	2	5	K-feldspar	65.97		17.89						15.66									0.47										99.99
49B	2	6	Albite	68.41		19.05					12.55																				100.01
49B	2	7	Pyrite				27.47							72.04							0.49										100
49B	2	8	Orthoclase	66.83		18.29					5.99	8.43									0.45										99.99
49B	2	9	Calcite		4.59		1.07			93.26											1.08										100
49B	2	10	Pyrite				27.94							71.62							0.45										100.01
49B	2	11	Calcite				1.11			98.14											0.75										100
49B	2	12	Fluoroapatite	2.99		2.1	3.04		0.81	41.82			40.31		8.39						0.52										99.98
49B	2	13	K-feldspar	64.8		17.99						15.04									0.61				1.55						99.99
49B	2	14	Albite	68.75		18.61					12.65																				100.01
49B	2	15	K-feldspar	65.8		17.89						15.66									0.65										100
49B	2	16	Pyrite				27.81							71.69							0.5										100
49B	2	17	K-feldspar	65.65		17.97						15.24									0.34				0.82						100.02
49B	2	18	Albite	69.1		18.65					11.95	0.3																			100
49B	2	19	Albite	69.44		18.29					12.28																				100.01
49B	2	20	Fluoroapatite	6.5		3.51	8.27		1.59	35.57			37.9		6.01						0.65										100
49B	2	21	Chlorite	30.57	10.28	17.82	22.64		17.2									0.98			0.52										100.01
49B	3	1	Rutile	7.38	70.68	4.06	7.81		3.2					6.09							0.8										100.02
49B	3	2	Calcite				1.2			97.97											0.83										100
49B	3	3	Chlorite	33.29		25.02	27.93		11.92	1.29											0.55										100
49B	3	4	Calcite		9.79		0.84			88.43											0.96										100.02
49B	3	5	Rutile + Others	14.01	66.94	6.97	6.72		3.03			0.81						0.73			0.78										99.99
49B	3	6	Albite	68.95		18.95					12.11																				100.01
49B	3	7	Albite	68.24	0.38	18.63					12.23	0.52																			100
49B	3	8	Chlorite + K2O	35.06		22.24	28.78		12.19			0.76						0.42			0.55										100
49B	3	9	Chlorite	32.15		23.56	32.81		10.56									0.38			0.56										100.02
49B	3	10	Chlorite	38.23		21.18	26.73		13.36												0.49										99.99
49B	3	11	Rutile		93.73					5.54											0.72										99.99
49B	3	12	Rutile + Others	6.78	68.04	3.87	7.38		3.38	9.92											0.62										99.99
49B	3	13	Rutile + Others	13.39	62.7	6.93	10.42		6.12	0.45											0										100.01
49B	3	14	Rutile	3.14	92.58	1.28	1.3		1.28												0.42										100
49B	3	15	Chlorite + CaO	33.5	0.48	24	27.54		11.97	1.8											0.68										99.97
49B	3	16	Calcite				0.96			97.99											1.05										100
49B	3	17	Calcite				1.02			97.62											1.37										100.01
49B	4	1	Pyrite				28.2							71.82																	100.02
49B	4	2	Calcite				1.07			98.25		0.69																0			100.01
49B	4	3	K-feldspar	65.78		17.95						15.31													0.96						100
49B	4	4	K-feldspar	66.25		17.84						15.92																			100.01
49B	4	5	K-feldspar	66.49		17.76						15.73																			99.98
49B	4	6	K-feldspar	65.42		17.25					0.53	15.14		0.8											0.85						99.99
49B	4	7	Albite	69.72		18.71					11.57																				100
49B	4	8	Calcite							100																					100
49B	4	9	Calcite				1.02			98.98																					100
49B	4	10	Pyrite				27.89							72.12																	100.01
49B	4	11	Albite	69.22		18.54					12.24																				100
49B	4	12	K-feldspar	66.34		17.97						15.7																			100.01
49B	4	13	K-feldspar	66.44		17.91						15.63																			99.98
49B	4	14	Chlorite	34.08		26.36	29.72		9.85																						100.01

Sample	Site	Pos.	Mineral	SiO_2	TiO_2	Al_2O_3	FeO_t	MnO	MgO	CaO	Na_2O	K_2O	P_2O_5	SO_3	F	Cl	V_2O_5	Cr_2O_3	CoO	NiO	ZnO	SrO	ZrO_2	MoO_3	BaO	La_2O_3	Ce_2O_3	Yb_2O_3	WO_3	PbO	Total
49B	4	15	Chlorite	35.68		24.79	28.02		10.98								0.52														99.99
49B	4	16	Calcite	1.43						97.5		1.08																0			100.01
49B	4	17	Albite	69.01		18.9					12.09																				100
49B	4	18	Albite	68.95		18.57					12.09	0.4																			100.01
49B	4	19	Albite	68.65	0.75	18.48					11.46	0.67																			100.01
49B	4	20	Albite	66.57	3.3	18.18					11.53	0.42																			100
49B	4	21	K-feldspar	66.4		17.95						15.66																			100.01
49B	4	22	K-feldspar	66.06		17.95						15.97																			99.98
49B	4	23	K-feldspar	66.91		17.54						15.55																			100
49B	4	24	K-feldspar	66.44		17.76					0.53	15.26																			99.99
49B	4	25	K-feldspar	66.87		17.65						15.47																			99.99
49B	4	26	K-feldspar	66.68		17.74						15.57																			99.99
49B	4	27	K-feldspar	66.79		18.03						15.18																			100
49B	4	28	Pyrite				27.48							72.54																	100.02
49B	5	1	Pyrite				28.1							71.92																	100.02
49B	5	2	Pyrite				28.14							71.87																	100.01
49B	5	3	K-feldspar	66.06		17.95						15.98																			99.99
49B	5	4	K-feldspar	65.63		18.2						15.13													1.05						100.01
49B	5	5	Calcite				1.44			98.56																					100
49B	5	6	Calcite				0.9			99.11																					100.01
49B	5	7	Calcite				0.77			99.23																					100
49B	5	8	Calcite				1			99.01																					100.01
49B	5	9	Albite	69.12		18.65					11.69	0.55																			100.01
49B	5	10	Albite	68.9		18.82					12.28																				100
49B	5	11	Albite	69.44		18.76					11.78																				99.98
49B	5	12	Albite	69.29		18.74					11.96																				99.99
49B	5	13	Albite	69.35		18.56					12.09																				100
49B	5	14	K-feldspar	65.25		18.37						15.43													0.96						100.01
49B	5	15	Albite	69.74		18.54					11.73																				100.01
49B	5	16	K-feldspar	66.08		18.05						15.24													0.63						100
49B	5	17	Calcite				1.58			98.42																		0			100
49B	5	18	Rutile + Others	4.56	83.27	2.91	4.46		2.24	0.27				2.32																	100.03
49B	5	19	Pyrite				27.75							72.27																	100.02
49B	5	20	Pyrite + Others	10.03	7.59	6.86	27.02		5.02	6.74				36.76																	100.02
49B	5	21	Calcite	6.97		2.19		0.79		88.71	1.32																				99.98
49B	5	22	Calcite							100																					100
49B	5	23	K-feldspar	66.51		17.8						15.7																			100.01
456A	1	1	Clinopyroxene	46.78	2.85	8.35	6.3		12.7	23																					99.98
456A	1	2	Clinopyroxene	50.38	1.85	5.91	4.66		14.16	23.03																					99.99
456A	1	3	Clinopyroxene	47.25	2.25	8.54	5.47		13.02	22.92								0.57													100.02
456A	1	4	Clinopyroxene	49.16	2.4	6.01	6.81		13.02	22.21								0.41													100.02
456A	1	5	Clinopyroxene	49.82	1.75	6.2	5.87		13.33	23.03																					100
456A	1	6	Clinopyroxene	51.58	0.83	3.04	11.73	0.37	10.25	21.34	0.84																				99.98
456A	1	7	Clinopyroxene + K20	53.99	1.1	6.22	9.84		7.74	17.07	1.31	2.73																			100
456A	1	8	Clinopyroxene	51.4	1.1	3.31	12.81	0.41	9.29	20.29	1.39																				100
456A	1	9	Clinopyroxene	47.58	3.07	6.2	10.2	0.36	11.36	21.23		0																			100
456A	1	10	Clinopyroxene	49.82	0.97	6.76	9.88		12.55	19.25	0.77																				100
456A	1	11	Clinopyroxene	47.6	2.19	8.58	7.19		11.84	21.79	0.82																				100.01
456A	1	12	Clinopyroxene	48.15	2.04	7.69	4.59		13.22	23.94								0.38													100.01

Sample	Site	Pos.	Mineral	SiO_2	TiO_2	Al_2O_3	FeO_t	MnO	MgO	CaO	Na_2O	K_2O	P_2O_5	SO_3	F	Cl	V_2O_5	Cr_2O_3	CoO	NiO	ZnO	SrO	ZrO_2	MoO_3	BaO	La_2O_3	Ce_2O_3	Yb_2O_3	WO_3	PbO	Total
456A	1	13	Clinopyroxene	48.26	2.72	7.18	5.9		12.9	23.03																					99.99
456A	1	14	Clinopyroxene + TiO2	43.64	10.09	5.05	6.72		11.09	23.41																					100
456A	1	15	Clinopyroxene	47	2.89	8.22	6.27		12.35	23.3																					100.03
456A	1	16	Clinopyroxene	49.27	2.04	6.37	4.76		13.95	23.35								0.26													100
456A	1	17	Clinopyroxene	49.82	1.85	6.25	4.49		13.91	23.35								0.31													99.98
456A	1	18	Clinopyroxene	48.28	2.15	7.86	4.81		13.18	23.17								0.54													99.99
456A	1	19	Clinopyroxene	49.37	1.85	9.75	4.67		12.2	20.96		0.88						0.32													100
456A	1	20	Clinopyroxene	51.51	0.98	3.72	11	0.34	9.95	21.23	1.27																				100
456A	1	21	Clinopyroxene	52.03	0.75	2.72	12.88	0.45	9.29	20.62	1.25																				99.99
456A	1	22	Clinopyroxene	55.47		14.17	3.4		3.71	10.56		8.9													3.79						100
456A	1	23	Clinopyroxene	48.52	1.4	7.22	7.94		11.11	20.54	2.31	0.96																			100
456A	1	24	Clinopyroxene	52.11	0.82	3.34	10.24		10.66	21.74	1.08																				99.99
456A	1	25	Clinopyroxene	52.2	0.62	2.14	13.28	0.44	9.35	20.83	1.15																				100.01
456A	1	26	Clinopyroxene	51.75	0.62	2.48	12.9	0.37	9.37	21.72	0.8																				100.01
456A	1	27	Clinopyroxene + others	33.65	6.31	10.83	22.14	0.4	9.8	14.8	1	0.26						0.82													100.01
456A	1	28	Titanite	34.93	29.07	3.67	1.48		1.87	28.99																					100.01
456A	1	29	Clinopyroxene	50.34	1.65	6.18	4.48		14.26	22.64								0.45													100
456A	1	30	Clinopyroxene	47.96	2.17	7.86	5.27		13.38	22.92								0.44													100
456A	1	31	Clinopyroxene	45.16	3.5	10.47	6.01		11.89	22.97																					100
456A	1	32	Clinopyroxene	48.75	1.65	7.41	7.15	0.4	11.34	23.28																					99.98
456A	2	1	Clinopyroxene	46.57	2.94	7.43	6.5		12.19	23.91	0.47																				100.01
456A	2	2	Clinopyroxene	46.36	2.9	7.86	6.51		12.17	24.22																					100.02
456A	2	3	Clinopyroxene	47.88	2.27	7.07	5.13		13.45	23.83								0.37													100
456A	2	4	Clinopyroxene	51.26	1.42	3.44	7.51		12.54	23.35	0.49																				100.01
456A	2	5	Clinopyroxene	44.69	0.48	10.39	11.32	0.65	11.64	20.02	0.5							0.31													100
456A	2	6	Clinopyroxene	50.57	0.38	3.65	11.89	0.35	11.41	21.04	0.73																				100.02
456A	2	7	Clinopyroxene	50.19	1.6	4.74	5.75		13.58	24.12																					99.98
456A	2	8	Clinopyroxene	47.92	2.25	7.22	5.09		13.12	23.94								0.45													99.99
456A	2	9	Clinopyroxene	45.99	2.87	7.37	6.86		12.52	24.4																					100.01
456A	2	10	Clinopyroxene	49.05	2	6.01	4.64		13.6	24.19								0.5													99.99
456A	2	11	Oxyhornblende (Alt)	37.61	2.32	15.32	16.53		16.86	10.12		1.24																			100
456A	2	12	Clinopyroxene	49.86	1.47	3.99	8.22		12.1	22.99	1	0.36																			99.99
456A	2	13	Clinopyroxene	48.94	1.8	5.63	6.95		13.02	23.66																					100
456A	2	14	Clinopyroxene	44.35	1.22	10.07	13.25	0.3	14.03	16.79																					100.01
456A	2	15	Clinopyroxene	52.99	0.37	1.1	10.65	0.3	11.79	21.72	1.08																				100
456A	2	16	Clinopyroxene	49.86	1.7	4.55	6.38		13.35	24.15																					99.99
456A	2	17	Clinopyroxene	51.98	1	2.02	8.01		12.88	23.38	0.73																				100
456A	2	18	Clinopyroxene	49.01	2.34	5.63	6.45		12.64	23.95																					100.02
456A	2	19	Clinopyroxene	49.61	1.78	5.56	6.96		12.12	22.23	1.25	0.51																			100.02
456A	2	20	Clinopyroxene	52.92	0.47	1.34	8.74		12.62	23.3	0.61																				100
456A	2	21	Clinopyroxene	53.48	0.38	1.02	9.71		12.17	22.53	0.69																				99.98
456A	2	22	Clinopyroxene	53.35	0.57	1.25	9.16		12.57	22.39	0.71																				100
456A	2	23	Clinopyroxene	52.03	0.7	2.46	8.77	0.3	12.32	23.44																					100.02
456A	2	24	Clinopyroxene	48.71	2.15	6.05	5.15		13.8	23.88								0.29													100.03
456A	2	25	Clinopyroxene	47.34	3.32	6.78	6.82		12.27	23.45																					99.98
456A	2	26	Oxyhornblende (Alt)	44.79	0.38	14.21	14.29	0.3	16.03	6.09		3.89																			99.98
456A	3	1	Clinopyroxene	45.35	2.7	9.62	7.95		11.91	22.47																					100
456A	3	2	Clinopyroxene	52.39	1.05	3.46	7.69		13.02	21.7	0.69																				100
456A	3	3	Clinopyroxene	53.09	0.63	2.82	8.56	0.36	12.39	20.97	1.2																				100.02

Sample	Site	Pos.	Mineral	SiO_2	TiO_2	Al_2O_3	FeO_t	MnO	MgO	CaO	Na_2O	K_2O	P_2O_5	SO_3	F	Cl	V_2O_5	Cr_2O_3	CoO	NiO	ZnO	SrO	ZrO_2	MoO_3	BaO	La_2O_3	Ce_2O_3	Yb_2O_3	WO_3	PbO	Total
456A	3	4	Clinopyroxene	53.65	0.78	2.72	8.13		12.47	21.13	1.12																				100
456A	3	5	Clinopyroxene	53.22	0.68	2.85	8.36		12.68	21.2	1																				99.99
456A	3	6	Clinopyroxene	52.17	1.12	4.04	8.66		12.07	20.71	1.2																				99.97
456A	3	7	Clinopyroxene	45.74	0.88	5.57	9.79		11.11	25.54	1.36																				99.99
456A	3	8	Clinopyroxene	51.9	1.13	3.8	8.76		12.14	21.16	1.11																				100
456A	3	9	Clinopyroxene	51.62	1.12	3.8	8.57		12.42	21.38	1.09																				100
456A	3	10	Clinopyroxene	52.17	1.05	3.72	8.56		12.49	21	1.01																				100
456A	3	11	Clinopyroxene	52.09	1.12	3.99	8.92		11.72	20.74	1.42																				100
456A	3	12	Clinopyroxene	51.58	1.15	4.5	9.15		11.56	20.78	1.28																				100
456A	3	13	Clinopyroxene	50.96	1.05	4.01	8.7		11.26	22.97	1.05																				100
456A	3	14	Clinopyroxene	47.7	2.84	8.14	4.62		13.51	22.72								0.47													100
456A	3	15	Clinopyroxene	48.47	0.77	17.23	11.59		11.09	5.58		5.25																			99.98
456A	3	16	Clinopyroxene	48.26	2.19	7.48	4.55		13.71	23.23								0.58													100
456A	3	17	Clinopyroxene	52.71	1.08	2.83	7.69		13.32	22.37																					100
456A	3	18	K-feldspar	59.21		18.01	1.25		0.88	2.62		11.47													6.55						99.99
456A	3	19	K-feldspar	61.82		17.82	2.53		1.03	1.94		13.3													1.54						99.98
456A	3	20	Clinopyroxene	51.45	1.1	4.35	9.1		11.51	21.27	1.21																				99.99
456A	3	21	Clinopyroxene	52.2	1.18	3.82	8.77		11.91	20.88	1.25																				100.01
456A	3	22	Clinopyroxene	52.28	1.15	3.51	8.67		12.15	20.81	1.42																				99.99
456A	3	23	Clinopyroxene	49.84	1.93	5.99	6.27		13.38	22.6																					100.01
456A	3	24	Clinopyroxene	45.67	1.98	8.81	6.97		9.48	26.56	0.51																				99.98
456B1	1	1	Oxyhornblende (Alt)	46.33	2.14	13.4	9.83		10.93	11.54		3.44	1.86								0.52										99.99
456B1	2	1	Oxyhornblende (Alt)	45.12	2.29	11	10.45		13.99	12.96	0	1.66	2.02								0.55										100.04
456B1	2	2	Oxyhornblende (Alt)	45.59	2.44	13	11.12		11.26	11.42	0.98	2.87	1.33																		100.01
456B1	2	3	Oxyhornblende (Alt)	45.93	1.75	14.06	10.27		11.66	11.29	1.78	3.28																			100.02
456B1	3	1	Oxyhornblende (Alt)	45.42	3.4	11.47	8.86		11.54	14.13		2.83	2.34																		99.99
456B1	3	2	Oxyhornblende (Alt)	48.24	2.75	13.49	8.67		8.39	12.16		4.34	1.95								0										99.99
456B1	3	3	Oxyhornblende (Alt)	46.01	2.75	12.26	10.65		10.83	13.24		2.65	1.6																		99.99
456B1	3	4	Calcite	5.6		2.04	1.62			90.72																					99.98
456B1	3	5	Ba-feldspar	47.49		23.37					0.85	5.97													22.32						100
456B1	3	6	Oxyhornblende (Alt)	41.97	2.69	12.17	12.59		12.35	14.2		1.41	2.61																		99.99
456B1	3	7	Oxyhornblende (Alt)	45.91	2.3	13.72	10.46	0.4	10.02	12.28		3.59	1.31								0										99.99
456B1	3	8	Oxyhornblende (Alt)	45.46	2.35	12.7	10.77	0.3	10.6	12.65		2.98	1.79								0.41										100.01
456B1	3	9	Oxyhornblende (Alt)	44.99	3.65	10.56	12.49		11.71	16.59																					99.99
456B1	4	1	Ba-feldspar	47.06		24.17						6.4									0.46				21.92						100.01
456B1	4	2	Calcite + Mix	18.82	1.22	8.07	8.75		7.96	54.75		0.45																			100.02
456B1	4	3	Oxyhornblende (Alt)	45.63	2.39	13.3	10.97		10.88	12.82		2.63	1.35																		99.97
456B1	4	4	Oxyhornblende (Alt)	43.98	2.19	13.08	11.96		12.47	12.24		2.23	1.86																		100.01
456B1	4	5	Oxyhornblende (Alt)	45.93	2.64	12.77	10.38		10.6	12.59		3.16	1.63								0.3										100
456B1	5	1	Chlorite	39.64		18.97	15.5		23.03	1.65		1.2																			99.99
456B1	5	2	Chlorite	35.96		20.6	19		23.99			0.45																			100
456B1	5	3	K-feldspar	64.2		18.37	0.77		0.66			14.01													2						100.01
456B1	5	4	Chlorite +K20	37.01		20.44	17.88		23.16			1.48																			99.97
456B1	5	5	Chlorite +K20	36.69		19.92	18.45	0.58	23.58			0.79																			100.01
456B1	5	6	Mix -?	43.9	10.84	5.16	5.02		9.62	24.46								1.01													100.01
456B1	5	7	Chlorite	36.56		19.76	19.45		23.43			0.82																			100.02
456B1	5	8	Albite	68.95		19.24					11.84																				100.03
456B1	5	9	Albite	70.21		19.82					9.96																				99.99
456B1	5	10	Chlorite	36.52		20.41	19		23.18			0.89																			100

Sample	Site	Pos.	Mineral	SiO_2	TiO_2	Al_2O_3	FeO_t	MnO	MgO	CaO	Na_2O	K_2O	P_2O_5	SO_3	F	Cl	V_2O_5	Cr_2O_3	CoO	NiO	ZnO	SrO	ZrO_2	MoO_3	BaO	La_2O_3	Ce_2O_3	Yb_2O_3	WO_3	PbO	Total
456B1	5	11	Albite	68.65		19.39					11.99																				100.03
456B1	5	12	Oxyhornblende (Alt)	39.7		17.74	15.33		21.42	4.46		1.32																			99.97
456B1	5	13	Oxyhornblende (Alt)	39.92	0.97	16.29	13.26		16.65	9.84		2.7						0.39													100.02
456B1	5	14	Albite	68.22		19.2				0.42	12.16																				100
456B1	5	15	Oxyhornblende (Alt)	44.17	2.07	10.66	9.73		14.86	14.66		1.24	2.61																		100
456B1	5	16	Albite	68.73		19.03					11.53	0.7																			99.99
456B1	5	17	Galena + Mix	20.15		9.15						5.28		19.53																45.9	100.01
456B1	5	18	Pentlandite	1.67		1.51	17.79		1.92					48.99					5.98	22.13											99.99
456B1	6	1	Pentlandite				17.89							52.14					6.27	23.71											100.01
456B1	6	2	Chlorite	36.71		19.78	18.77	0.44	23.43			0.87																			100
456B1	6	3	Albite	67.58		18.76	1		0.88		11.45	0.33																			100
456B1	6	4	Chlorite	38.31		20.61	17.92		22			1.14																			99.98
456B1	6	5	Wulfenite																					28.99						71.02	100.01
456B1	6	6	K-feldspar	64.77		18.8						14.13													2.31						100.01
456B1	6	7	Titanite	34.55	33.88	2.27	1.49		0.78	26.32								0.73													100.02
456B1	6	8	Albite	67.79		19.22	0.62		0.61		11.77																				100.01
456B1	6	9	K-feldspar	58.96		19.52	2.24		2.4			11.9													5						100.02
456B1	6	10	Chlorite + TiO2	32.97	10.14	8.62	16.02		4.74	19.94								7.57													100
456B1	6	11	Allanite	41.09		25.02	10.14		0.85	14.75																3.07	5.08				100
456B1	6	12	Chlorite + K20	42.55		15.46	14.65		20.36	1.75		5.23																			100
456B1	6	13	K-feldspar	64		18.27	0.42					14.84													2.46						99.99
456B1	7	1	Albite	68.33		19.03				0.39	12.27																				100.02
456B1	7	2	Chlorite	38.42		18.74	17.08		18.31	6.97		0.47																			99.99
456B1	7	3	Albite	68.65		19.52					11.82																				99.99
456B1	7	4	Chlorite	38.51		18.88	17.08		24.39			1.16																			100.02
456B1	7	5	Clinopyroxene	50.53	1.75	6.14	4.62		15.06	21.91																					100.01
456B1	7	6	K-feldspar	64.84		18.57						14.55													2.04						100
456B1	7	7	Albite	68.65		19.12	0.35				11.88																				100
456B1	7	8	Chlorite + K20	42.63		16.06	15.5		22.07			3.73																			99.99
456B1	7	9	Clinopyroxene	55.36	1.08	1.76	6.57		13.17	22.07																					100.01
456B1	7	10	Albite	68.43		18.78				0.42	11.2	1.16																			99.99
456B1	7	11	Titanite	34.48	26.11	5.44	4.94		4.76	22.25								2.03													100.01
456B1	7	12	Clinopyroxene	53.99	0.6	3.27	7.73		13.9	20.5																					99.99
456B1	7	13	Chlorite	37.65		19.56	17.87	0.43	22.98			1.52																			100.01
456B1	7	14	Chlorite	38.08		19.25	17.48		23.76	1.08		0.35																			100
456B1	7	15	Titanite	30.91	20.62	11.79	12.56		6.75	16.78								0.58													99.99
456B1	7	16	Clinopyroxene	54.4	1.45	9.9	4.79		9.5	15.8		4.14																			99.98
456B1	8	1	Chlorite	37.26		19.58	18.06		24.34			0.76																			100
456B1	8	2	Pentlandite				18.27							52.79					6.14	22.8											100
456B1	8	3	Albite	68.78		19.12					12.11																				100.01
456B1	8	4	K-feldspar	67.81		19.16	0.85		0.8		7.91	3.44																			99.97
456B1	8	5	Titanite	34.23	35.3	1.81	1.18			26.36		0.3						0.83													100.01
456B1	8	6	Chlorite + K20	39.43		17.61	14.95		15.97	9.96		2.07																			99.99
456B1	8	7	Chlorite + K20	39.94		17.67	16.47		22.63	0.87		2.43																			100.01
456B1	8	8	Chlorite + K20	42.4	0.67	15.23	14.23		18.92	6.31		2.25																			100.01
456B1	8	9	Clinopyroxene	48.73	2.79	7.2	6.47		13.23	21.58																					100
456B1	8	10	Chlorite + K20	37.35		19.95	18.27		23.83			0.59																			99.99
456B1	8	11	Chlorite + K20	40.41		16.95	16.39		22.52			3.71																			99.98
456B1	8	12	Albite	68.07		19.27	0.57		0.73		11.1	0.28																			100.02

Sample	Site	Pos.	Mineral	SiO_2	TiO_2	Al_2O_3	FeO_t	MnO	MgO	CaO	Na_2O	K_2O	P_2O_5	SO_3	F	Cl	V_2O_5	Cr_2O_3	CoO	NiO	ZnO	SrO	ZrO_2	MoO_3	BaO	La_2O_3	Ce_2O_3	Yb_2O_3	WO_3	PbO	Total
456B1	8	13	Chlorite + K20	36.75		19.97	17.46	0.49	24.23			1.11																			100.01
456B1	8	14	Chlorite + K20	37.12		20.07	18.23		23.93			0.66																			100.01
456B1	8	15	Clinopyroxene	49.12	2.05	7.1	7.68		13.3	20.76																					100.01
456B1	8	16	Clinopyroxene	50.19	1.75	6.73	4.99		14.82	21.52																					100
456B1	8	17	Titanite + others	34.89	14.26	8.09	8.34		3.18	24.86								6.37													99.99
456B1	8	18	Albite	68.67		19.16					12.17																				100
456B1	8	19	Titanite	32.43	33.33	2.27	0.67			28.39			2.91																		100
456B1	8	20	Pentlandite	1.28		1	18.01		1.26					50.72					5.57	22.14											99.98
456B1	8	21	Fluoroapatite	6.5		1.57	0.59			42.27	0.81		42		5.74	0.54															100.02
456B2	1	1	Ba-feldspar	53.05		22.16						8.44													16.36						100.01
456B2	1	2	Ba-feldspar	45.54		38.17						8.52													7.77						100
456B2	1	3	Ba-feldspar	45.48		38.89						8.17													7.48						100.02
456B2	1	4	Ba-feldspar	51.73		31.78						9.9													6.58						99.99
456B2	1	5	Ba-feldspar	53.09		22.92						8.59													15.41						100.01
456B2	1	6	Calcite	5.22		4.88				89.12		0.78																			100
456B2	1	7	Albite	68.95		19.01					12.05																				100.01
456B2	1	8	Albite	68.6		19.12					12.27																				99.99
456B2	1	9	Ba-feldspar	45.61		24.81						4.99													24.6						100.01
456B2	1	10	Oxyhornblende (Alt)	44.24	2.07	10.01	11.87		14.34	15.57			1.63			0.25															99.98
456B2	1	11	Oxyhornblende (Alt)	43.68	1.93	10.85	12.5		13.53	14.93		0.82	1.76																		100
456B2	1	12	Oxyhornblende (Alt)	43.25	2.19	10.6	12.4		14.58	14.92		0.36	1.72																		100.02
456B2	1	13	Titanite	36.32	31.64	3.63	1.74			26.65																					99.98
456B2	1	14	Titanite	30.16	20.63	8.31	9.15		7.18	20.09			4.47																		99.99
456B2	1	15	Oxyhornblende (Alt)	43.4	2.17	10.11	12.66	0.36	14.19	15.56			1.56																		100.01
456B2	1	16	Oxyhornblende (Alt)	45.27	0.58	18.57	11.62		10.86	6.94		4.61	1.56																		100.01
456B2	1	17	Mix	42.25		23.88	11.13		3.3	17.25																	2.19				100
456B2	1	18	Chlorite	27.62		15.57	13.53		18.07	25.19																					99.98
456B2	2	1	Oxyhornblende (Alt)	44.77	1.97	12.47	10.7		11.84	14.15		2.2	1.88																		99.98
456B2	2	2	Oxyhornblende (Alt)	44.11	2.42	13.04	11.77		12.29	13.03		1.72	1.63																		100.01
456B2	2	3	Oxyhornblende (Alt)	42.89	2.35	13.51	12.52		13.2	12.12		1.84	1.56																		99.99
456B2	2	4	Oxyhornblende (Alt)	41.78	2.44	11.66	12		13.46	14.48	0.84	1.02	2.31																		99.99
456B2	2	5	Ba-feldspar	51.92		21.26	7.17		6.53	3.65		7.22													2.24						99.99
456B2	2	6	Ba-feldspar	53.82		22.18						8.72													15.26						99.98
456B2	2	7	Ba-feldspar	54.34		21.33						9.48													14.86						100.01
456B2	2	8	Oxyhornblende (Alt)	42.76	2.04	11.39	12.09	0.41	13.81	14.76		0.64	2.11																		100.01
456B2	2	9	Oxyhornblende (Alt)	44.35	2.14	11.92	11.71		13.2	14.1		1.16	1.42																		100
456B2	3	1	Chlorite + K2O	36.82		20.71	18.11		23.05			1.31																			100
456B2	3	2	Chlorite	37.69		19.5	18.2	0.43	23.51			0.67																			100
456B2	3	3	Chlorite	35.92		20.46	18.4		23.98			0.77						0.47													100
456B2	3	4	Albite	68.41		19.16	0.42				12.01																				100
456B2	3	5	Clinopyroxene	50.38	1.7	6.61	4.22		15.19	21.52								0.38													100
456B2	3	6	Clinopyoxene + TiO2	38.27	12.13	9.16	10.79		3.55	26.12																					100.02
456B2	3	7	Clinopyroxene	53.2	1.4	4.36	6.65		12.64	21.74																					99.99
456B2	3	8	Titanite	33.99	23.12	8.3	9.21		4.46	20.93																					100.01
456B2	3	9	Pentlandite				17.88							52.39					6.6	23.13											100
456B2	3	10	Pentlandite				18.24							53.01					6.18	22.59											100.02
456B2	3	11	Titanite	34.85	27.19	5.5	5.13		5.07	20.53								1.74													100.01
456B2	3	12	Chlorite + K2O	38.31		19.24	17.55		23.66			1.24																			100
456B2	3	13	Titanite	28.71	20.53	9.07	9.34	0.76	3.61	22.9								5.09													100.01

Sample	Site	Pos.	Mineral	SiO_2	TiO_2	Al_2O_3	FeO_t	MnO	MgO	CaO	Na_2O	K_2O	P_2O_5	SO_3	F	Cl	V_2O_5	Cr_2O_3	CoO	NiO	ZnO	SrO	ZrO_2	MoO_3	BaO	La_2O_3	Ce_2O_3	Yb_2O_3	WO_3	PbO	Total
456B2	3	14	Titanite	35.57	28.67	4.86	4.19		4.61	21.81		0.29																			100
456B2	3	15	Clinopyroxene	50.76	1.57	6.18	4.36		14.69	22.02								0.42													100
456B2	3	16	Clinopyroxene	46.78	3.39	9.86	6.25		12.15	21.56																					99.99
456B2	3	17	Chlorite + K2O	36.9		19.8	18.23	0.44	23.45			1.18																			100
456B2	3	18	Titanite	34.57	33.44	3.27	1.85		1.84	25.02																					99.99
456B2	3	19	Titanite	35.28	34.63	2.55	0.95			26.58																					99.99
456B2	3	20	Chlorite + K2O	37.37		19.92	18.01		23.98			0.73																			100.01
456B2	3	21	Titanite	35.02	32.83	2.85	2.5		1.66	25.13																					99.99
456B2	3	22	Clinopyroxene	48.41	2.54	7.88	6.02		13.27	21.88																					100
456B2	3	23	Clinopyroxene	53.44	3.05	2.31	6.7		12.72	21.79																					100.01
456B2	3	24	Clinopyroxene	49.57	2.5	7.24	5.76		13.51	21.42																					100
456B2	4	1	Chlorite + K2O	37.78		19.61	17.75		23.73			1.11																			99.98
456B2	4	2	Chlorite + K2O	37.39		20.46	18.1		23.73			0.34																			100.02
456B2	4	3	Albite	67.56		19.1	0.51		0.9		11.28	0.64																			99.99
456B2	4	4	Ba-feldspar	45.42		24.38						4.71													25.5						100.01
456B2	4	5	Ba-feldspar	51.79		22.84						7.08													18.28						99.99
456B2	4	6	Titanite	34.89	35.01	3.38				26.71																					99.99
456B2	4	7	Albite	68.52		19.16					12.32																				100
456B2	4	8	Chlorite	36.32		20.88	18.56	0.36	23.84																						99.96
456B2	4	9	Celcian	45.37		24.81						4.42													25.4						100
456B2	4	10	Pentlandite	1.6		1.57	17.47		1.91					50.34					5.66	21.45											100
456B2	4	11	Titanite	35.53	31.29	3.72	2.37		2.67	24.42																					100
456B2	4	12	Oxyhornblende (Alt)	38.31		19.29	14.87		20.31	4.56																1.27	1.39				100
456B2	4	13	Mix	27.57	6.66	9.13	18.22	0.66		21.51							0.66	14.12			1.48										100.01
456B2	4	14	Chlorite	36.11		20.71	19.4		23.79																						100.01
456B2	4	15	Chlorite	36.45		21.35	18.94		23.25																						99.99
456B2	4	16	Chlorite	37.59		20.43	17.51		23.96			0.54																			100.03
456B2	4	17	Chlorite	36.45		20.41	18.33	0.37	23.89			0.54																			99.99
456B2	4	18	Chlorite	36.34		21.05	18.77		23.83																						99.99
459C	1	1	Calcite				2.02			97.99																					100.01
459C	1	2	Calcite							100																					100
459C	1	3	Calcite							100																					100
459C	1	4	Calcite				1.54			98.46																					100
459C	1	5	K-feldspar	60.54		16.19	6.7		5.95			10.6																			99.98
459C	1	6	K-feldspar	60.71		16.89	6.34		5.92			10.12																			99.98
459C	1	7	Calcite							100																					100
459C	1	8	Chlorite + Calcite	32.49		22.75	24.47		8.31	10.63		1.35																			100
459C	1	9	Chlorite	40.6		24.49	24.51		7.79			2.6																			99.99
459C	1	10	Chlorite	42.59		24.9	20.78		8.19			3.54																			100
459C	1	11	Chlorite	43.51		23.92	20.51		8.39			3.67																			100
459C	1	12	K-feldspar	59.38		18.71	6.47		5.65			9.78																			99.99
459C	1	13	K-feldspar	59.9		18.33	5.85		5.34			10.59																			100.01
459C	1	14	K-feldspar	60.88		16.84	6.25		5.82			10.21																			100
459C	1	15	K-feldspar	60.22		16.89	6.9		5.65			10.33																			99.99
459C	1	16	Chlorite	35.1		23.73	29.29		11.21			0.66																			99.99
459C	1	17	Calcite				1.24			98.76																					100
459C	1	18	Albite	69.01		19.14					11.85																				100
459C	1	19	Chlorite	33.76		24.19	29.85		11.54	0.67																					100.01
459C	1	20	Chlorite	33.78		24.62	30.05		11.52																						99.97

Sample	Site	Pos.	Mineral	SiO_2	TiO_2	Al_2O_3	FeO_t	MnO	MgO	CaO	Na_2O	K_2O	P_2O_5	SO_3	F	Cl	V_2O_5	Cr_2O_3	CoO	NiO	ZnO	SrO	ZrO_2	MoO_3	BaO	La_2O_3	Ce_2O_3	Yb_2O_3	WO_3	PbO	Total
459C	1	21	Calcite	14.27	2.67	4.46				75.93	2.7																				100.03
459C	2	1	Chlorite	33.86		21.88	30.53		13.71																						99.98
459C	2	2	Calcite							100																					100
459C	2	3	Calcite				1.22	1.02		97.76																					100
459C	2	4	Chlorite + TiO2	37.84	12.76	19.35	18.26		9.3	0.45	2.05																				100.01
459C	2	5	Calcite				1.75			98.25																					100
459C	2	6	Chlorite	32.17	0.98	22.86	31.56		11.86	0.57																					100
459C	2	7	Calcite				2.35			97.65																					100
459C	2	8	Chlorite	32.82		22.15	29.37		11.52	4.16																					100.02
459C	2	9	Chlorite	37.59		23.07	26.71		10.28	0.5		1.84																			99.99
459C	2	10	Chlorite	40.9		23	24.47		9.09			2.55																			100.01
459C	2	11	Chlorite	33.01		21.69	31.22		14.09																						100.01
459C	2	12	Chlorite	33.63		22.16	30.55		13.65																						99.99
459C	2	13	Chlorite	34.1		20.96	30.99		13.96																						100.01
459C	2	14	Chlorite	33.71		23.01	30.62		12.65																						99.99
459C	2	15	Chlorite +CaO	33.5		22.81	30.31		11.31	2.07																					100
459C	2	16	Chlorite +CaO	32.37		22.98	31.83		10.51	1.82								0.51													100.02
459C	2	17	Calcite		1.7		1.54			96.77																					100.01
459C	3	1	Calcite				1.04			98.97																					100.01
459C	3	2	Calcite				1.18			98.81																					99.99
459C	3	3	Calcite				1.36			98.64																					100
459C	3	4	Mix	23.72		13.72	22.23		5.52	33.86		0.94																			99.99
459C	3	5	Chlorite	32.41		24.24	31.79		11.09									0.48													100.01
459C	3	6	Chlorite	33.63		21.28	30.39		14.09									0.6													99.99
459C	3	7	Chlorite	34.59		21.75	29.28		13.46			0.92																			100
459C	3	8	Chlorite	37.67		23.96	24.66		10.93			2.77																			99.99
459C	3	9	K-feldspar	52.07		24.3	10.79		5.49			7.34																			99.99
459C	3	10	K-feldspar + mix	44.11		23.88	19.08		8.42			4.11						0.41													100.01
459C	3	11	Chlorite	36.88		23.88	27.53		10.43			1.29																			100.01
459C	3	12	Chlorite	35.62		22.41	28.95		12.44			0.6																			100.02
459C	3	13	Chlorite	32.92		24.24	31.09		11.21									0.53													99.99
459C	3	14	Calcite	3.83		2.99	5.92		1.91	85.37																					100.02
459C	3	15	Calcite				3.22			96.8																					100.02
459C	3	16	Chlorite	33.56		23.24	30.98		12.22																						100
459C	3	17	Chlorite	33.46		24.64	30.34		11.56																						100
459C	3	18	Calcite	18.35		6.82	1.98			66.5	6.36																				100.01
459C	3	19	Chlorite	34.12		24.04	29.61		12.24																						100.01
459C	3	20	Calcite				2.34			97.66																					100
459C	3	21	Chlorite	33.78		20.26	29.15		13.58	2.2		0.41						0.63													100.01
459C	3	22	Chlorite + K2O	31.92		20.63	27.08		10.84	8.26		0.73						0.54													100
459C	3	23	Chlorite + K2O	38.55		22.83	26.03		10.61			1.99																			100.01
459C	3	24	Albite	67.83	1.67	18.06					11.26	1.18																			100
459C	3	25	Chlorite + K2O	37.07		21.94	27.8		10.84	0.6		1.02						0.75													100.02
459C	3	26	Rutile	3.91	87.91	1.91	2.47		1.64	2.15																					99.99
459C	3	27	Rutile	8.62	80.83	3.8	2.7		1.03	0.39	2.62																				99.99
459C	3	28	Calcite				1.14			98.87																					100.01
459C	3	29	Calcite	3.68		2.23				93.45		0.65																			100.01
459C	3	30	Calcite	7.14		1.8	1.2			88.08	1.78																				100
459C	3	31	Chlorite	34.23		24.92	29.52		10.88									0.45													100

Sample	Site	Pos.	Mineral	SiO_2	TiO_2	Al_2O_3	FeO_t	MnO	MgO	CaO	Na_2O	K_2O	P_2O_5	SO_3	F	Cl	V_2O_5	Cr_2O_3	CoO	NiO	ZnO	SrO	ZrO_2	MoO_3	BaO	La_2O_3	Ce_2O_3	Yb_2O_3	WO_3	PbO	Total
459C	4	1	Chlorite	32.9		25.07	30.22		11.81																						100
459C	4	2	Chlorite	33.2		24.49	29.96		12.34																						99.99
459C	4	3	Chlorite	33.35		23.37	31.34		11.94																						100
459C	4	4	Calcite				1.45			98.55																					100
459C	4	5	Calcite							100																					100
459C	4	6	Calcite							100																					100
459C	4	7	Calcite				1.44			98.56																					100
459C	4	8	Chlorite + K2O	34.89		23.09	29.72		11.67			0.63																			100
459C	4	9	Chlorite	33.44		23.73	31.16		11.66																						99.99
459C	4	10	Calcite				1.66			98.34																					100
459C	4	11	Chlorite + K2O	36.26		24.17	27.41		10.76			1.41																			100.01
459C	4	12	Calcite				2.39			97.61																					100
459C	4	13	Calcite				1.52			98.48																					100
459C	4	14	Chlorite + K2O	38.48		22.43	25.05		10.58	0.6		2.3						0.56													100
459C	4	15	Chlorite + K2O	39.53		23.96	24.21		9.67			2.64																			100.01
459C	4	16	Chlorite + K2O	34.8		21.81	29.2		12.93			0.46					0.8														100
459C	4	17	Calcite				2.92			97.08																					100
459C	4	18	Chlorite	33.59		24.21	30.01		12.2																						100.01
459C	4	19	Chlorite	34.27		22.13	30.45		13.15																						100
459C	4	20	Calcite	7.44			1.18			91.38																					100
459C	4	21	Albite	67.62	2.15	18.08					11.22	0.93																			100
459C	4	22	Titanite	17.99	60.73	8.47	6.75		2.85		3.2																				99.99
459C	4	23	Chlorite	32.32		21.9	32.74		11.87								0.57	0.58													99.98
459C	4	24	Calcite	2.29			4.05			93.66																					100
459C	4	25	Chlorite	33.63		21.71	30.79		13.88																						100.01
459C	4	26	Calcite				2.65			97.34																					99.99
459C	4	27	Calcite				3.14			96.87																					100.01
459C	4	28	Chlorite	35.62		23	28.75		11.57			1.05																			99.99
459C	4	29	K-feldspar	46.87		24.6	16.38		6.93			5.22																			100
459C	4	30	K-feldspar + Mix	38.66		23.03	25.83		10.23			2.24																			99.99
459C	4	31	K-feldspar + Mix	41.82		24.26	21.56		8.94			2.84						0.57													99.99
459C	4	32	Chlorite + K2O	32.88		23.18	30.9		10.63	1.29		0.47						0.64													99.99
459C	4	33	Calcite	13.52		10.51	15.23		5.27	55.48																					100.01
459C	5	1	Calcite							100																					100
459C	5	2	Calcite							100																					100
459C	5	3	K-feldspar	47.55		24.47	15.26		6.96			5.75																			99.99
459C	5	4	Calcite				2.48			97.52																					100
459C	5	5	Chlorite + K2O	3.64		3.42	5.27		2.07	85.59																					99.99
459C	5	6	Chlorite	32.47		20.84	26.72		10.38	8.4		0.64						0.56													100.01
459C	5	7	Calcite	8.17		7.05	12.43		4.29	68.06																					100
459C	5	8	Calcite				2.1			97.9																					100
459C	5	9	K-feldspar	39.7		20.48	15.75		6.85	13.14		4.07																			99.99
459C	5	10	K-feldspar	57.84		24.77	3.54		4.31			9.53																			99.99
459C	5	11	K-feldspar	57.33		25.24	3.85		4.21			9.37																			100
459C	5	12	K-feldspar	46.48		24.85	15.57		6.78			5.85						0.48													100.01
459C	5	13	K-feldspar	49.22		24.64	13.51		6.72			5.9																			99.99
459C	5	14	K-feldspar	52.86		24.73	9.88		4.88			7.66																			100.01
459C	5	15	K-feldspar	57.76		25.21	3.11		4.06			9.85																			99.99
459C	5	16	K-feldspar	45.31		24.21	18.15		7.94			4.38																			99.99

Sample	Site	Pos.	Mineral	SiO_2	TiO_2	Al_2O_3	FeO_t	MnO	MgO	CaO	Na_2O	K_2O	P_2O_5	SO_3	F	Cl	V_2O_5	Cr_2O_3	CoO	NiO	ZnO	SrO	ZrO_2	MoO_3	BaO	La_2O_3	Ce_2O_3	Yb_2O_3	WO_3	PbO	Total
459C	5	17	K-feldspar	44.52		24.15	19.12		7.35			4.42						0.48													100.04
459C	5	18	Chlorite + K2O	38.74		24.21	25.41		9.55			2.1																			100.01
459C	5	19	K-feldspar	42.53		24.11	21.16		8.46			3.75																			100.01
459C	5	20	K-feldspar	57.48		24.96	3.94		4.1			9.54																			100.02
459C	5	21	Chlorite + K2O	36.84		24.51	26.13		10.25			1.76						0.54													100.03
459C	5	22	K-feldspar	53.24		24.58	9.53		5.01			7.62																			99.98
459C	5	23	K-feldspar	41.82		24.77	21.56		8.64			3.2																			99.99
459C	5	24	K-feldspar	47.17		24.83	15.89		6.68			5.44																			100.01
459C	5	25	Chlorite + K2O	35.6		24.32	28.01		9.85			1.73						0.5													100.01
459C	5	26	Chlorite + K2O	37.54		23.96	27.09		9.68			1.7																			99.97
459C	5	27	Chlorite + K2O	37.05		23.47	26.45		10.81			1.81						0.44													100.03
459C	5	28	Mix	30.33		18.67	25.25		9.27	15.11		1.39																			100.02
459C	5	29	Calcite	13.24		4.42	1.76			78.08	2.49																				99.99
459C	5	30	Chlorite + CaO	33.54		23.45	30.3		11.39	1.32																					100
459C	5	31	Chlorite	33.44		22.2	29.91		13.71								0.73														99.99
459C	5	32	Calcite				1.85			98.15																					100
459C	5	33	Calcite				3.77			96.24																					100.01
459C	5	34	Chlorite + CaO	34.55		22.18	28.78		11.39	1.71		0.86						0.56													100.03
459C	5	35	Chlorite	32.77		23.41	33.38		10.43																						99.99
459C	5	36	Chlorite + CaO	33.67		23.32	28.68		10.26	4.07																					100
459C	6	1	Calcite				1.29			98.71																					100
459C	6	2	Calcite	12.24		3.44	1.7			82.11		0.53																			100.02
459C	6	3	Chlorite	34.7		22.98	29.56		11.67	0.53								0.56													100
459C	6	4	Calcite				2.07		1.49	96.45																					100.01
459C	6	5	Chlorite	35.81		23.66	28.15		11.47			0.93																			100.02
459C	6	6	Mix	18.5		11.9	13.03		6.28	49.36		0.92																			99.99
459C	6	7	Chlorite	35.49		23.43	28.57		10.71			1.26						0.54													100
459C	6	8	Chlorite	33.44		23.86	29.85		12.85																						100
459C	6	9	Chlorite	33.44		21.48	31.16		13.95																						100.03
459C	6	10	Chlorite + Others	37.89		23.51	25.36		10.41	0.76		2.08																			100.01
459C	6	11	Chlorite + Others	35.62		22.07	24.78		10.4	5.53		1.61																			100.01
459C	6	12	Calcite				1.07			98.94																					100.01
459C	6	13	Chlorite	32.88		21.5	31.13		14.48																						99.99
459C	6	14	Mix	13.52		7.52	16.27		3.78	58.89																					99.98
459C	6	15	Chlorite + K2O	40.47		22.56	23.81		10.33			2.83																			100
459C	6	16	Chlorite + K2O	35.08		23.92	28.62		10.94			1.42																			99.98
459C	6	17	Chlorite + K2O	34.65		23	29.82		10.55			1.46						0.54													100.02
459C	6	18	Chlorite	32.9		22.03	31.39		12.62								0.59	0.47													100
459C	6	19	Chlorite	33.07		21.58	30.66		13.95								0.73														99.99
459C	6	20	Chlorite	33.67		21.79	29.37		13.88								0.61	0.69													100.01
459C	6	21	Chlorite	32.92		21.28	30.22		14.89								0.7														100.01
459C	6	22	Chlorite + K2O	41.07		23.88	23.31		8.79			2.94																			99.99
459C	6	23	Chlorite + K2O	37.22		24.04	27.03		10.05			1.67																			100.01
459C	6	24	Chlorite + K2O	37.07		23.9	26.81		10.65			1.57																			100
459C	6	25	Chlorite + K2O	35.47		22.18	28.21		11.08	1.06		1.4					0.61														100.01
459C	6	26	Calcite				1.97			98.03																					100
459C	6	27	Albite	68.09	0.6	18.33				0.39	11.93	0.67																			100.01
459C	6	28	Chlorite	34.06		20.65	30.53		14.28									0.48													100
459C	6	29	Chlorite	30.33	10.48	20.56	27.05		11.59																						100.01
459C	6	30	Chlorite	33.59		25.89	29.27		11.28																						100.03
459C	6	31	Calcite	4.77		1.57				93.65																					99.99
459C	6	32	Albite	63.38	6.44	17.59	0.44				11.19	0.95																			99.99

APPENDIX B

Backscattered Electron Images (BSE)

(Sample numbers, sites, and analysis number refer to analyses in Appendix A)

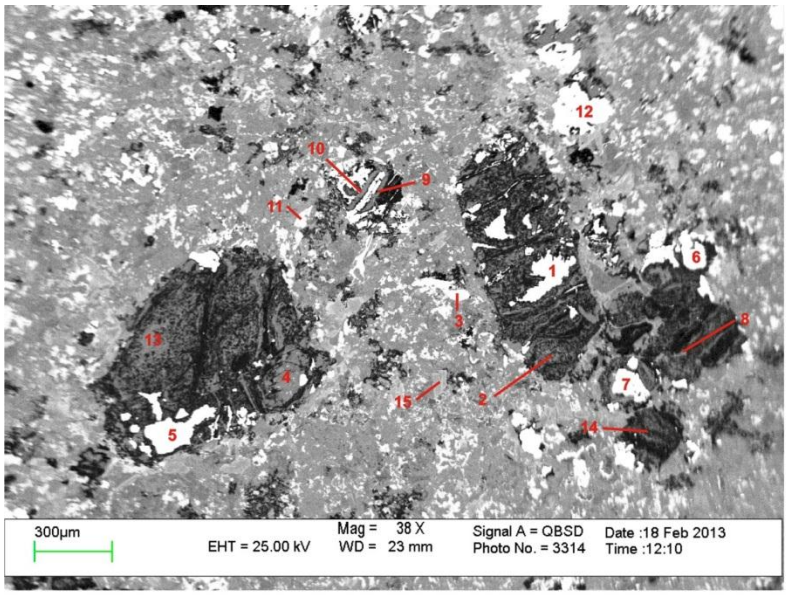

1	Pyrite
2	Wollastonite
3	Fluoroapatite
4	Calcite
5	Pyrite
6	Pyrite
7	Pyrite
8	Quartz
9	Calcite
10	Calcite
11	Fluoroapatite
12	Pyrite
13	Wollastonite
14	Wollastonite
15	Oxyhornblende (Alt)

Sample: 46A
Site: 1

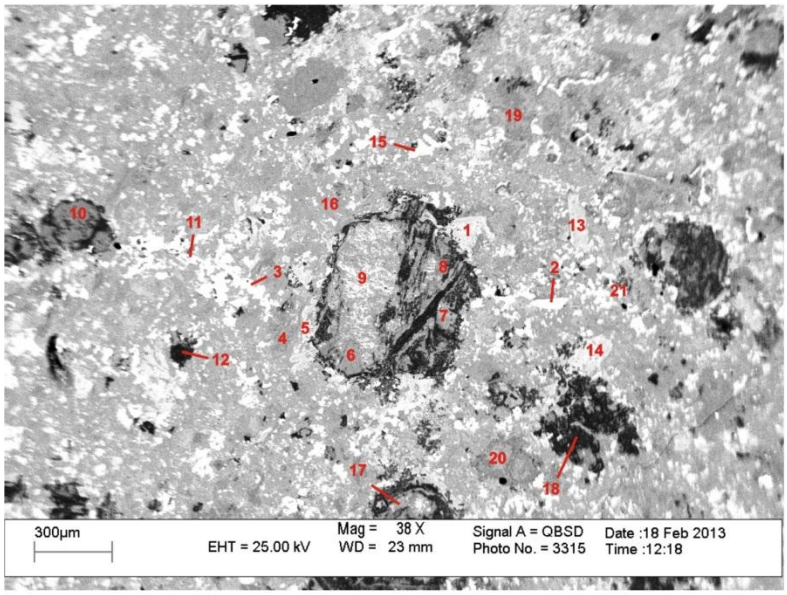

1	Phlogopite
2	Fluoroapatite
3	Fluoroapatite
4	Chlorite
5	Phlogopite
6	Calcite
7	Calcite
8	Calcite
9	Alstonite
10	Calcite
11	Ba-feldspar
12	Quartz
13	Phlogopite
14	Chlorite + K2O
15	Titanite
16	Chlorite + K2O
17	Calcite
18	Quartz
19	Chlorite + K2O
20	Chlorite + K2O
21	Titanite

Sample: 46A
Site: 2

[Top] Xenoliths of Wollastonite pseudomorphed by calcite, in mafic volcanic flow. Alteration of groundmass by quartz, calcite, and chlorite

[Bottom] Xenoliths of Alstonite pseudomorphed by calcite. Alteration of groundmass by quartz, calcite, and chlorite, in a mafic volcanic flow.

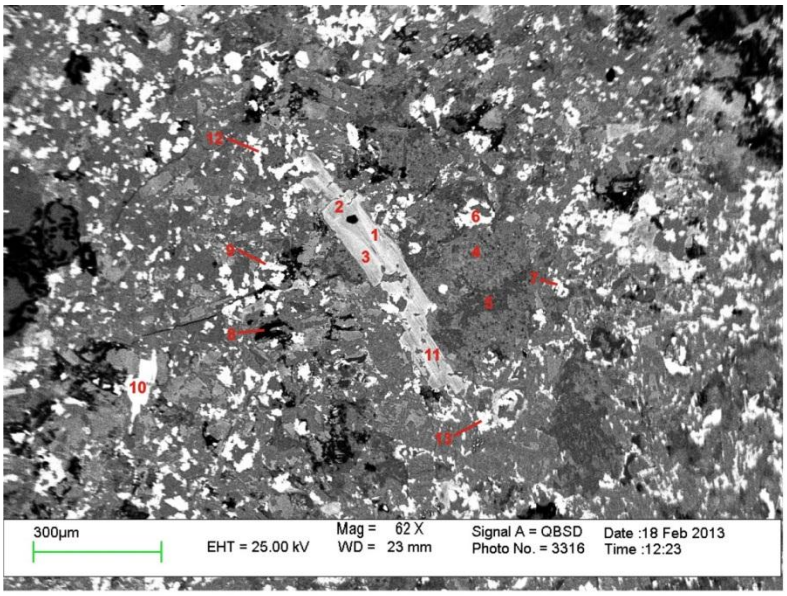

1-3	Phlogopite
4	Chlorite + K2O
5	Calcite
6	Titanite
7	Titanite
8	Quartz
9	Titanite
10	Fluoroapatite
11	Phlogopite
12	Titanite
13	Titanite

Sample: 46A
Site: 3

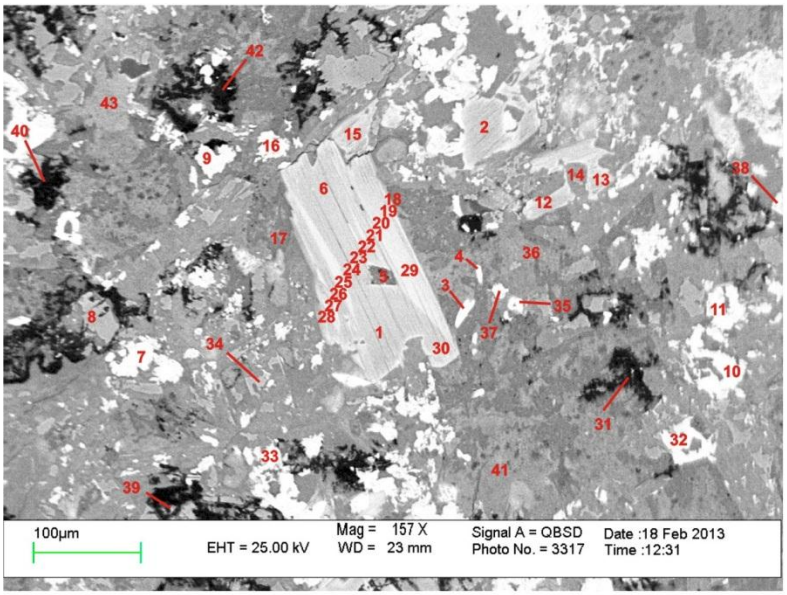

1-2	Phlogopite
3-4	Fluoroapatite
5	Calcite
6	Phlogopite
7	Titanite
8	Clinopyroxene
9-11	Titanite
12-13	Phlogopite
14	Clinopyroxene
15	Phlogopite
16	Titanite
17	Calcite
18-30	Phlogopite
31	Quartz
32	Titanite
33	Titanite
34-35	Clinopyroxene
36	Chlorite
37	Ba-feldspar
38	Titanite
39-40	Quartz
41	K-feldspar
42	Quartz
43	Chlorite +K2O

Sample: 46A
Site: 4

[Top] Phenocrysts of phlogopite, showing resorbed grain boundaries. Alteration in groundmass by chlorite, quartz and calcite.

[Bottom] Phenocrysts of phlogopite, showing resorbed grain boundaries and alteration by chlorite.

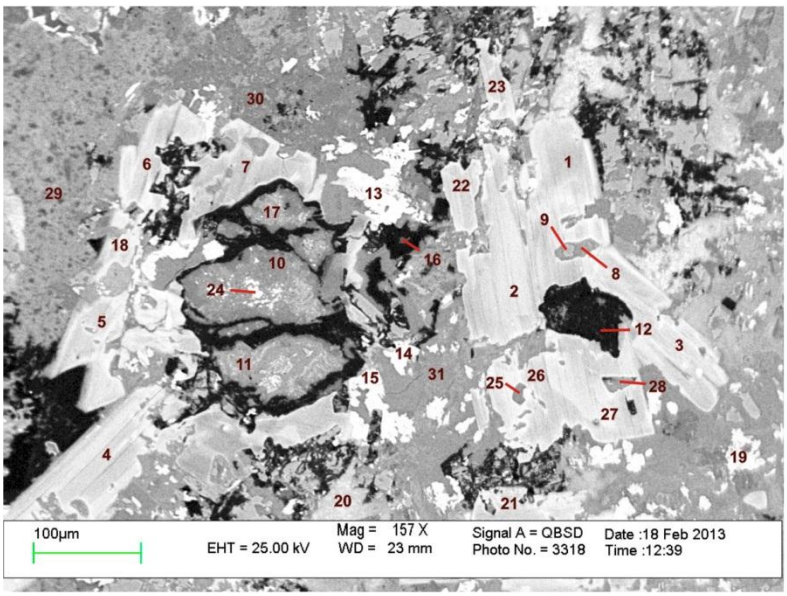

1-7	Phlogopite
8	Chlorite
9	Clinopyroxene
10	Calcite
11	Calcite
12	Quartz
13-15	Titanite
16	Chlorite + SiO2
17	Calcite
18	Phlogopite
19	Titanite
20	Mix
21-23	Phlogopite
24	Alstonite
25	Mix
26	Phlogopite
27	Phlogopite
28	Chlorite
29	Phlogopite
30	Mix
31	Chlorite

Sample: 46A
Site: 5

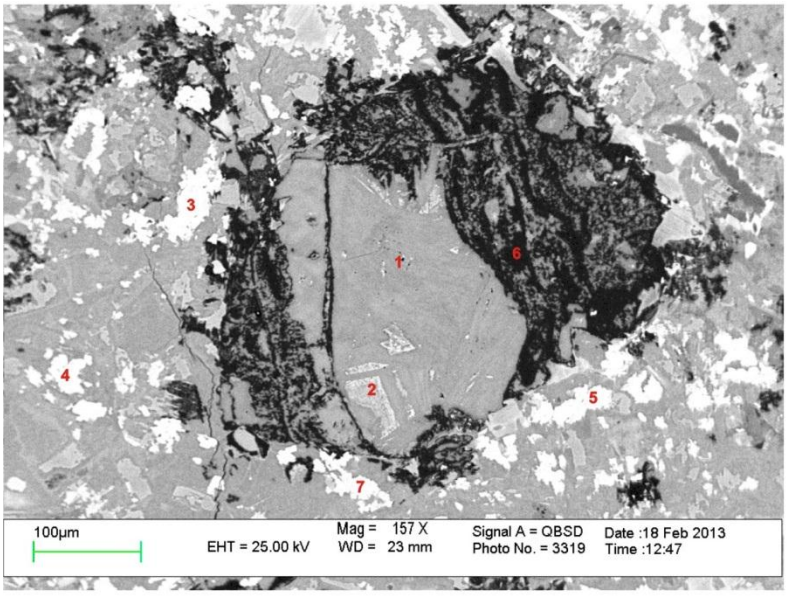

1	Calcite
2	Calcite
3	Titanite
4	Titanite
5	Titanite
6	Quartz
7	Titanite

Sample: 46A
Site: 6

[Top] Phenocrysts of phlogopite, showing resorbed grain boundaries and xenoliths pseudomorphed by calcite.

[Bottom] Calcite replacement of xenolith, plus alteration of groundmass

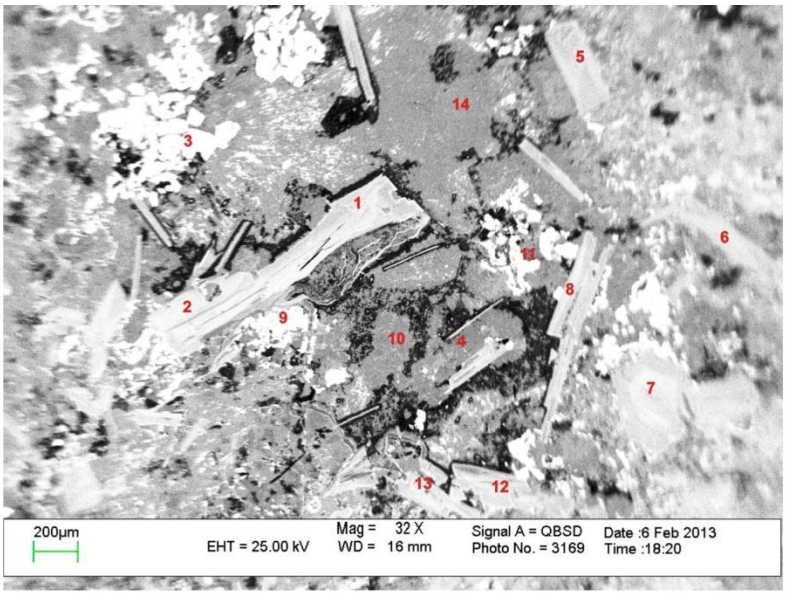

1	Phlogopite
2	Phlogopite
3	Celsian
4	Calcite
5	Phlogopite
6	Phlogopite
7	Phlogopite
8	Phlogopite
9	Ba-feldspar
10	Calcite
11	Ba-feldspar
12	Phlogopite
13	Phlogopite
14	Calcite

Sample: 46A
Site: 7

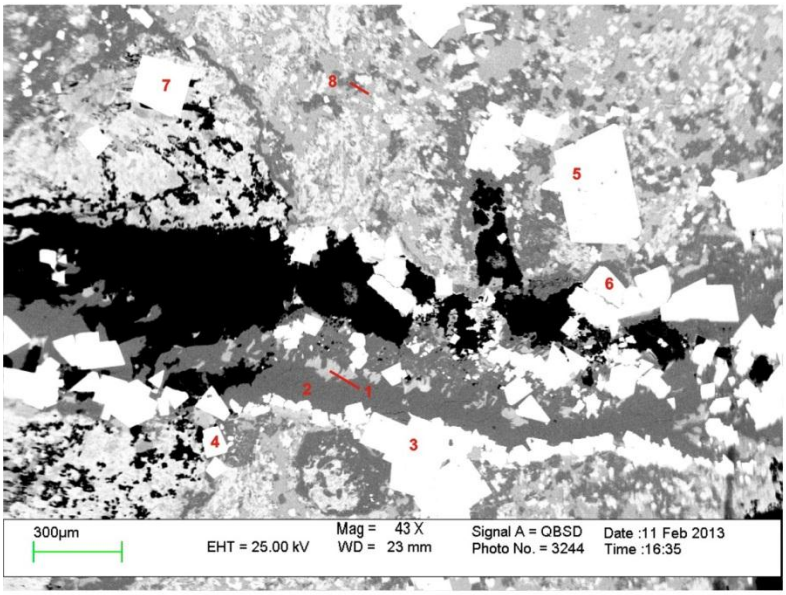

1	Chlorite
2	Quartz
3	Pyrite
4	Pyrite
5	Pyrite
6	Pyrite
7	Pyrite
8	Mix

Sample: 47E
Site: 1

[Top] Phenocrysts of phlogopite and Ba-feldspar showing resorbed grain boundaries.

[Bottom] Secondary pyrite ± alteration minerals in quartz vein.

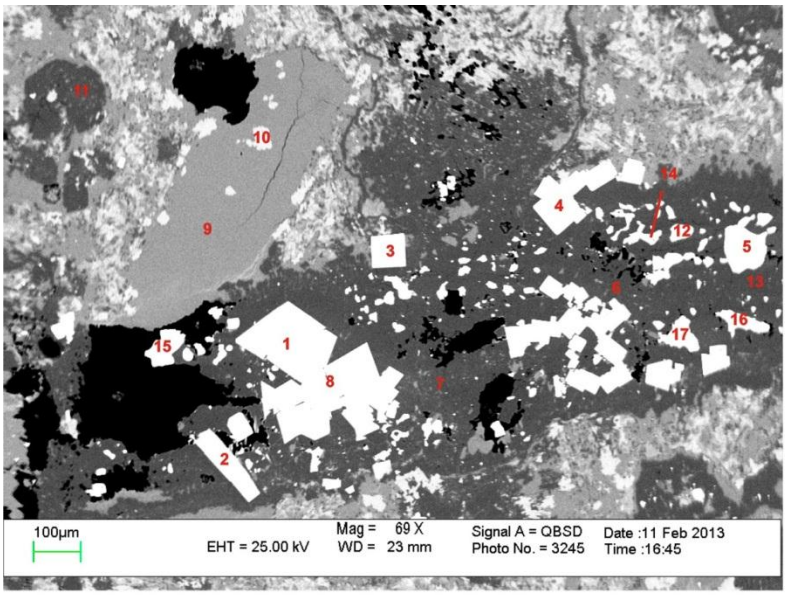

1	Pyrite
2	Pyrite
3	Pyrite
4	Pyrite
5	Barite
6	Quartz
7	Quartz
8	Quartz
9	Olivine
10	Titanite
11	Quartz
12-17	Barite

Sample: 47E
Site: 2

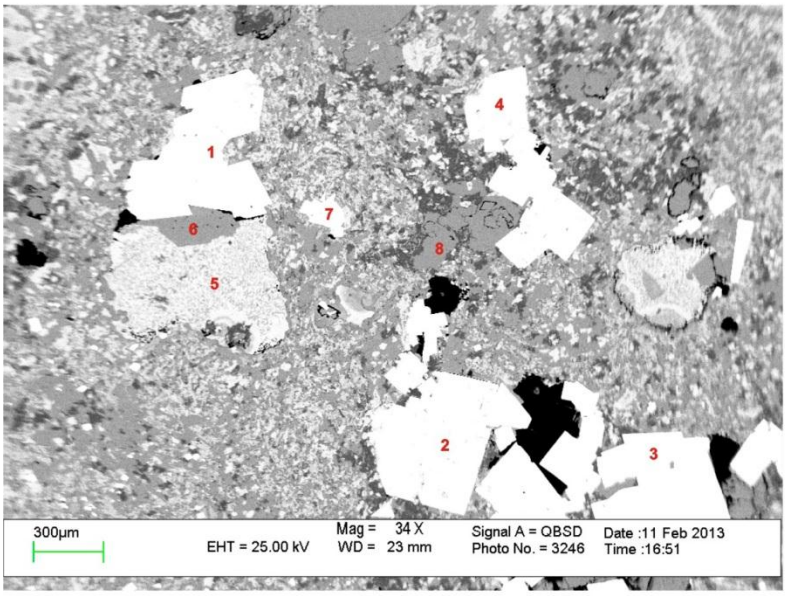

1	Pyrite
2	Pyrite
3	Pyrite
4	Pyrite
5	Alstonite + Qartz
6	Calcite
7	Pyrite
8	Chlorite

Sample: 47E
Site: 3

[Top] Phenocrysts of olivine showing resorbed grain boundaries, with alteration of pyrite ± barite in quartz vein.

[Bottom] Secondary pyrite, with alteration of groundmass by chlorite and calcite, with Alstonite xenolith pseudomorphed by calcite

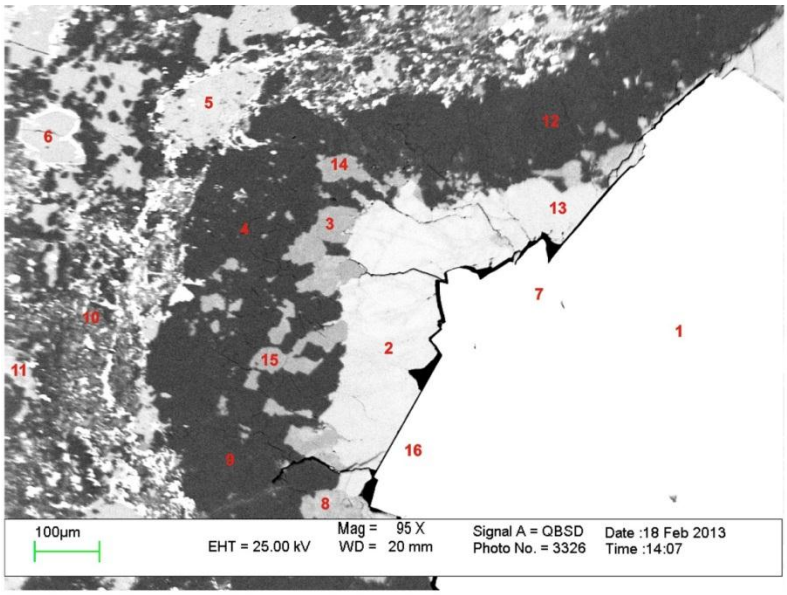

1	Pyrite
2	Calcite
3	K-feldspar
4	Albite
5	Calcite
6	Calcite
7	Pyrite
8	Calcite
9	Albite
10	Mix
11	Calcite
12	Albite
13	Calcite
14	K-feldspar
15	K-feldspar
16	Pyrite

Sample: 49B
Site: 1

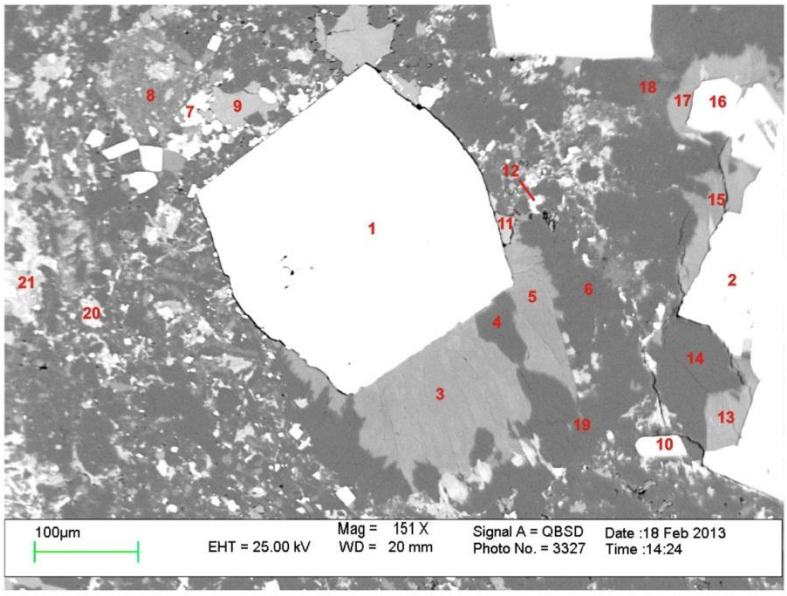

1	Pyrite
2	Pyrite
3	K-feldspar
4	Albite
5	K-feldspar
6	Albite
7	Pyrite
8	Orthoclase
9	Calcite
10	Pyrite
11	Calcite
12	Fluoroapatite
13	K-feldspar
14	Albite
15	K-feldspar
16	Pyrite
17	K-feldspar
18	Albite
19	Albite
20	Fluoroapatite
21	Chlorite

Sample: 49B
Site: 2

[Top/Bottom] Hydrothermal/alteration assemblage of K-fsp ± albite ± pyrite

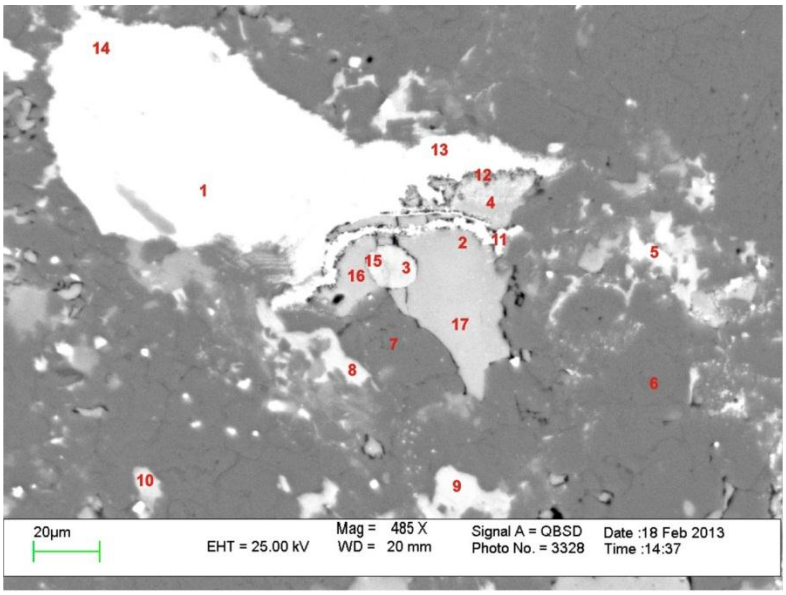

1	Rutile
2	Calcite
3	Chlorite
4	Calcite
5	Rutile + Others
6	Albite
7	Albite
8	Chlorite + K2O
9	Chlorite
10	Chlorite
11	Rutile
12	Rutile + Others
13	Rutile + Others
14	Rutile
15	Chlorite + CaO
16	Calcite
17	Calcite

Sample: 49B
Site: 3

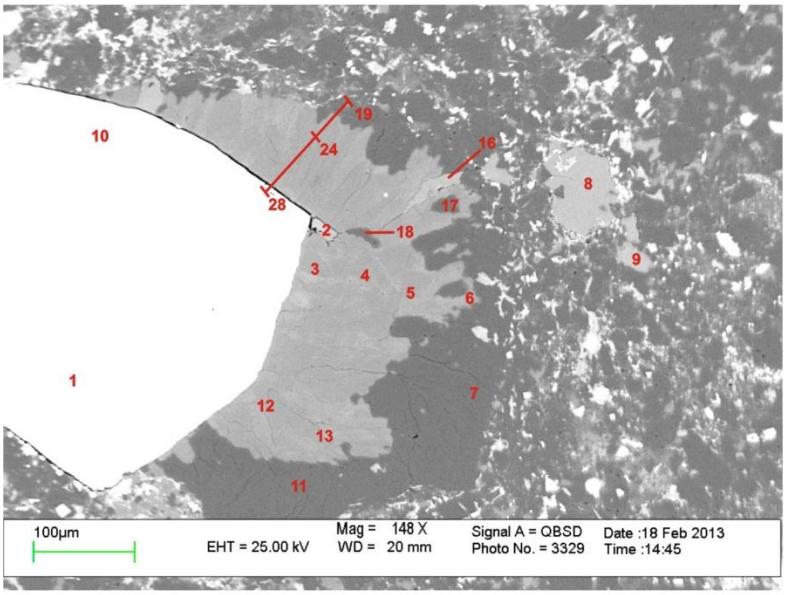

1	Pyrite
2	Calcite
3	K-feldspar
4	K-feldspar
5	K-feldspar
6	K-feldspar
7	Albite
8	Calcite
9	Calcite
10	Pyrite
11	Albite
12	K-feldspar
13	K-feldspar
14	Chlorite
15	Chlorite
16	Calcite
17	Albite
18	Albite
19	Albite
20	Albite
21-27	K-feldspar
28	Pyrite

Sample: 49B
Site: 4

[Top/Bottom] Hydrothermal/alteration assemblage of K-fsp ± albite ± pyrite

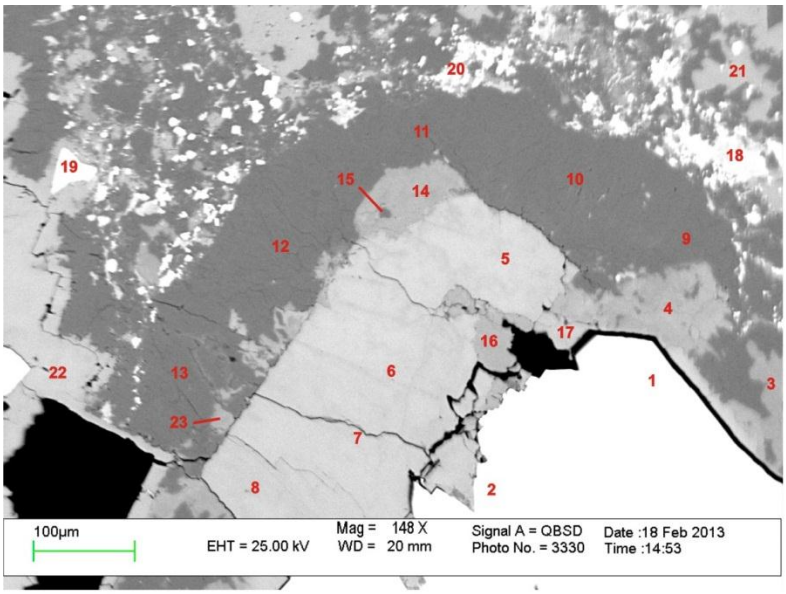

1	Pyrite
2	Pyrite
3	K-feldspar
4	K-feldspar
5	Calcite
6	Calcite
7	Calcite
8	Calcite
9-13	Albite
14	K-feldspar
15	Albite
16	K-feldspar
17	Calcite
18	Rutile + Others
19	Pyrite
20	Pyrite + Others
21	Calcite
22	Calcite
23	K-feldspar

Sample: 49B
Site: 5

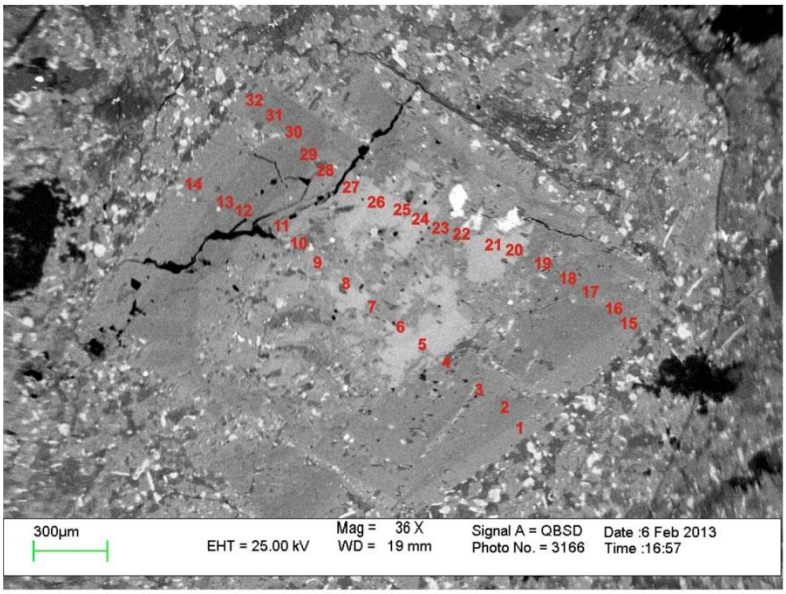

1-6	Clinopyroxene
7	Clinopyroxene + K20
8-13	Clinopyroxene
14	Clinopyroxene + TiO2
15-26	Clinopyroxene
27	Clinopyroxene + others
28	Titanite
29	Clinopyroxene
30	Clinopyroxene
31	Clinopyroxene
32	Clinopyroxene

Sample: 456A
Site: 1

[Top] Hydrothermal/alteration assemblage of K-fsp ± albite ± pyrite.

[Bottom] Zoned clinopyroxene, showing euhedral rims with resorbed cores.

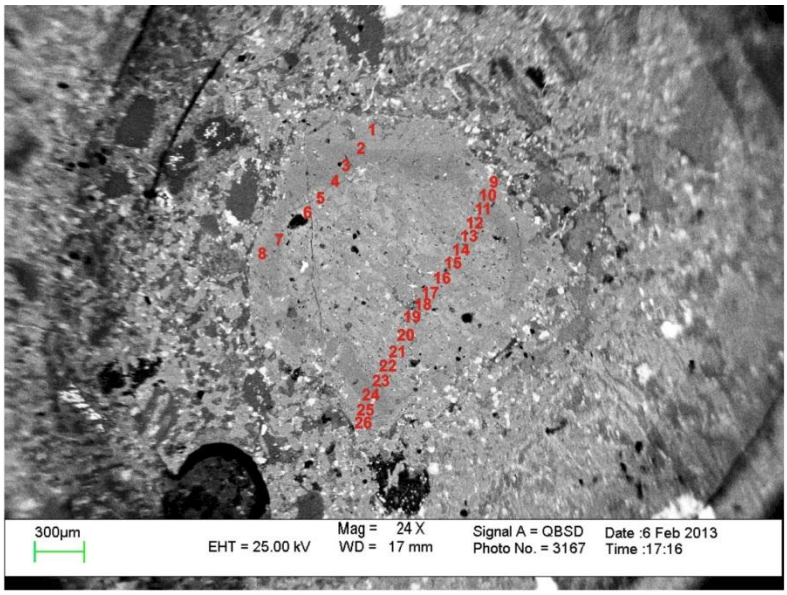

1-9	Clinopyroxene
10	Clinopyroxene
11	Oxyhornblende (Alt)
12	Clinopyroxene
13-23	Clinopyroxene
24	Clinopyroxene
25	Clinopyroxene
26	Oxyhornblende (Alt)

Sample: 456A
Site: 2

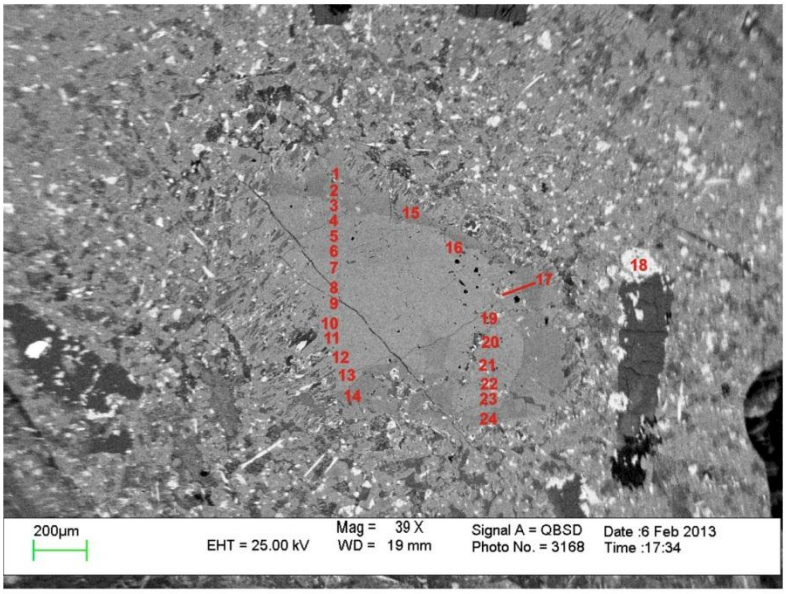

1-16	Clinopyroxene
17	Clinopyroxene
18	K-feldspar
19	K-feldspar
20	Clinopyroxene
21	Clinopyroxene
22	Clinopyroxene
23	Clinopyroxene
24	Clinopyroxene

Sample: 456A
Site: 3

[Top] Zoned clinopyroxene, showing euhedral rims with resorbed cores.

[Bottom] Zoned clinopyroxene, showing euhedral rims with resorbed cores, in macrocrystic basalt

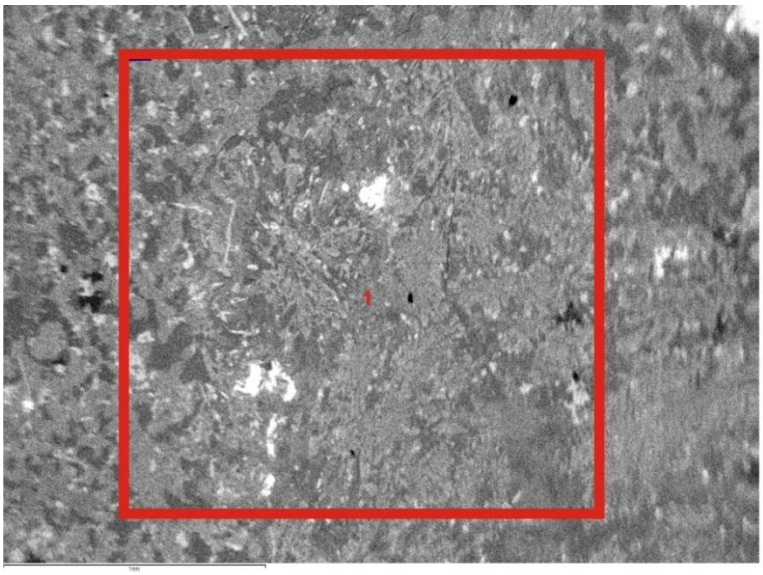

1 Oxyhornblende (Alt)

Sample: 456B1
Site: 1

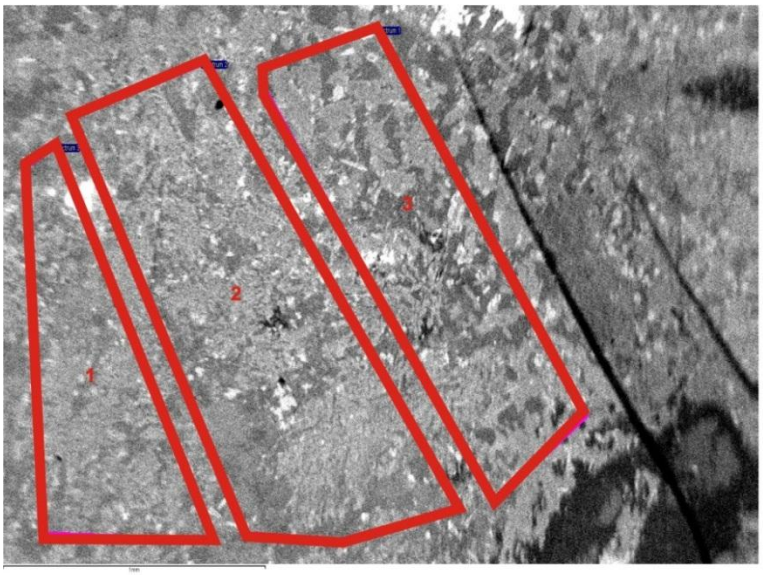

1 Oxyhornblende (Alt)
2 Oxyhornblende (Alt)
3 Oxyhornblende (Alt)

Sample: 456B1
Site: 2

[Top] Single raster analysis of ocelli showing plumose textures of oxyhornblende.

[Bottom] Raftered analyses away from ocelli edged (line in image), with oxyhornblende composition. See analyses from 456B1 (sites 3 & 4) and 456B2 (sites 1 &2).

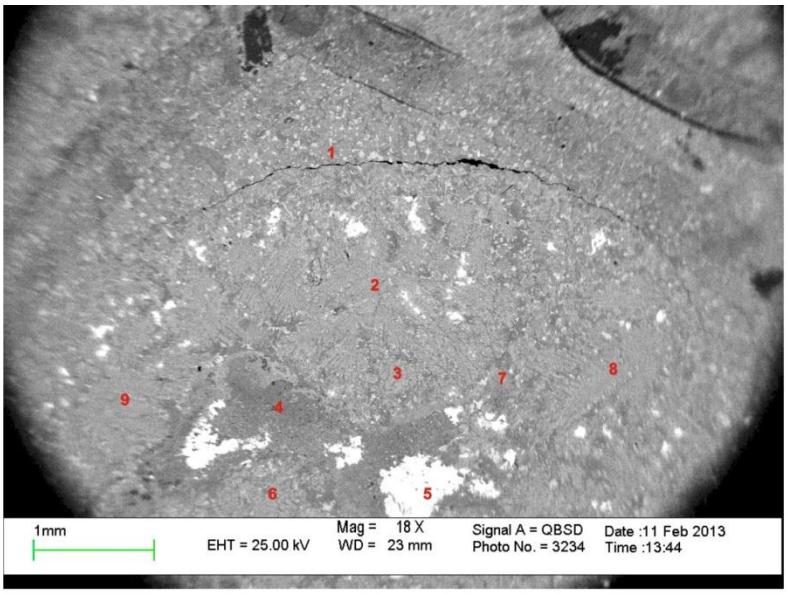

1 Oxyhornblende (Alt)
2 Oxyhornblende (Alt)
3 Oxyhornblende (Alt)
4 Calcite
5 Ba-feldspar
6 Oxyhornblende (Alt)
7 Oxyhornblende (Alt)
8 Oxyhornblende (Alt)
9 Oxyhornblende (Alt)

Sample: 456B1
Site: 3

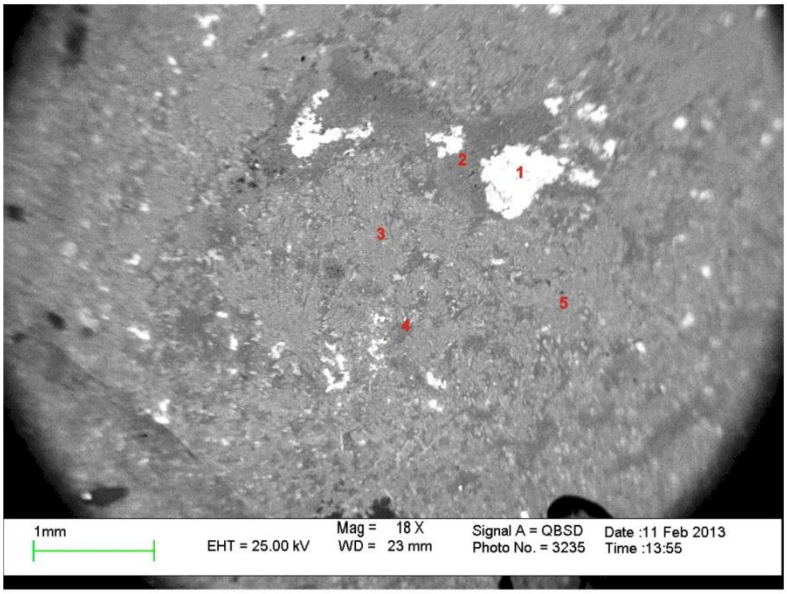

1 Ba-feldspar
2 Calcite + Mix
3 Oxyhornblende (Alt)
4 Oxyhornblende (Alt)
5 Oxyhornblende (Alt)

Sample: 456B1
Site: 4

[Top/Bottom] Analyses of ocelli, showing dendritic/plumose texture of oxyhornblende, with cores Ba-feldspar, and varying chlorite and calcite alteration.

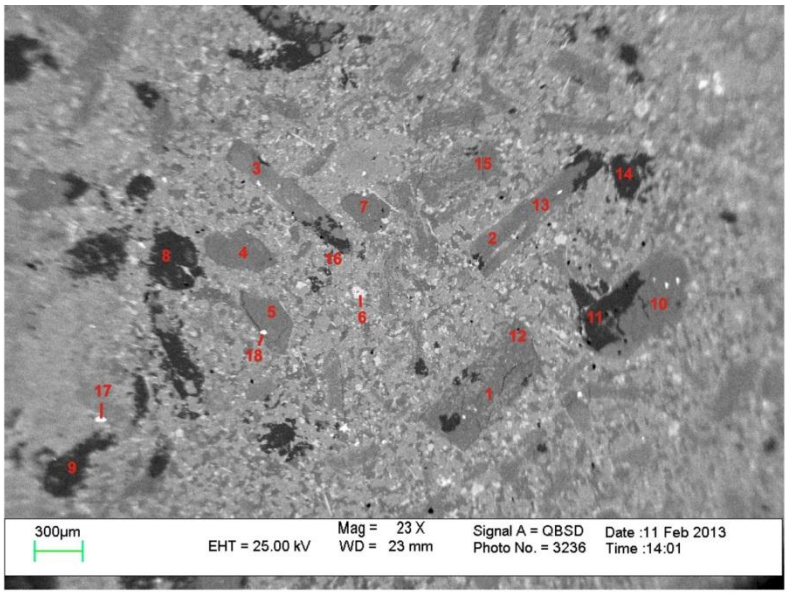

1	Chlorite
2	Chlorite
3	K-feldspar
4	Chlorite +K20
5	Chlorite +K20
6	Mix -?
7	Chlorite
8	Albite
9	Albite
10	Chlorite
11	Albite
12	Oxyhornblende (Alt)
13	Oxyhornblende (Alt)
14	Albite
15	Oxyhornblende (Alt)
16	Albite
17	Galena + Mix
18	Pentlandite

Sample: 456B1
Site: 5

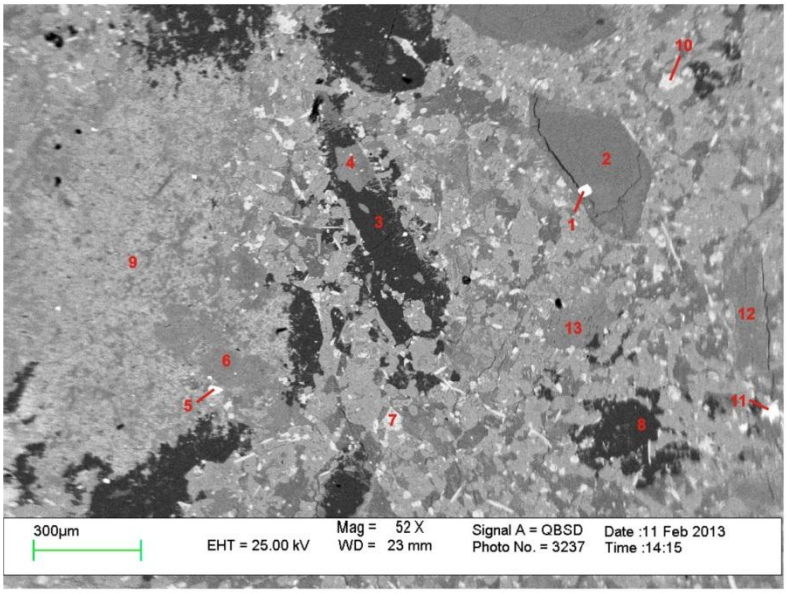

1	Pentlandite
2	Chlorite
3	Albite
4	Chlorite
5	Wulfenite
6	K-feldspar
7	Titanite
8	Albite
9	K-feldspar
10	Chlorite + TiO2
11	Allanite
12	Chlorite + K20
13	K-feldspar

Sample: 456B1
Site: 6

[Top/Bottom] Phenocrysts of olivine with orthorhombic habit pseudomorphed by calcite. Alteration of groundmass by chlorite and calcite in microcrystic basalt.

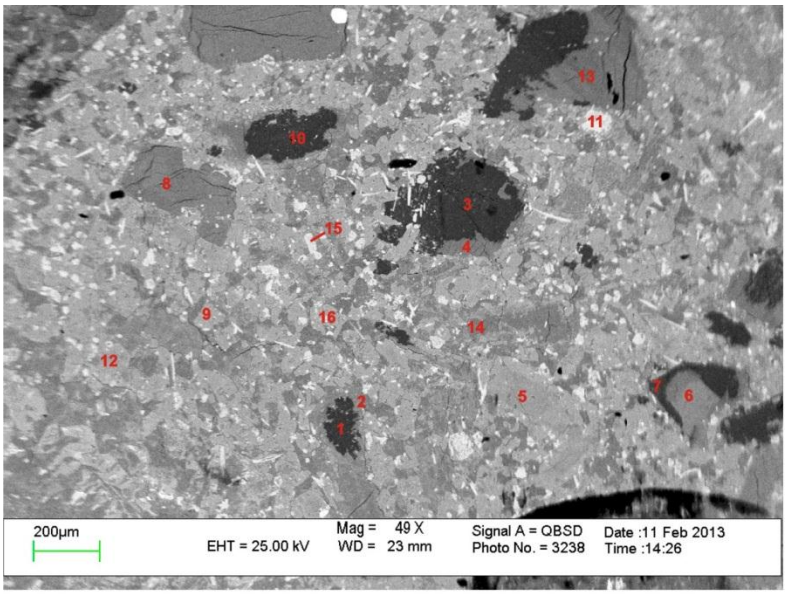

1	Albite
2	Chlorite
3	Albite
4	Chlorite
5	Clinopyroxene
6	K-feldspar
7	Albite
8	Chlorite + K20
9	Clinopyroxene
10	Albite
11	Titanite
12	Clinopyroxene
13	Chlorite
14	Chlorite
15	Titanite
16	Clinopyroxene

Sample: 456B1
Site: 7

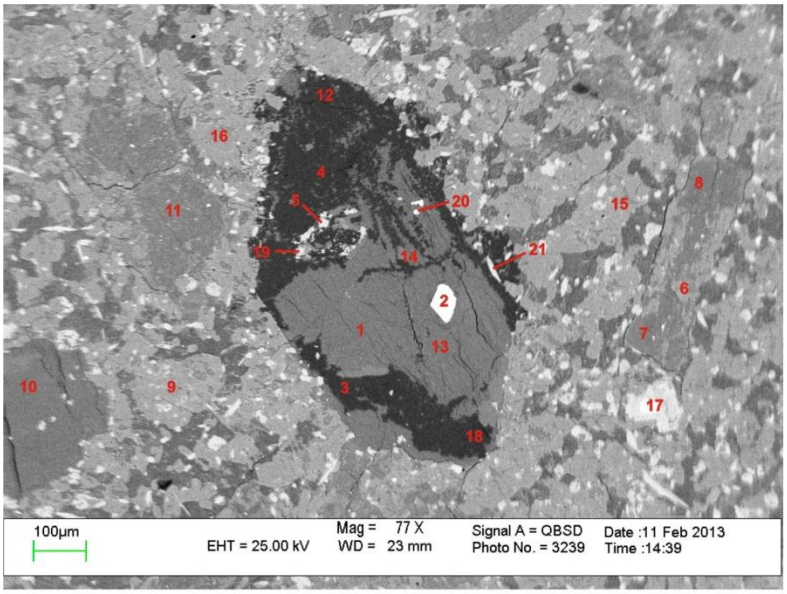

1	Chlorite
2	Pentlandite
3	Albite
4	K-feldspar
5	Titanite
6	Chlorite + K20
7	Chlorite + K20
8	Chlorite + K20
9	Clinopyroxene
10	Chlorite + K20
11	Chlorite + K20
12	Albite
13	Chlorite + K20
14	Chlorite + K20
15	Clinopyroxene
16	Clinopyroxene
17	Titanite + others
18	Albite
19	Titanite
20	Pentlandite
21	Fluoroapatite

Sample: 456B1
Site: 8

[Top/Bottom] Phenocrysts of olivine with orthorhombic habit pseudomorphed by chlorite and calcite in microcrystic basalt.

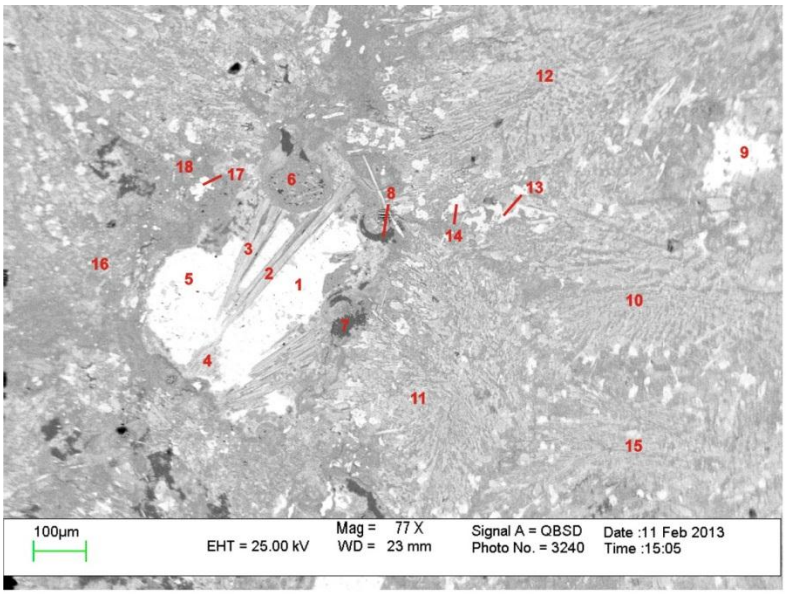

1	Ba-feldspar
2	Ba-feldspar
3	Ba-feldspar
4	Ba-feldspar
5	Ba-feldspar
6	Calcite
7	Albite
8	Albite
9	Ba-feldspar
10	Oxyhornblende (Alt)
11	Oxyhornblende (Alt)
12	Oxyhornblende (Alt)
13	Titanite
14	Titanite
15	Oxyhornblende (Alt)
16	Oxyhornblende (Alt)
17	Mix
18	Chlorite

Sample: 456B2
Site: 1

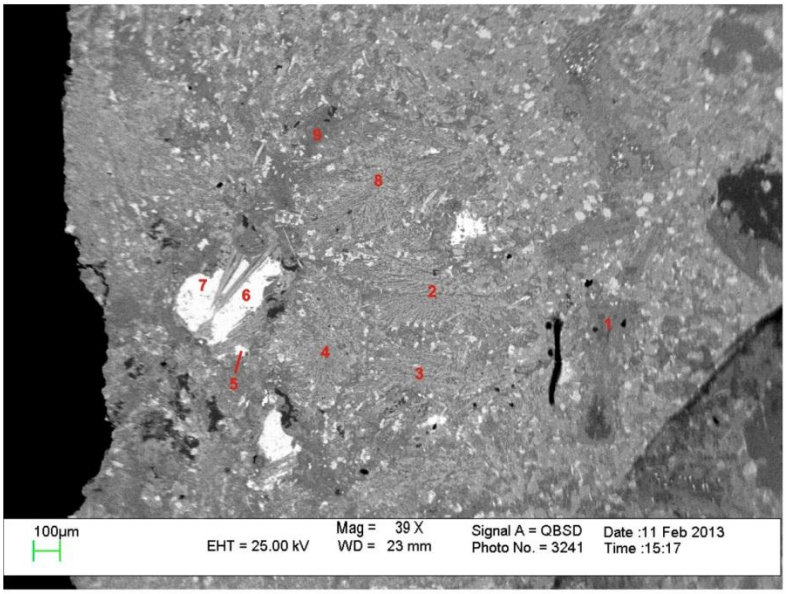

1	Oxyhornblende (Alt)
2	Oxyhornblende (Alt)
3	Oxyhornblende (Alt)
4	Oxyhornblende (Alt)
5	Ba-feldspar
6	Ba-feldspar
7	Ba-feldspar
8	Oxyhornblende (Alt)
9	Oxyhornblende (Alt)

Sample: 456B2
Site: 2

[Top] Ocelli showing plumose texture oxyhornblende, and Ba-feldspar cores.

[Bottom] Ocelli showing plumose texture of oxyhornblende and resorbed grain boundaries of Ba-feldspar.

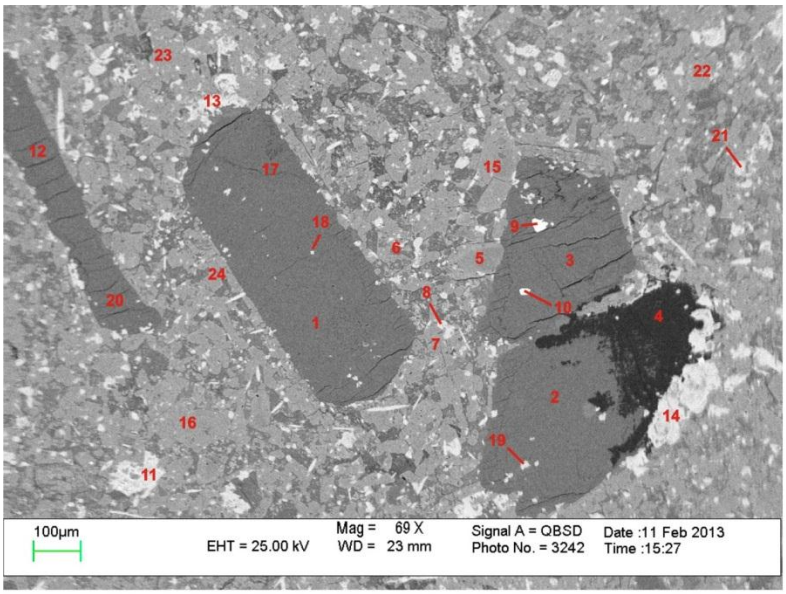

1	Chlorite + K2O
2-3	Chlorite
4	Albite
5	Clinopyroxene
6	Clinopyoxene + TiO2
7	Clinopyroxene
8	Titanite
9	Pentlandite
10	Pentlandite
11	Titanite
12	Chlorite + K2O
13-14	Titanite
15-16	Clinopyroxene
17	Chlorite + K2O
18	Titanite
19	Titanite
20	Chlorite + K2O
21	Titanite
22-24	Clinopyroxene

Sample: 456B2
Site: 3

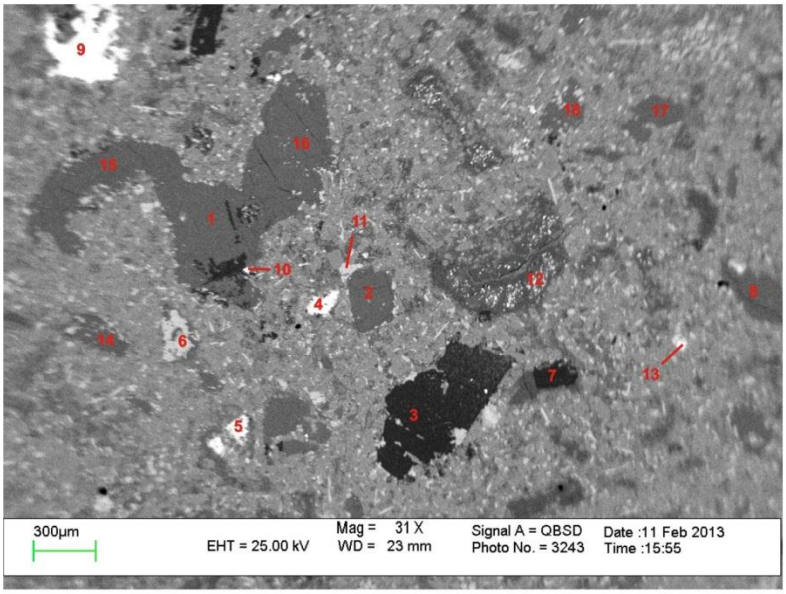

1	Chlorite + K2O
2	Chlorite + K2O
3	Albite
4	Celsian
5	Ba-feldspar
6	Titanite
7	Albite
8	Chlorite
9	Celsian
10	Pentlandite
11	Titanite
12	Oxyhornblende (Alt)
13	Mix
14-18	Chlorite

Sample: 456B2
Site: 4

[Top/Bottom] Phenocrysts of olivine with orthorhombic habit pseudomorphed by chlorite. Alteration of groundmass by chlorite and calcite in microcrystic basalt.

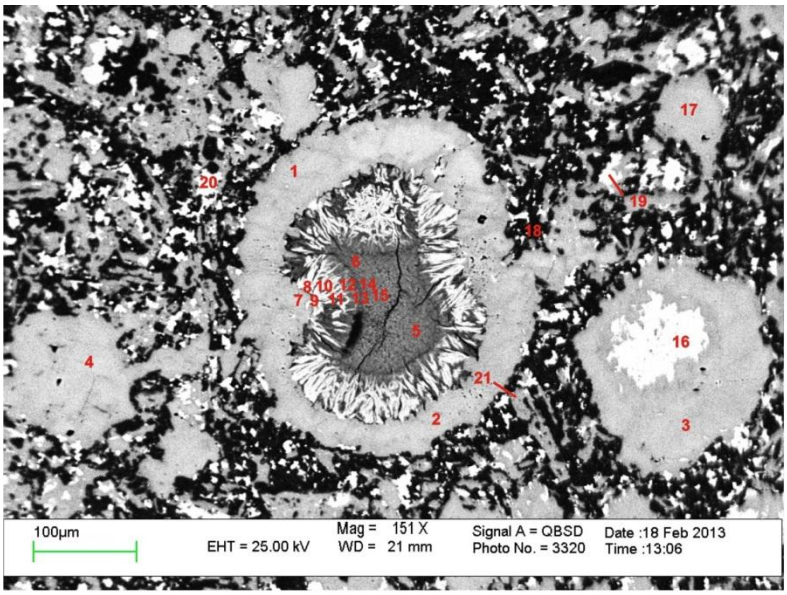

1-4	Calcite
5	K-feldspar
6	K-feldspar
7	Calcite
8	Chlorite + Calcite
9-11	Chlorite
12-15	K-feldspar
16	Chlorite
17	Calcite
18	Albite
19	Chlorite
20	Chlorite
21	Calcite

Sample: 459C
Site: 1

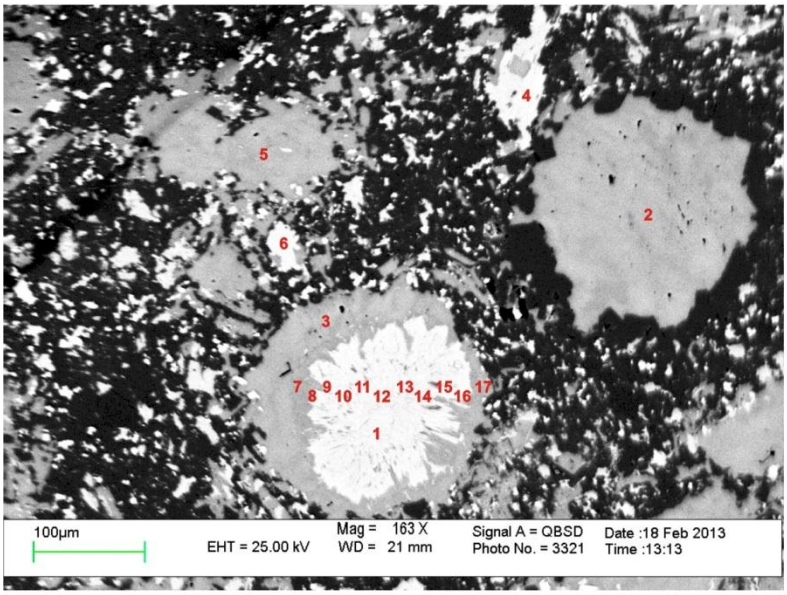

1	Chlorite
2	Calcite
3	Calcite
4	Chlorite + TiO2
5	Calcite
6	Chlorite
7	Calcite
8-14	Chlorite
15	Chlorite +CaO
16	Chlorite +CaO
17	Calcite

Sample: 459C
Site: 2

[Top/Bottom] Zoning of amygdale, in massive amygdaloidal basalt.

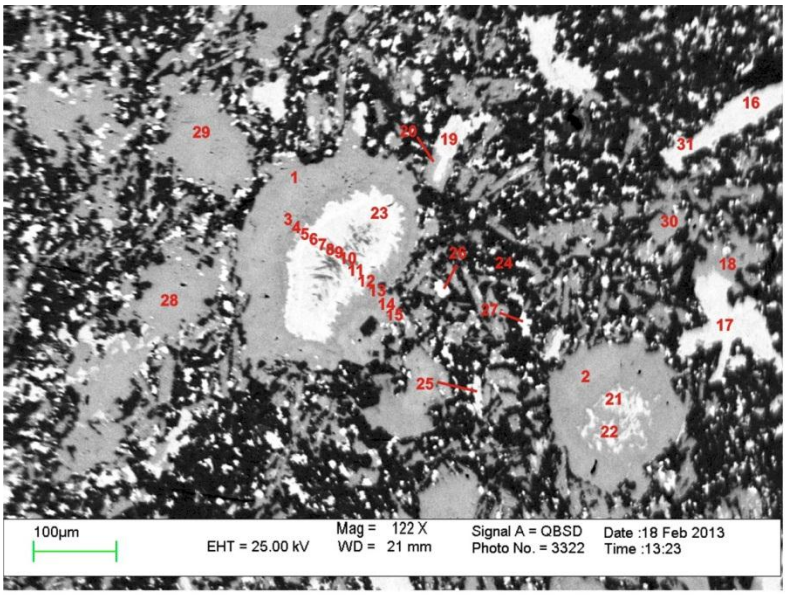

1-3	Calcite
4	Mix
5-8	Chlorite
9	K-feldspar
10	K-feldspar + mix
11-13	Chlorite
14-15	Calcite
16-17	Chlorite
18	Calcite
19	Chlorite
20	Calcite
21	Chlorite
22	Chlorite + K2O
23	Chlorite + K2O
24	Albite
25	Chlorite + K2O
26	Rutile
27	Rutile
28-30	Calcite
31	Chlorite

Sample: 459C
Site: 3

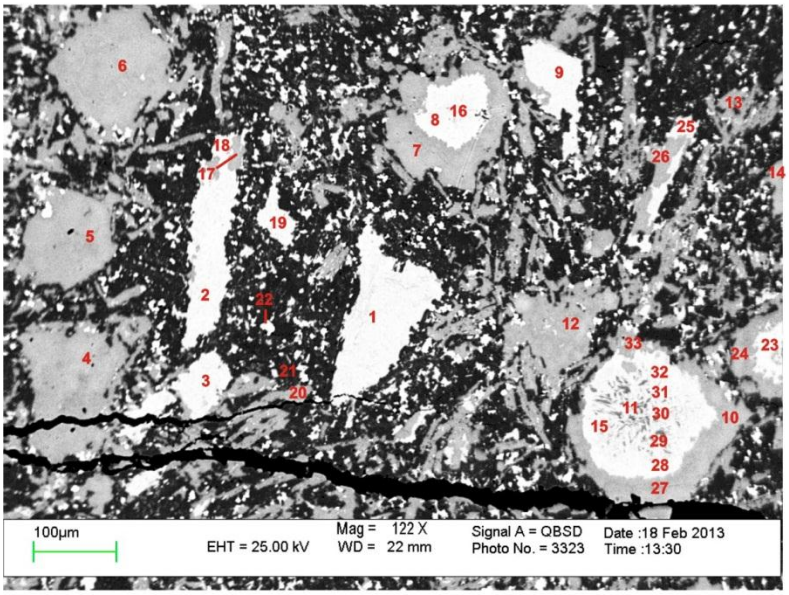

1-3	Chlorite
4-7	Calcite
8	Chlorite + K2O
9	Chlorite
10	Calcite
11	Chlorite + K2O
12	Calcite
13	Calcite
14-16	Chlorite + K2O
17	Calcite
18-19	Chlorite
20	Calcite
21	Albite
22	Titanite
23	Chlorite
24	Calcite
25	Chlorite
26-27	Calcite
28	Chlorite
29	K-feldspar
30	K-feldspar + Mix
31	K-feldspar + Mix
32	Chlorite + K2O
33	Calcite

Sample: 459C
Site: 4

[Top/Bottom] Zoning of amygdale, with alteration of glassy groundmass by chlorite ± calcite in massive amygdaloidal basalt.

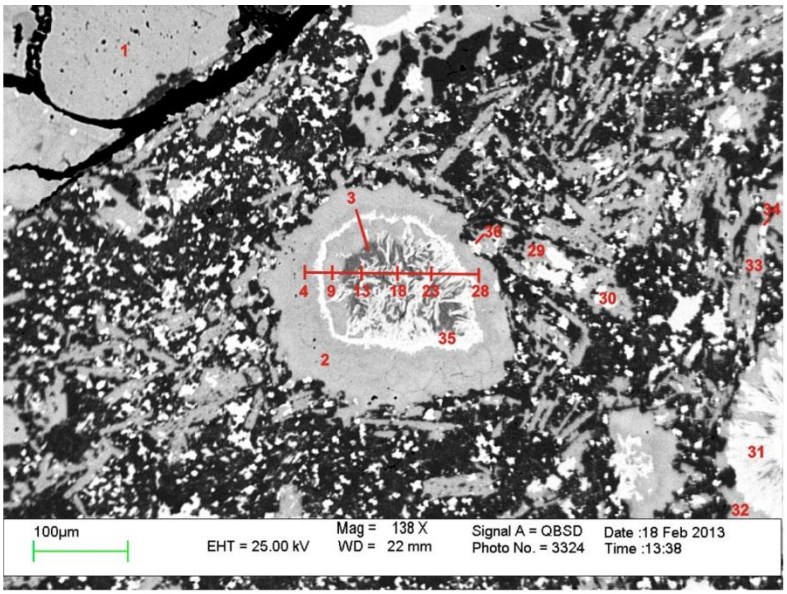

Sample: 459C
Site: 5

1-2	Calcite
3	K-feldspar
4	Calcite
5	Chlorite + K2O
6	Chlorite
7-8	Calcite
9-17	K-feldspar
18	Chlorite + K2O
19	K-feldspar
20	K-feldspar
21	Chlorite + K2O
22	K-feldspar
23	K-feldspar
24	K-feldspar
25-27	Chlorite + K2O
28	Mix
29	Calcite
30	Chlorite + CaO
31-33	Chlorite
34	Chlorite + CaO
35	Chlorite
36	Chlorite + CaO

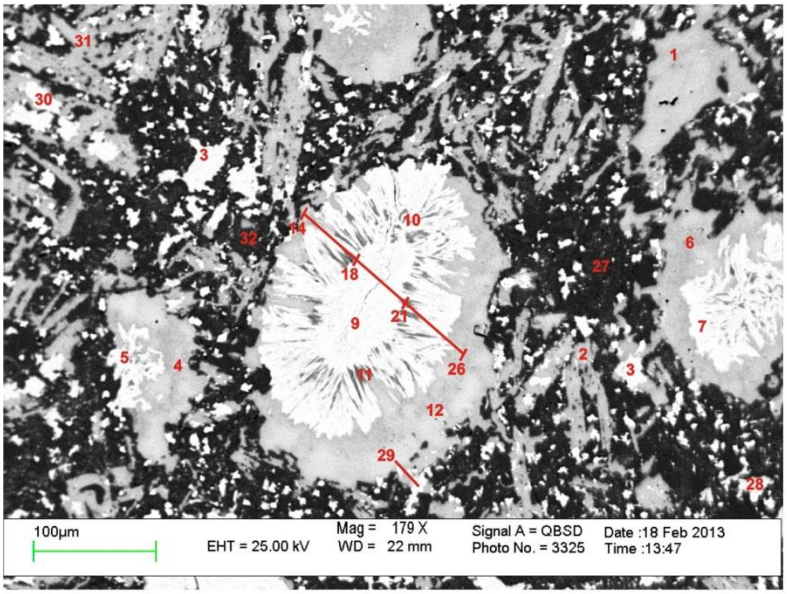

Sample: 459C
Site: 6

1-2	Calcite
3	Chlorite
4	Calcite
5	Chlorite
6	Mix
7-9	Chlorite
10	Chlorite + Others
11	Chlorite + Others
12	Calcite
13	Chlorite
14	Mix
15-17	Chlorite + K2O
18-21	Chlorite
22-25	Chlorite + K2O
26	Calcite
27	Albite
28-30	Chlorite
31	Calcite
32	Albite

[Top/Bottom] Zoning of amygdale, with alteration of glassy groundmass by chlorite ± calcite in massive amygdaloidal basalt.